# Foetal Advanced Speckle Tracking for the Assessment of Cardiac Function

## (FAST-I Study)

**C E Blunt**

**DClinSci 2025**

# Foetal Advanced Speckle Tracking for the Assessment of Cardiac Function

# (FAST-I Study)

**CARLA ELIZABETH BLUNT**

A thesis submitted in partial fulfilment of the requirements of the Manchester Metropolitan University for the degree of **Doctor of Clinical Science**

Department of Life Sciences,

Faculty of science and engineering, Manchester Metropolitan University

2025

## Declaration by the candidate

I hereby declare that this thesis is entirely my own work and has not been copied from any other sources. It has not been submitted or accepted for any other degree at any University. To the best of my knowledge, this thesis does not contain any material that has been previously written or distributed previously by other parties.

## Acknowledgements

This project was conducted as part of a Doctorate in Clinical Sciences. The National School of health Care Science (NSHCS) and University hospitals of Leicester (UHL) as part of the Higher Specialist Scientific Training (HSST) Programme provided funding for this work. This programme was possible due to the collaborative efforts of congenital and foetal cardiology units at UHL and Manchester metropolitan University (MMU). I am truly grateful for the opportunity to have embarked on this programme.

I would like to sincerely thank my work place supervisors Dr Katie Linter and Mrs Deborah Ip for your continued support and encouragement throughout this process. You both supported me in a clinical doctorate that was both new and challenging, which we all navigated together. I would not have seen this project to completion without the support and direction of you both. You believed in me when I did not believe in myself.

I am grateful for the supervision and contributions that I have received from Dr Rehan Junejo and Dr Llwyd Orton, you have both played a vital role in the organisation, planning and execution of this research project to completion. Thank-you, for your valuable knowledge, guidance and experience.

Special thanks go to Dr Suhair Shebani, Dr Oscar Nolan, Mrs Sharon Bowcutt and Mrs Linda O'Hare your expertise and enthusiasm in foetal cardiology and your support and encouragement for this research project has allowed it to be completed. I would also like to thank Professor Tommy Mousa for the time you gave in the conceptualisation and planning of this project.

I could not have completed the project or this programme without the support of the congenital cardiac physiology team, you have given me time, support and encouragement throughout this whole process for which I am so deeply thankful.

I would like to thank all the participants of this study for giving their time, without them, the research would not be possible.

Finally, to my dear family and friends, who have been through the highs and lows of this programme every step of the way with me! I really cannot thank-you enough.

## Abstract

**Introduction:** Speckle tracking echocardiography (STE) is an advanced imaging technique used to assess myocardial deformation through global sphericity index (GSI) and global longitudinal strain (GLS). However, its use in foetal cardiology is still limited. This study explores the application of STE in the foetal heart, assessing its feasibility and reproducibility in routine practice and defining normal values across gestational age (GA) groups. Further, ventricular disproportion of the foetal heart is the main indication of an obstructive lesion such as coarctation of the aorta (CoA). However, its diagnosis before birth remains challenging. STE may provide an additional diagnostic marker for the presence of foetal CoA. The primary objective of this study was to evaluate the use of foetal 2D STE in the clinical setting and to assess reproducibility, reliability and clinical applicability. Additionally, this study explores STE's role in detecting obstructive lesions associated with ventricular disproportion and its potential application in foetal tachyarrhythmia cases. **Methods:** In a prospective study, using STE, 120 normal foetal four-chamber heart views from 72 participants from 18 to 37 weeks of gestation, 22 studies from 16 foetuses with ventricular disproportion were analysed and compared. Further, seven tachyarrhythmia patients were recruited and a case series was conducted to evaluate the use of STE in this cohort compared to healthy controls. Foetal HQ software was used to assess GSI and GLS of the left ventricle (LV) and right ventricle (RV). Statistical analysis was conducted to assess reproducibility, reliability and to establish normal reference ranges; ventricular disproportion and tachyarrhythmia data were compared against the normal control group. Reference ranges and Z-scores were produced for GSI, LV, and RV GLS across GA groups 19-37 weeks. **Results:** STE has proven to be a feasible and reliable tool for assessing

foetal cardiac function in a clinical setting, with high reproducibility (ICC GSI: 0.93, LV GLS: 0.92, RV GLS: 0.84). A significant relationship was observed between gestational age (GA) and both LV and RV GLS ($p < 0.05$), Notably RV GLS values were higher than LV GLS with a statistically significant difference ($p < 0.05$). In cases of ventricular disproportion with confirmed obstructive lesions, a significant reduction in LV GLS and GSI was observed compared to normal cohorts ($p < 0.05$). Similarly in foetuses with tachyarrhythmia, both GSI and LV GLS were significantly reduced compared to controls ($p < 0.05$). Foetuses with atrial flutter exhibited the lowest GSI values (< 1.1), suggesting potential cardiac remodelling. **Conclusion:** STE is a reliable tool for foetal cardiac assessment and can be easily incorporated into routine foetal examination with normal reference ranges established here for GSI and LV and RV GLS. Additionally, STE analysis may be a valuable tool for assessing foetuses with ventricular disproportion and could aid in predicting obstructive lesions such as CoA. Furthermore, the use of STE in foetal tachyarrhythmia may offer additional insight into myocardial function before clinical signs of foetal cardiac failure or hydrops develop. However further research is needed to validate its utility in these clinical cases.

## Key words

Cardiac function, foetal cardiac, foetal echocardiography, ventricular function, left ventricle, right ventricle, ventricular disproportion, speckle tracking echocardiography, obstructive lesion, foetal tachyarrhythmia, Coarctation of aorta, four-chamber view, Supraventricular tachycardia

# Table of Contents

## List of Abbreviations

| | |
|---|---|
| 2D | Two Dimensional |
| 3D | Three Dimensional |
| ASD | Atrial Septal Defect |
| BCCA | British Congenital Cardiac Association |
| CFI | Colour Flow Imagining |
| CI | Chief Investigator |
| CoA | Coarctation of the Aorta |
| EMCHC | East Midlands Congenital Heart Centre |
| ECHO | Echocardiography |
| EF | Ejection Fraction |
| EPR | Electronic Patient Record |
| GLS | Global Longitudinal Strain |
| FASP | Fetal Anomaly Screening Programme |
| FE | Foetal Echocardiography |
| GE | General Electric |
| GSI | Global Sphericity Index |

| | |
|---|---|
| HSST | Higher Specialist Scientist Training |
| ICF | Informed Consent Form |
| IT | Information Technology |
| LA | Left Atrium |
| LRI | Leicester Royal Infirmary |
| LV | Left Ventricle |
| LVOT | Left Ventricular Outflow Tract |
| LVEF | Left Ventricular Ejection Fraction |
| MAPSE | Mitral Annular Plane Systolic Excursion |
| MMU | Manchester Metropolitan University |
| MPI | Myocardial Performance Index |
| MV | Mitral Valve |
| N/A | Not applicable |
| PA | Pulmonary Artery |
| PV | Pulmonary Valve |
| REC | Research ethic committee |
| RV | Right Ventricle |
| STE | Speckle – Tracking Echocardiography |
| SVT | Supraventricular Tachycardia |

| | |
|---|---|
| TAPSE | Tricuspid Annular Plane Systolic Excursion |
| TDI | Tissue Doppler Imaging |
| TTE | Transthoracic echocardiography |
| TV | Tricuspid Valve |
| UHL | University Hospitals of Leicester |
| UK | United Kingdom |

# Table of Figures

## Chapter 2



## Chapter 3

## Chapter 4



## Chapter 5

## Chapter 6

# List of Tables

## Chapter 2



## Chapter 3



## Chapter 4

## Chapter 5



## Chapter 6

## Thesis Overview

This thesis is a traditional style thesis divided into sections and subjections.

**Chapter 1** seeks to briefly introduce the overview of foetal echocardiography (FE).

**Chapter 2** introduces the topics of FE, foetal cardiac function and speckle tracking of the foetal heart. This chapter looks at the potential uses of speckle tracking echocardiography (STE) in the presentation of ventricular disproportion and post foetal arrhythmia. A detailed literature review on the functional assessment of the foetal heart, the techniques used and the introduction of STE will be included in this chapter. Foetal ventricular disproportion including potential causes such as coarctation of the aorta and foetal tachyarrhythmia will also be discussed. The rationale behind this study and its hypothesis is also included in this chapter. Chapter two ends with the aims and objectives of this thesis and provides an impact statement.

**Chapter 3** Discusses the methods used, including ethical approvals, eligibility and recruitment. This chapter also includes a detailed piece on the experimental protocol and techniques used for the acquisition of echocardiographic images, extrapolation and analysis of data for the Fetal HQ software.

**Chapter 4** will discuss the feasibility and reproducibility of foetal heart STE in the assessment of global sphericity index (GSI) and the global longitudinal strain (GLS) of the right ventricle (RV) and the left ventricle (LV). It will include a brief introduction to the use of foetal STE in the clinical setting, the aims and objectives of this research, relevant methods describing data acquisition, analysis for reproducibility

assessment, and reliability statistics as well as normal reference values. The chapter will conclude with a discussion of the strengths and the limitations of this study.

**Chapter 5** looks at the use of STE in the assessment of GSI and GLS in cases of ventricular disproportion. During this chapter, there will be discussions on the potential use of STE in the diagnosis of coarctation of the aorta and other obstructive lesions. An initial introduction detailing ventricular disproportion and a literature review of recent studies involving STE commence this chapter. This will then be followed by the methods used for the study and the aims and objectives. Results present the data obtained from the disproportion cases compared with the normal reference ranges and values established in earlier chapter. Chapter concludes with the discussion of the findings, limitations and a conclusion.

**Chapter 6** is a case series investigating foetal tachyarrhythmia and the use of STE to quantify GSI, LV, and RV GLS once the foetal heart has reverted into sinus rhythm. The chapter begins with an introduction on foetal tachyarrhythmia and the functional assessment in these cases. Demographics of the case series are discussed including the presentation, treatment and management of the patients. Results include the data obtained with a discussion and a conclusion to end.

**Chapter 7** is a general discussion of the three results chapters. Within this chapter, the strengths and limitations encountered throughout the study will be discussed. The findings from this study are compared with existing literature and current clinical practice. Particular consideration is given to the impact on services and service users. The chapter conclude with recommendation for improvement in any future research and any future studies that may be continued because of this study.

# Chapter 1 – Introduction – Foetal Echocardiography Overview

Foetal echocardiography (FE) was initially introduced for the assessment and diagnosis of structural heart defects (Simpson et al., 2018) and is currently the standard method for defining foetal cardiac anomalies (Archer and Manning, 2018). FE is a vital tool in the antenatal diagnosis of congenital heart disease (CHD), which is the primary cause of mortality and morbidity in neonates (Agarwal et al., 2016). Although studies looking at the prevalence of congenital heart disease do vary slightly, the consensus is that congenital heart disease occurs in approximately 8-9 per 1000 live births (Agarwal et al., 2016; Van der Linde et al., 2011). Using FE to detect complex congenital anomalies before birth is challenging, but has been shown to decrease morbidity and improve surgical outcomes (Agarwal et al., 2016; Maulik et al., 2017 and Rajiah et al., 2011). Having the ability to detect cardiac anomalies during the antenatal period can alter the obstetric course and outcome (Maulik et al., 2017). Rajiah et al., (2011) discussed this theory further by proposing that early detection can enable parental reassurance, foetal therapy, mode of delivery, and better support a postnatal referral to a specialist cardiac centre with a multi-disciplinary team available with the expertise to manage congenital cardiac patients.

With the development of new techniques, it is now possible to not only detect structural abnormalities of the foetal heart but to also allow the assessment of foetal cardiac function (Crispi et al., 2013). Advancing technology has allowed foetal echocardiographers to move away from a purely subjective assessment of myocardial contractility to more quantifiable methods such as M-mode echocardiography and Doppler based techniques. Modalities such as M-mode, two-dimensional (2D), and Doppler echocardiography have been utilised in the assessment of cardiac dysfunction. However, none of these modalities is preferable

to another with all demonstrating their own limitations, such as foetal position, maternal habitus and gestational age (Simpson et al., 2018). .

More recently, STE has emerged as a tool in the assessment of foetal cardiac function. It offers advantages over conventional FE methods, as it is the only technique that can investigate the deformation of the myocardium (Simpson, 2011). 2D STE techniques allow myocardial deformation to be quantified by using frame-by frame tracking of bright myocardial areas (speckles) which are natural acoustic markers which are formed by the interaction of the myocardium and the ultrasound waves (Bijnens et al., 2009). These speckles are unique to small regions of tissue thereby making them reliable for tracking motion over time. Post-processing analysis of 2D images allows myocardial strain and strain rate to be measured. Despite its potential advantages in the assessment of foetal cardiac function, STE in foetal cardiology is a developing technique that still requires investigation for use in the foetal heart (Germanakis et al., 2012; Day et al., 2019).

STE has been described in the adult population since 2004 (Leitman et al., 2004). It has gained pace within adult cardiology and has increasingly become a part of the routine echocardiographic evaluation. In 2015, the European Association of Cardiovascular Imaging and the American Society of Echocardiography published a consensus document to standardise the use of 2D STE for deformation analysis for the adult population. The British Society of Echocardiography (Robinson et al., 2024) highlighted the benefits of 2D STE for longitudinal strain but expressed caution due to inter-vendor variation.

However, even with increasing interest and growing recognition in the adult population of the usefulness of STE, the technique has not been widely used in the

assessment of foetal cardiac function. Interest in the technique is now increasing for assessment of foetal cardiac function, as heart failure in the foetus is usually a late event that can be recognized by cardiomegaly, atrioventricular insufficiency, and foetal hydrops (Huhta, 2004). In the early stage, the heart is able to adapt and there is a long subclinical period of cardiac dysfunction before end-stage heart failure (Huhta, 2004). During this period of cardiac adaptation, changes in cardiac function, as well as in the heart's shape and size, can be measured. This phase of adaption is known as cardiac remodelling. (Opie et al., 2006). It is during this stage that foetal STE could detect subtle subclinical myocardial dysfunction before it is evident through routine FE. Nonetheless, it is still predominantly used within research and is not routinely utilised within the clinical setting in centres across the United Kingdom.

During the Initial review of relevant literature for this study, it became evident that there is a dearth of studies investigating the application of STE of the foetal heart as a potential diagnostic marker in foetuses presenting with ventricular disproportion. There was however, a recent study by DeVore et al (2021) where the use of STE in the detection of coarctation of the aorta (CoA). CoA is a narrowing within the descending aorta that can obstruct the blood flow from the heart to the body. It was concluded in the study that the use of STE on the last examination during the third trimester and prior to delivery could potentially assist in the detection of CoA, as they demonstrated changes in the foetal heart shape and function compared to the control group. However further investigation was recommended. While STE has been investigated to assess myocardial function in various clinical conditions such as congenital heart disease and foetal growth restriction, its application in foetal cardiac arrhythmias remains unexplored. This absence in literature highlights a gap in the

understanding of how myocardial mechanics quantified by STE, may be altered in cases of foetal arrhythmias.

# Chapter 2 – Background and literature review

## 2.1 Cardiac Function

FE is used in the assessment of cardiovascular well-being of the foetus. Advancement in research and clinical expertise has seen a shift from foetal echocardiography being used solely for the detection of structural anomalies to also being utilised in the assessment of foetal cardiac function (Crispi and Gratacós, 2012; Godfrey et al., 2012; Crispi et al., 2013).

In order to perform an accurate functional assessment of the foetal heart it is important to understand the physiology and cardiac function of a normal heart. By understanding the challenges that a small foetal heart presents, and to understand the limitations, which echocardiography-imaging devices can present, can aid in the accurate assessment of foetal cardiac function. Cardiac function is the heart's ability to meet the metabolic demands of the body (Carreiro, 2009). The heart's main function is to provide adequate circulation of blood through the body and to provide sufficient perfusion of the organs (Chaudhry et al., 2022). Myocardium is the term used to describe heart's muscle. It is made of cardiac muscle fibres (myofibrils) which are uniquely arranged to wrap around the heart and its four chambers in varying orientation. Cardiac chambers consist of two superior atria and inferior ventricles. The unique orientation of myofibrils enables the ventricles to contract in several directions simultaneously. It is these movements that enable the heart to be an effective pump. Functionally this consists of six movements: narrowing, lengthening, and shortening, widening, twisting and uncoiling (Buckberg et al., 2018, Crispi et al., 2013). These six movements make up the three-directional myocardial motion of radial, longitudinal and circumferential contractility (Crispi et al., 2013). It is the varying orientation of the myocardial fibres within the left ventricle that permit

these movements to occur enabling the left ventricle to contact in a highly sophisticated way. The contractility of the myocardium can be evaluated with the use of ultrasound by measuring either motion or deformation. Myocardial Deformation is defined by the change in length or thickness between two points. Myocardial motion is the distance covered by one point and determined by displacement and velocity (Crispi et al., 2013). Figure 2.1 provides a schematic view of these movements.

**Longitudinal function –** These muscle fibres are adjacent to the endocardium and are longitudinally orientated. Longitudinal function represents the magnitude of motion from the base of the heart towards the apex (Figure 2.1).

**Radial function –** Muscle fibres within the myocardium are ordinated circularly around the short axis of the LV. It is the contraction of these fibres that result in the diameter of the LV cavity decreasing. (Robinson et al., 2024) (Figure 2.1)

**Circumferential Function** – This is the twisting contraction of the LV. Muscle fibres adjacent to the epicardium are orientated approximately 60° in relation to the fibres within the myocardium. Contraction of these fibres result in a twisting motion of the entire LV, the basal section twists clockwise and the apex has a counter clockwise twist; this twisting motion is known as circumferential shortening (Figure 2.1, Figure 2.2).

The overall function of the left ventricle relies on adequate radial, longitudinal and circumferential contraction. All these movements occur simultaneously with the basal segments being pulled towards the apex. This motion results in the LV shortening in both length and circumference in a twisting motion, this motion decreases the cavity size in order to expel blood into the aorta. (Crispi et al., 2013). In comparison to the left ventricles shortening and twisting motion, right ventricular (RV) contractility relies

mainly on the contraction of the longitudinal muscle fibres seen from the base to the apex of the chamber. (DeVore et al., 2019).

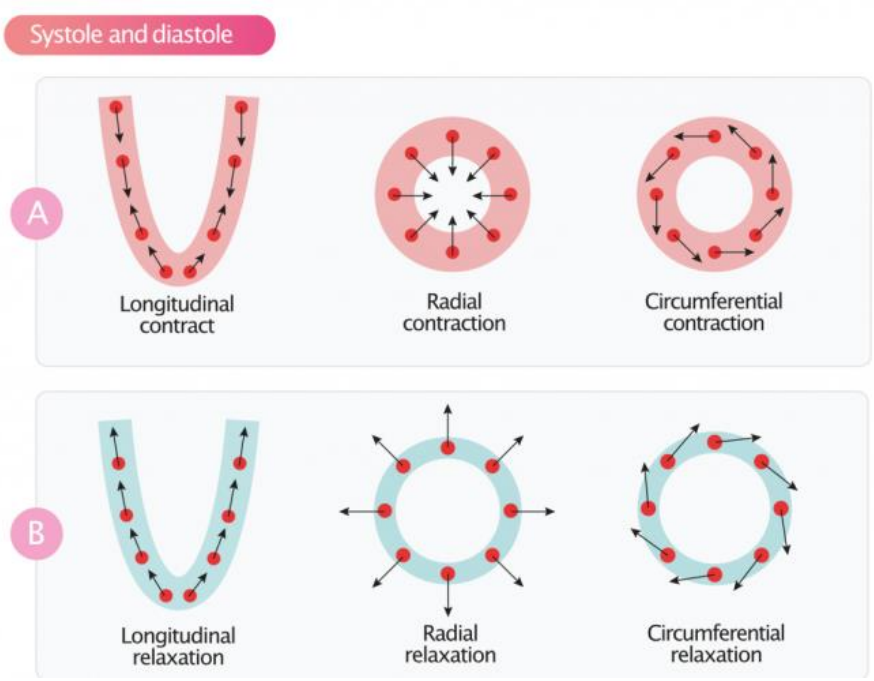


**Figure 2.1**: Myocardial deformation during the cardiac cycle, demonstrating fibre orientation and directional strain. **Panel A** – illustrates systolic contraction in three directions longitudinal (base-apex), radial (inward thickening), and circumferential. **Panel B** – shows corresponding diastolic relaxation with myocardial lengthening, wall thinning and expansion. (Image Adapted from Clinical Echocardiography, 2021)

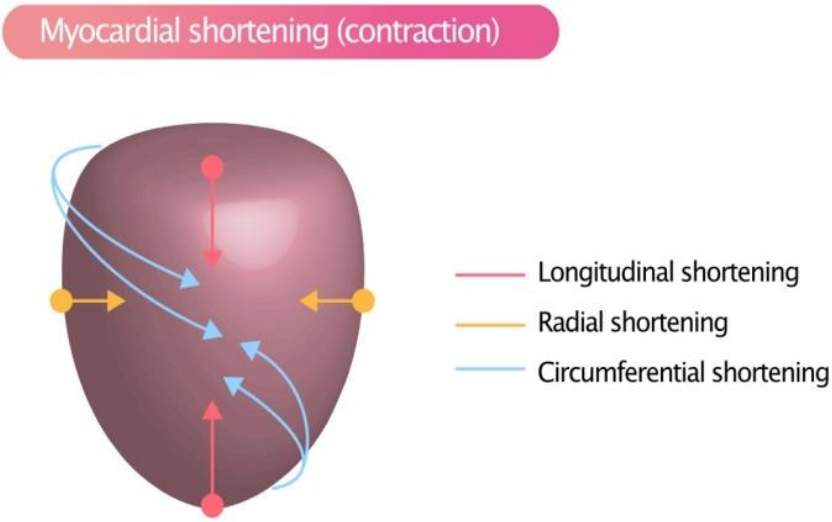


**Figure 2.2**: Illustrates a three-dimensional representation of left ventricular myocardial fibre shortening during systole. The diagram highlights longitudinal (red arrows), radial (yellow arrows) and circumferential (blue arrows) shortening, this reflects the coordinated contraction of myocardial fibres in multiple planes. (Adapted from Clinical Echocardiography, 2021)

The right ventricle (RV) is the anterior cardiac chamber in the normal heart and is positioned immediately behind the sternum. Its geometry is notably more complex compared to the conical shape of the left ventricle (LV). When viewed laterally the RV presents a triangular shape, whereas in cross-section, it appears crescent-shaped (Ho and Nihoyannopoulos, 2006; Wang et al., 2021).

Structurally, the RV can be divided into three functional components figure 2.3.

1. Inlet region; this encompasses the tricuspid valve, chordae and papillary muscles
2. Apical trabecular region; this includes the trabeculated myocardium forming the apical part of the RV.
3. Outlet region; This extends to the pulmonary valve and infundibulum

(Goor and Lillehei, 1997)

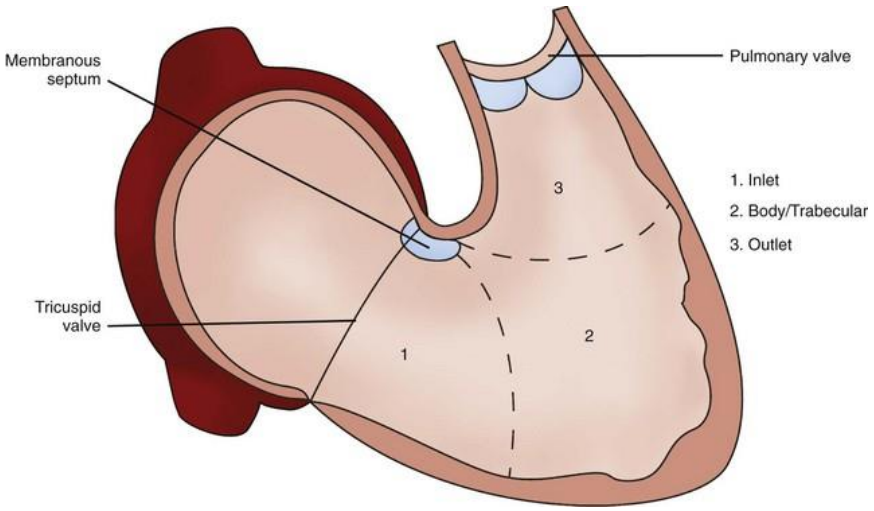


**Figure 2.3**: Anatomical illustration of the right ventricle, demonstrating the three functional components. **1. Inlet** (receiving flow from the tricuspid valve. **2. Trabecular body** and **3. Outlet** (leading to the pulmonary valve). These structural divisions contribute to the distinct contractile mechanics of the right ventricle compared to the left ventricle. (Adapted from Thoracic Key, 2016)

The RVs contractile mechanics are distinct from those of the LV, incorporating three separate mechanisms these can be seen in figure 2.4:

1. Inward motion of the free wall (bellows effect); this contributes to the radial shortening of the chamber.
2. Longitudinal fibre contraction: Responsible for the majority of RV shortening, occurring along the long axis of the chamber.
3. Traction from the LV: The shared myocardial attachments between the RV and LV facilitate contraction via secondary tethering forces generated by LV contraction.

Unlike the LV, that relies heavily on twisting and rotational movements during systole. The RVs contraction relies predominantly on longitudinal shortening to ensure effective RV systolic function. (Ho and Nihoyannopoulos, 2006).

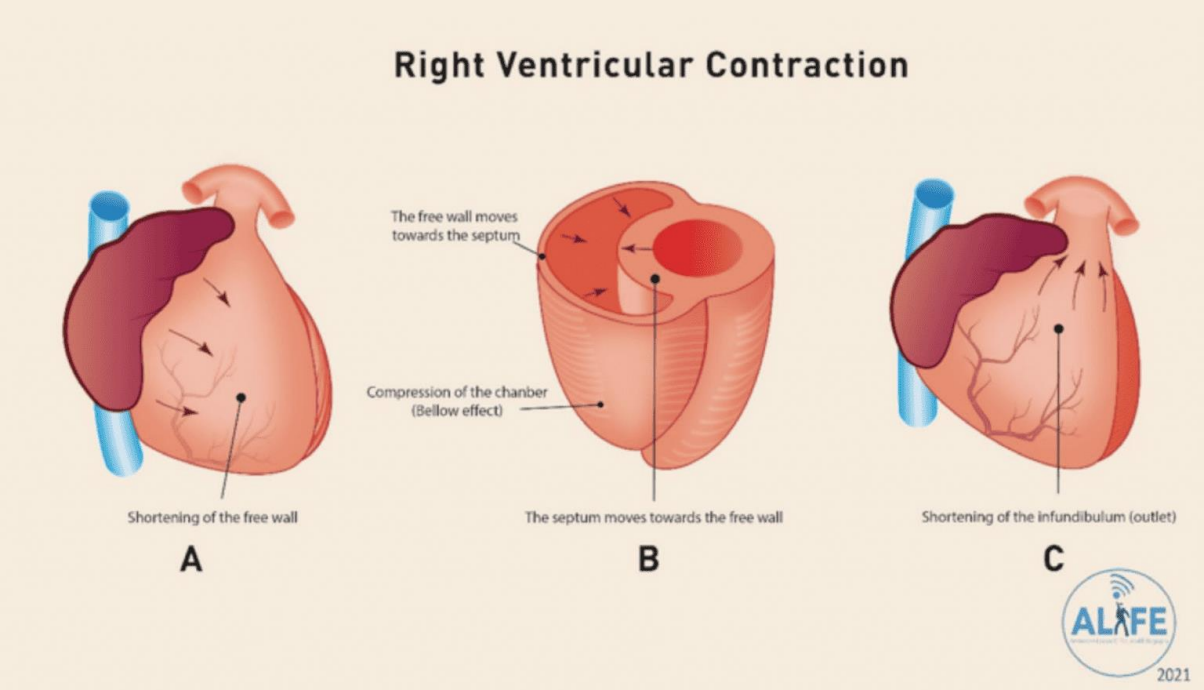


**Figure 2.4**: This figure depicts the three primary components of RV contraction. **A** illustrates the shortening of the free wall. During systole, the free wall moves inwards towards the septum. Image **B** highlights the "bellows effect" in which the interventricular septum moves towards the free wall. Image **C** focuses on the shortening of the infundibulum (the outflow tract), which contributes to overall efficiency of the RV ejection phase (Image adapted from Kraemer et al., 2021)

## 2.2 Foetal Embryology and Assessment of Foetal Cardiac Function

### Foetal Embryology

The development of the human heart is a highly coordinated process which begins in the third week post-conception and is complete by the end of week eight (Archer and Manning, 2018). It involves the differentiation of mesodermal cells into the cardiogenic regions known as the first heart field (FHF) and the second heart field (SHF), forming the cardiac crescent illustrated in figure 2.5. At around day 21 the bilateral cardiac crescent fields fuse at the midline to create the primitive heart tube, which give rise to distinct cardiac structures (Abuhamad and Chaoui, 2022). The primitive heart tube undergoes looping by folding on itself in a rightward and anterior

motion, resulting in the future atria, ventricles and outflow tracts, (Abuhamad and Chaoui, 2022; Archer and Manning, 2018). This occurs with the bulging of the tube and looping to the right as the primitive ventricle moves downwards and to the right, and the primitive atria moving upward and to the left behind the ventricle the process of the formation of the foetal heart from the cardiac crescent to the chamber formation is illustrated in figure 2.5.

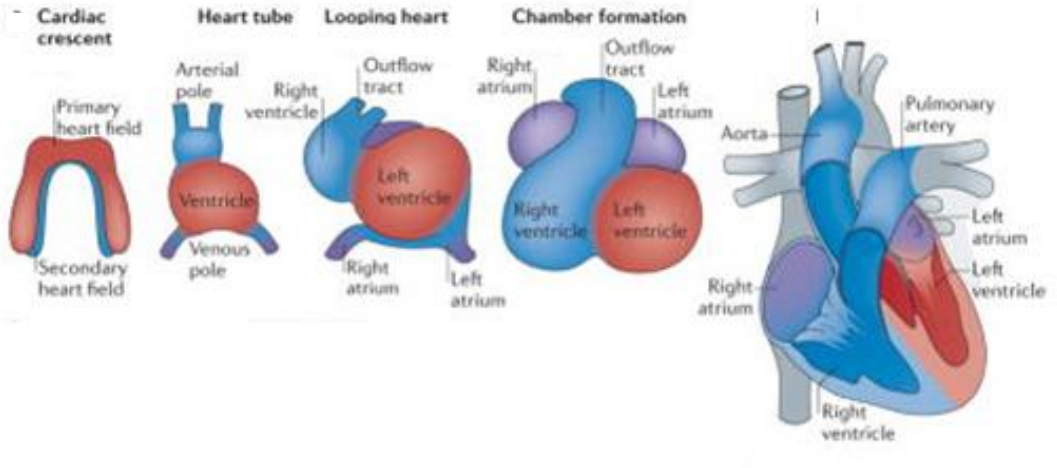


**Figure 2.5**: The image illustrates embryological development of the human heart from the cardiac crescent to the four-chambered structure. Key stages of early cardiac formation beginning with the cardiac crescent (~Day 15-16) and progressing through heart tube formation (~Day 20-21), looping (~Day 23-28) and chamber formation (~Week 4-8). Sequential development is shown from the primitive heart field culminating in the structurally mature four-chambered heart at 8 weeks post-conception. (Image adapted from OpenStax College, 2013)

Chamber formation continues through the process of septation at weeks 4-8, where the heart tube divides into distinct chambers and major vessels. (Abuhamad and Chaoui, 2022). Cardiac septation is the process by which heart tube divides into for separate chambers and two outflow tracts (Anderson, et al., 2003). This occurs between 4 and 8 weeks of gestation. Septation of the atria involves the development

of the septum primum and the septum secundum, forming the foreman ovale, which functions as a right to left shunt in foetal circulation, which allows blood to bypass the lungs during foetal life. (Anderson, et al., 2003). Ventricular septation occurs as the muscular wall (the interventricular septum) grows upward from the apex of the heart. This joins with tissue from the endocardial cushions and conotruncal ridges to complete the separation of the left and right ventricles. (Anderson, et al., 2003). Outflow tract septation is guided by spiralling ridges and contributions from the cardiac crest cells to divide the single vessel the truncus arteriosus into the aorta and pulmonary artery. These coordinated processes ensure the formation of the functional, four-chambered heart with separate systemic and pulmonary circulations. (Sadler, 2018).

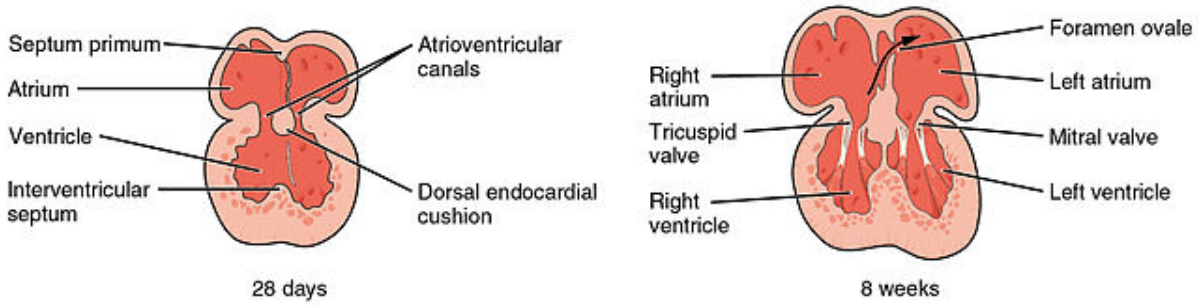


**Figure 2.6:** The illustration demonstrates the process of septation. At 28 days post conception septation begins with the appearance of the primum septum, the atrioventricular canals and the endocardial cushions. By ~8 weeks gestation septation has occurred, creating right and left atria and ventricles and the valves are developed. The foreman ovale is visible, permitting right-left shunting in foetal circulation. (Image adapted from OpenStax College, 2013)

**Foetal Cardiac Function**

The assessment of foetal cardiac function is now an integral part of the FE, allowing detailed evaluation of contraction and relaxation of the myocardial fibres and evaluation of the foetal heart's capacity to maintain cardiac output (CO) (Rocha et al., 2019). Accurate functional assessment of the foetal heart can aid in the prognosis and management of the foetus (Maulik et al., 2017; Rocha et al., 2019). Following the completion of cardiac septation by approximately 8 weeks of gestation, the foetal heart becomes functionally active and amenable to detailed echocardiographic assessment (Sadler, 2018). The transition from embryonic development to physiological functionality is a critical period in foetal cardiology, as it allows for the early detection of abnormalities in myocardial performance and chamber configuration that may precede overt structural anomalies (Abuhamad and Chaoui, 2022; Sadler, 2018).

There have been many echocardiographic methods developed over the years, which have allowed the transformation of foetal cardiac assessment from a purely subjective assessment of myocardial contractility to development of techniques, which allow the accurate quantification of size and function of the foetal heart (Simpson et al., 2018; Day et al., 2019). Most of these echocardiographic methods were developed for the assessment of the adult heart and have since been adapted for use in the foetal heart (Godfrey et al., 2012).

## 2.3 Echocardiographic Assessment of Foetal Cardiac Function – literature review

Several methods have been adapted from the adult and paediatric population for use in foetal echocardiography. These being: 2-Dimensional (2D) echocardiography,

Motion-mode (M-mode) echocardiography, and Pulsed wave Doppler. These will be discussed in detail later in the chapter. In more recent years through increasing research has advanced techniques such as Tissue Doppler, 4D Spatio-temporal image correlation (STIC) and 2D STE which can also be utilised in the assessment of foetal cardiac function (Archer and Manning, 2018). Early research in cardiac function of the foetal heart reviewed the use of M-mode and pulsed Doppler ultrasound to examine cardiac function. Two early studies carried out by DeVore (2005) and Simpson (2004) reviewed methods used for the assessment of foetal cardiac function, including M-mode and Doppler techniques. Using data from previous studies, DeVore (2005) and Simpson (2004) looked at the different methods used within foetal cardiology to assess foetal cardiac function. DeVore (2005) had a more technical approach; he included many reference ranges for normal values across gestations from 14 – 40 weeks within his report. Conversely, Simpson et al (2004) took a more descriptive approach with detailed explanations of how the measurements were obtained and the limitations of these techniques.

Both of these reviews concluded that although there were a wide variety of echocardiographic methods available to evaluate foetal cardiac function, there were limitations with all methods in the accuracy of the data derived due to either poor reproducibility or lack of validity. Both studies however agreed that selective use of one or more of these methods could be beneficial in the clinical setting.

### M-mode

M-mode echocardiography is the study of two-dimensional motion of all structures along an ultrasound beam over time (Godfrey et al., 2012). M-mode has been used in foetal echocardiography since the 1980's. It allows for the quantification of ventricular chamber size, ventricular wall thickness and ventricular function (DeVore,

2005; Simpson, 2004). Simpson (2004) and DeVore (2005) discuss the difficulty in M-mode quantification of ventricular function. To obtain an accurate M-mode for functional assessment the M-mode cursor must be positioned perpendicular to the ventricular septum. This is to enable visualisation of systole and diastole in the absence of an electrocardiogram (DeVore, 2005). This perpendicular view is not always achievable during FE due to foetal movement or foetal position. Figure 2.7 below, shows the position required of the foetal heart to obtain accurate M-mode measurements.

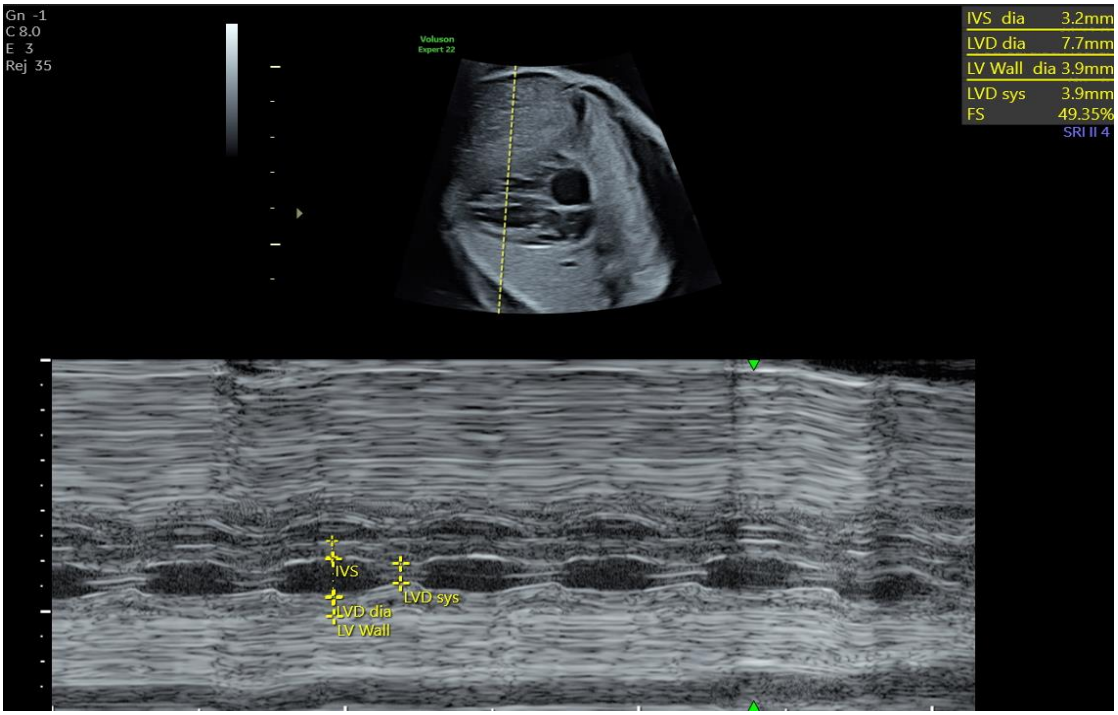


**Figure 2.7***:* Illustrates M-mode functional measurements for fractional shortening, obtained from the foetal heart with M-mode cursor perpendicular to the ventricular septum. (Image obtained with consent)

### Annular excursion/displacement

Mitral annular plane systolic excursion (MAPSE) and tricuspid annular plane systolic excursion (TAPSE) have the capability of evaluating longitudinal systolic function which has been shown to be affected in the earlier stages of cardiac dysfunction

(Koestenberger et al., 2009). Carvalho et al, (2001) performed a pilot study looking at the feasibility of determining mitral and tricuspid annular plane systolic excursion as a measurement for longitudinal function in the foetal heart. Although this was only a short study over a 3 month period with a small cohort of patients (Mitral -18, Tricuspid-14), they indicated that long-axis function of the foetal heart was feasible and could overcome the limitations of conventional M-mode due to foetal lie as mentioned previously. Nevertheless, due to its small cohort and short timeframe the conclusions derived from this study data would have to be taken with care. They were unable to generate any reference ranges and there was no mention of reproducibility within the study. In a study performed by Germanakis et al (2012), looking at the feasibility of performing offline TAPSE and MAPSE measurements found that measurements obtained off-line were similar to those obtained via conventional M-mode methods. They did indicate similar intra-observer variability indicating good reproducibility, however this again was still a small cohort of just 54 foetuses and it did not look at the feasibility of recording conventional M-mode. Some researchers recommend the use of TAPSE in the functional assessment of the foetal heart due to the importance of the right ventricle in utero and it being the dominant ventricle (Crispi and Gratacos, 2012). Yet, research and reference values in the foetal population are limited. Peixoto et al (2020) carried out a prospective study looking at the normal values for MAPSE and TAPSE in 360 low-risk pregnant women between 20 and 36+6 weeks gestation. Peixoto et al (2020) were able to produce reference values for foetal MAPSE and TAPSE due to its prospective design and large sample size. However, the reliability analysis performed indicated poor/moderate reproducibility. It was indicated that small changes in angle or location of the Doppler might explain this. Evidence indicates that although MAPSE

and TAPSE do have the capability of detecting longitudinal dysfunction in the foetal heal heart, even with studies as recent as 2020 there is still limited data on reference ranges and there is a need for caution when using this technique to assess cardiac function in the foetus.

### Conventional Doppler

Traditionally, foetal cardiac function was assessed by measuring blood flow using conventional Doppler. This technique allows assessment of blood's outflow (systolic) and inflow (diastolic) through the heart, as well as calculation of cardiac time periods. Assessment of cardiac output can then be calculated with the use of these measurements (Crispi et al., 2013; Hernandez-Andrade et al., 2012). To enable cardiac output to be evaluated stroke volume (SV) must be calculated. SV is a calculation of blood flow out of the heart in systole and is based on the measurement of the diameter of the aortic or pulmonary valve annulus multiplied by the flow across the chosen valve, dependent on which ventricle is being assessed. (Godfrey et al., 2012). The limitations with this method are the need to align perfectly with the direction of flow and the ability to have accurate measurements of the small valve structure. Small errors in these measurements could account for potentially large errors in the estimation of cardiac output, which is calculated using the formula SV x heart rate (Godfrey et al., 2012; Rocha et al., 2019; Simpson et al., 2018). Figure 2.8 illustrates the small structures involved and the accuracy needed in obtaining these measurements.

A 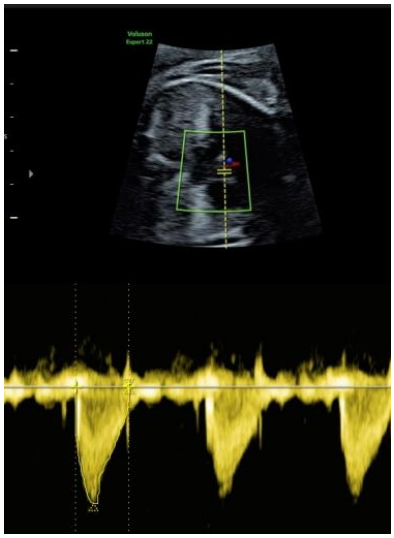

B 


**Figure 2.8**: Illustration of assessment of stroke volume to assess cardiac output using conventional Doppler technique. (A) Pulsed wave Doppler at aortic valve level with tracing to produce the velocity-time integral (VTI). (B) Left ventricular outflow tract (LVOT) measurement at aortic valve level. Image B demonstrates the small measurements needed to calculate cardiac output. (Images obtained with consent).

Research indicates that no one method has been found to replace another and foetal movement, position, size, or suspected cardiac lesion at the time of the echocardiogram could influence the modality used (Simpson, 2004; Crispi et al., 2012; Godfrey et al., 2012).

Moving forward and with the advancing technology and experience, foetal echocardiography is being utilised with more confidence for the detection of foetal cardiac dysfunction as well as structural abnormalities (Crispi et al., 2013); Godfrey et al., 2012). Crispi et al (2013) in their review on the assessment of foetal cardiac function explained that although foetuses rarely go into cardiac failure, there can be a long subclinical stage where the heart will attempt to adapt to the early stages of injury (Crispi et al., 2013; Huhta, 2004). During this stage, changes in the heart's shape, size and function can be seen. This process is known as cardiac remodelling (Crispi et al., 2013). Having the ability to assess the foetal heart for these subtle

changes in cardiac function in the subclinical stage before end-stage heart failure has occurred, may help to predict postnatal and long-term cardiac outcomes and allow early interventions to prevent end-stage heart failure (Crispi et al., 2013). Godfrey et al (2012) also recognised the potential benefit of being able to assess cardiac function, but it was highlighted that many of the assessments in current use were still blighted with limitations and that a standard method for assessment of cardiac function was still not feasible.

### Myocardial Performance Index

Myocardial performance index (MPI) consists of both systolic and diastolic components and can be applied to each ventricle individually. MPI utilises only time intervals meaning it is independent of heart rate and structural abnormalities, this is illustrated in Figure 2.9. Using only time intervals gives it an added advantage in the assessment of foetal cardiac function in congenital cardiac abnormalities, as subtle dysfunctions in foetal cardiac function may not be evident structurally. However, cardiac dysfunction may be evident in the altered timings of specific phases of the cardiac cycle (Godfrey et al., 2012). Van Mieghem et al, 2009 looked to validate the use of MPI in the foetal population between 20 and 36 weeks gestation. This was a prospective study including 117 healthy foetuses and 14 with suspected cardiac failure. Correlations were made between MPI and ejection fraction (EF). Results of this study showed a good correlation between MPI and EF with better inter-observer and intra-observer variability. Cruz-Martinez et al (2012) also found in their cross-sectional study that there was little variation in MPI during the first and second trimesters, they did however find a remarkable increase in MPI values between 34-41 weeks gestation. The strengths of this study compared to Van Mieghem et al are that this was a larger cohort consisting of 730 foetuses making the findings more

robust across the gestational ages. Neither of these studies investigated the effect of foetal heart rate on the components of the MPI measurement, but Cruz-Martinez (2012) did acknowledge that during left heart evaluation Doppler measurements of both the inflow and outflow were obtainable simultaneously thus eradicating the variation due to changes in foetal heart rate.

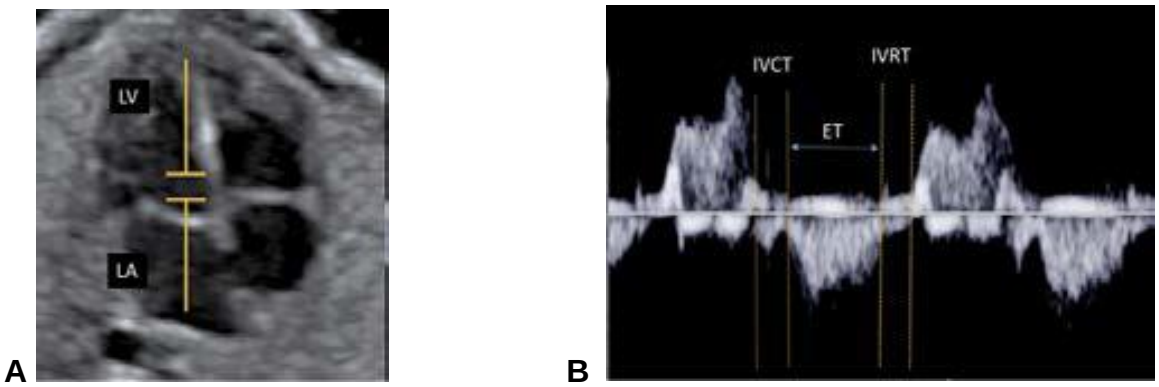


**Figure 2.9***:* Illustrates the position of the Doppler required (A) and the calculations needed (B), in order to obtain an accurate MPI. Images demonstrate the measurements required for the calculation of myocardial performance index (MPI). Image A illustrates where the cursor should be placed within the left ventricle (LV) and the left atrium (LA) to enable detection of inflow (mitral valve) and outflow (LVOT) on the same Doppler. Image B shows the measurements taken from the Doppler acquired in the 4-chamber view (A). MPI is calculated by Isovolumetric Contraction time (IVRT) + isovolumetric relaxation time (IVRT) / Ejection time (ET) (Rocha et al., 2019: Online).

Studies including MPI have mostly been tested on the left ventricle. Yet some techniques such as fractional shortening and MPI are still used in the assessment of the right ventricle, even though the right ventricle is anatomically and geometrically different to the left (Simpson, 2004; Godfrey et al., 2012).

### STE and strain / strain rate

STE is an emerging tool and is being used more frequently within the clinical setting in postnatal echocardiography in the assessment of myocardial wall deformation and cardiac function (Godfrey et al., 2012; Johnson et al., 2019). STE is a grey-scale based technique and is relatively angle independent. Therefore it allows a more sensitive and comprehensive assessment of ventricular size, shape and function. STE has the ability to track speckles, which are natural acoustic markers within the myocardium. The STE software will identify these speckles and then track them frame by frame to enable assessment of deformation of the heart (Bansal and Kasliwal, 2013; Godfrey et al., 2012). STE enables the calculation of deformation using the lagrangian method (figure 2.10) which is defined as deformation from an original length and is calculated using the formula below:

$$\varepsilon_L(t) = [L(t) - L(t_0)] / L(t_0)$$

STE is calculated using lagrangian strain as the base line. As end-diastole is always known it can be used as a reference (Hoit B, 2011).

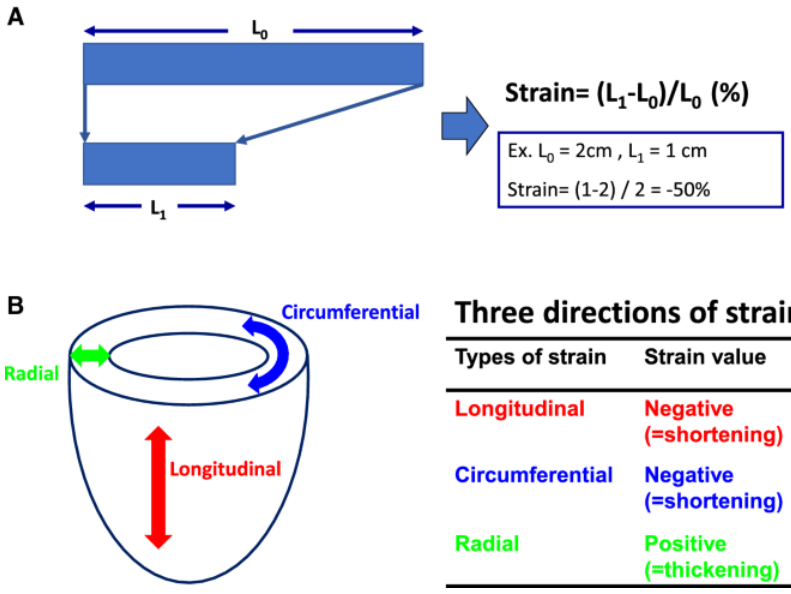


**Figure 2.10**: this figure demonstrates the concept of lagrangian strain and the definition and types of strain. Figure A; illustrates how strain is calculated as a change in the length of an object within a certain direction relative to its baseline length. Figure B shows the three directions of strain: Longitudinal, circumferential and radial. (Negishi and Negishi, 2022).

STE is a common technique used to measure strain. Strain is the measure of deformation of the myocardium throughout the cardiac cycle. It can measure the myocardium in multiple directions, these being: radial, longitudinal and circumferential. Once these speckles have been identified the specialist software can then generate strain (the amount of deformation the heart undergoes) and strain rate (the speed at which deformation occurs) curves. Strain is expressed as a fractional length change. The shortening is expressed as a negative value and the lengthening as a positive value. When used for the assessment of cardiac function and strain, the more negative the strain value is, the better the contractility. Global longitudinal strain is the most commonly used strain parameter within the clinical and research setting, with numerus studies performed in adults to enable standardised development of normal values within the healthy adult population to be achieved

(Yingchoncharoen, 2013). Longitudinal change indicates the change in length of the ventricular myocardium along the long axis of the LV, from the basal segment to the apex. Strain rate is the rate at which this deformation occurs. This process produces a negative value in systole and a positive value in diastole (Johnson et al., 2019). Strain is a dimensionless measure of myocardial deformation and is calculated using the formula:

$$\varepsilon = \frac{\Delta L}{L_0}$$

Where Ɛ represents strain and Δ$L$ is the change in myocardial segment length ($L$ - $L_0$), and $L_0$ being the original length of the myocardial segment measured at end-diastole.

### STE and strain/ strain rate of the foetal heart.

In more recent years, there has been an increasing interest in the use of STE for the evaluation of cardiac function and deformation of the foetal myocardium. (Simpson et al., 2018). From 16 weeks gestation, the foetal heart has reached a level of maturation that permits reproducible assessment of myocardial function through advanced imaging techniques, including STE. At this stage, myocardial fibres have begun to align longitudinally, enabling evaluation of both systolic and diastolic performance using functional markers such as GLS (Rychik and Tian, 2016; Van Oostrum et al., 2021). From 16 to 24 weeks gestation the maturation of myocardial deformation patterns coincides with stabilisation of cardiac output, making this window ideal for establishing functional baselines in both normal and high-risk pregnancies (Simpson, 2013). Functional perturbations during this period may be the

earliest indication of underlying pathology, for example coarctation of the aorta may manifest as reduced left ventricular strain despite normal anatomy on structural imaging due to the increased afterload (Rychik and Tian, 2016). Beyond 24 weeks, the foetal heart demonstrates more consistent myocardial contractility and ventricular symmetry (Matsui et al., 2020). GSI which reflects the hearts shape, provides an additional dimension to functional assessment, particularly in conditions with altered loading such as coarctation of the aorta or cardiac failure (GE Healthcare, 2020). Detection of abnormal functional patterns during this stage can inform prognosis and clinical management, progressive strain reduction may indicate cardiac decompensation whereas abnormal GSI values may suggest evolving ventricular remodelling or pressure overload (Abuhamad and Chaoui, 2022)

During foetal life, STE has been utilised in the assessment of global longitudinal strain. From 16 weeks gestation, STE could provide a sensitive method for early detection of subclinical myocardial dysfunction as this tends to become abnormal first and therefore is a sensitive marker for disease, Supporting surveillance and intervention strategies in at risk foetal populations (Simpson et al., 2018).

Normal reference ranges for foetal STE parameters – GLS and GSI have been increasingly reported across gestational age groups. These studies consistently show gestational trends in myocardial deformation and ventricular geometry (Ohira et al., 2020; Huntley et al., 2021; Wang et al., 2021). For GSI which reflects ventricular shape (length-to-width ratio), Wang et al, (2021) provided GSI reference ranges from 1.05 at 17 weeks gestation to 1.18 by 36 weeks. A GSI of >1.1 was considered normal. Huntley et al (2021) also demonstrated similar GSI values.

Recent studies have shown that LV GLS values tend to decrease with increasing gestation. Huntley et al. (2021) reported mean LV GLS values ranging from -23.5% at 16 weeks to -20.1% by 37 weeks, Ohira et al (2020) observed a similar trend across a larger cohort ranging from 18-38 weeks.

RV GLS values follow a comparable but slightly less steep decline with normal values seen higher than those reported for LV GLS. Ohira et al. (2020) reported mean RV GLS values from -25.6% at 18 weeks to -22.3% at term and Huntley et al. (2021) confirmed that RV values consistently exceeded those of the LV throughout.

Unlike M-mode and pulsed Doppler imaging as previously discussed, STE of ventricular chambers is independent of the orientation of the 4-chamber view relative to the ultrasound beam. This reduced dependence on the angle of insonation, which is a key factor in ultrasound imaging, represents a major advantage over alternative techniques, particularly in foetal cardiac assessment. Since STE does not require precise beam alignment to assess myocardial motion, it allows a more reliable evaluation of ventricular function. This is useful as it overcomes the challenges of highly variable foetal position or movement that may limit optimal insonation angles (DeVore et al., 2018; Simpson et al., 2018). The use of STE in congenital cardiology has not been widely studied. One of the earliest studies found on the assessment of congenital heart disease with the use of STE was that of Germanakis et al (2012). This study concluded that myocardial strain was within normal ranges for congenital heart disease that supports a biventricular repair. It was also indicated that in pathologies that would require univentricular pathway, the dominate ventricle revealed strain ratios within normal. Therefore, this could aid in the management and prognosis of these foetuses. Good cardiac function in these pathologies is essential for a successful surgical outcome. Although conclusions looked optimistic and STE

was deemed a potentially useful tool in the progress of myocardial function in foetuses with CHD, this was only a short study over a six-month timeframe with a small cohort. 28 foetuses were included 14 of which had serial echocardiograms totalling 55 studies. The pathologies included were extremely varied, 11 groups in total were included with only a small numbers in each group. Some groups with as little as n = 1 in each. Due to these small numbers, it would be difficult to determine that all CHD for biventricular repair would have a normal myocardial strain; larger numbers of different pathologies would be needed to make this conclusion. Comparisons were made with 144 normal foetuses; these were from the same time period and population. Yet there was no mention of cross matching of gestational age between CHD population and the normal reference ranges. Since the publication of this study, there have been advancements in research in the use of STE in the foetal population. Numerous studies have since reported that STE is both feasible and reproducible in the assessment of cardiac function in the foetal population. For example both Luo et al (2021) and Huntley et al (2021) studies involved small cohort numbers, with a structurally normal heart at 59 and 50 respectively. Huntley (2021) investigated just the normal population whereas Luo et al also included 50 patients with CHD. However, similar to Germanakis et als (2012) study, the CHD cohort in Luo et als (2021) paper were extremely varied with 18 subgroups in total. Many of these subgroups as with Germanakis et al (2012) only had n = 1 case of the differing pathologies. With such low numbers, data derived from the ability of STE analysis on particular pathologies would be difficult to reliably interpret. Table 2.1 details the key studies conducted evaluating the reproducibility and validity of foetal STE parameters.

**Table 2.1** – Summary of published studies reporting the repeatability and validity of foetal GLS and GSI measurements

| Study | Population | Parameter (s) | Key Findings | Repeatability/ Validity outcomes |
|---|---|---|---|---|
| **Di Salvo et al., 2008** | 100 healthy foetuses ( GA 20-32 wks) | LV and RV GLS | 1st validation study in foetal STE. Good inter and intra observer variability | CV <3% and <6% respectively |
| **Krause et al., 2017** | 30 healthy controls | GLS | Evaluated foetal GLS | Described as reproducible across observers, no ICC or CV reported |
| **Luo et al., 2021** | 40 healthy controls<br>20 CHD (TR) | GLS (LV and RV) | Feasible and reproducible in normal cohort | Described as reproducible across observers, no ICC or CV reported |
| **Ohira et al., 2020** | 109 healthy foetuses (18-38 weeks) | GLS (LV and RV) | GLS may be useful in quantifying foetal deformation | ICC >0.9 for all parameters |
| **Huntley et al., 2021** | 50 healthy foetuses (20-38 weeks) | GLS (LV and RV) GSI | Tracked gestational trends for LV/RV GLS and GSI | ICC >0.9 for all parameters; CV not reported |
| **Wang et al., 2021** | 58 healthy foetuses | GSI and GLS | Developed GSI reference ranges (17-40 weeks GA) GSI <1.1 = abnormal | ICC >0.90 for all parameters for inter and intra-observer |
| **Van Oostrum et al., 2022** | 124 healthy foetuses; >500 serial scans | GLS (LV/RV) | Large longitudinal study showing GA STE trends | Repeatability and validity not reported |

Summary of published studies evaluating the reproducibility and validity of foetal STE measurements, including GLS and GSI. Studies report key findings in both healthy and CHD cohorts, where available, repeatability is quantified using ICC or CV.

Day et al (2019) reviewed STE in the foetal heart and agreed that STE is a feasible and reproducible technique in the foetal heart and does have advantages over other methods, such as the ability to assess regional function as well as global function. It was highlighted however that there is a need for more research looking at the effect of foetal cardiac disease on myocardial deformation and the need for normal reference ranges at all gestational age groups. The table (2.2) below taken from Day et als (2019) review and illustrates that STE does have the ability to assess more areas of foetal cardiac function in comparison to alternative methods.

**Table 2.2** – A comparison of the techniques available for the evaluation of foetal cardiac function

| Technique | Systolic function | Diastolic function | Global function | Regional function |
|---|---|---|---|---|
| **M-mode** | Yes | No | Yes | No |
| **Conventional Doppler** | Yes | Limited | Yes | No |
| **Tissue Doppler** | Yes | Limited | Yes | No |
| **Speckle tracking** | Yes | Limited | Yes | Yes |

A comparison of different techniques used to assess foetal cardiac function, evaluating their ability to measure systolic, diastolic, global and regional function. (Day et al, 2019).

## 2.4 Rationale

The following study was designed to assess the feasibility of using STE for the assessment of foetal cardiac function within the clinical setting and to develop normative values from a normal cohort study to enable cut-off values to be developed to better inform patient management. The use of STE analysis in cases of ventricular disproportion, and within a case series of those who are being managed for foetal tachyarrhythmia is a novel contribution to the field.

Currently, STE is not used routinely for the assessment of foetal heart function within our department and its adoption into routine clinical practice nationally remains limited. STE could potentially give a wealth of information on foetal heart size, shape and function through simple assessment of the four-chamber view, which is routinely acquired in all cardiac scans.

## 2.5 Aims and Objectives

**Overall Research Aims**

To determine the clinical value of foetal 2D STE by assessing its reproducibility, reliability, and applicability for evaluating foetal cardiac shape and function using GSI and GLS.

**Overall Research Objectives**

1) **To establish normative data for foetal cardiac geometry (GSI) and myocardial function (GLS) from the four-chamber view of the foetal heart across gestations** – achieved by prospectively analysing four-chamber foetal heart images from 120 normal studies (18 – 37 weeks gestation) using fetal HQ software. GSI, LV GLS and RV GLS will be calculated and used to generate gestation-specific reference ranges and z-scores.
2) **To evaluate the reproducibility and reliability of STE derived GLS and GSI measurements in structurally normal hearts** – achieved by a subset of images being analysed by the same observer (intra-observer) and re-analysed by the second independent observer (inter-observer). Reproducibility will be assessed using intraclass correlation coefficients (ICC) and coefficients of variation (CV) for each parameter.
3) **To assess the utility of STE in detecting obstructive cardiac lesions in foetuses presenting with foetal cardiac ventricular disproportion** – achieved via STE measurements from the disproportion group being compared to gestational age-matched controls. Group differences in GSI and GLS will be analysed statistically and related to postnatal confirmation of obstruction, including cases of coarctation of the aorta.

4) **To explore the use of STE in assessing myocardial function in foetuses diagnosed with tachyarrhythmia** – achieved with the use of STE measurements from the tachyarrhythmia being analysed post arrhythmia (in sinus rhythm) GSI and GLS values will be compared to gestational age-matched controls to assess evidence of myocardial dysfunction.

## 2.6 Hypothesis

Foetal STE can be feasible and reliable within the clinical setting. Information obtained from STE could enable improved diagnostic and prognostic management in ventricular disproportion and arrhythmia.

# Chapter 3 – General Methodology

The study was performed at the University Hospitals of Leicester NHS trust, which is one of the biggest and busiest National Health Service (NHS) Trusts in the country, serving one million residents with increasingly specialist services over a much wider area. Nationally and internationally renowned specialist treatment and services in cardio-respiratory diseases, cancer and renal disorders reach a further two to three million patients from the rest of the country. The trust is spread over three sites with a team of more than 10,000 highly skilled staff from all disciplines. The antenatal clinic is based at the largest of the three sites, the Leicester Royal Infirmary (LRI). The foetal cardiology service at the university Hospitals of Leicester is part of the East Midlands Congenital Heart Centre (EMCHC). The foetal cardiology service at the EMCHC was first established in 2001 and provides a foetal cardiology provision to a large local and regional network. During the year 2021 – 2022, 726 foetal cardiac scans were performed comprising of 344 follow-up patients and 382 new patients. This study was a single-centre prospective cross-sectional observational pilot study. With participants recruited from the foetal cardiology clinic and the foetal medicine clinics at the LRI.

## 3.1 – Ethics

Ethical approval was provided by the East Midlands – Leicester Central Research Ethics Committee (Reference: 22/EM/0265) and validated by the Manchester Metropolitan University Science and Engineering Ethics Review Committee (EthOS ID: 36673). Studies presented herein abide by the latest version of the Declaration of Helsinki,

Written informed consent was obtained from all women who agreed to participate in the study. All participants were provided study information in a written format and

were allowed to ask questions prior to their signed consent. It was made clear that they were eligible to withdraw from the study at any time and that there would be no effect on the standard of care they received should they wish to withdraw.

## 3.2 – Recruitment

Women who were attending for foetal cardiac echo or the foetal Medicine clinic who fulfilled the inclusion criteria were initially approached to participate in the study by the specialists who were carrying out the assessment. These were members of their direct care team. The project was discussed with the patient and a patient information sheet was given. If they decided to participate in the research, a member of the research team then approached the patient to discuss the project further and answer any question they may have had. The patients were given ample time to consider whether they would wish to participate in the study and time to discuss the project and ask any further questions. Those who agreed to participate signed a consent form. Copies of the signed form were filed in the patient's notes and the study site file.

### Normal cohort

Healthy women with a single low-risk uncomplicated pregnancy and normal foetal echocardiogram confirmed at either a foetal medicine clinic or a foetal cardiac clinic were eligible for the study. Participants were excluded if they demonstrated any of the following exclusion criteria: a maternal age of less than 18 years at the time of booking; women with multiple pregnancies or multiple pregnancies but death of one of the twins; cases with confirmed diagnosis of chromosomal problem or genetic problem; and women who were incapable of giving consent. Studies were also excluded if there was poor image quality from the foetal echocardiogram. This was

because poor definition or poor position of the four-chamber view which could result in sub-optimal fetal HQ analysis.

In total, 120 echocardiographic studies were included, derived from seventy-two pregnant women who met the study's inclusion criteria. Some participants contributed measurements at different gestational ages, but not more than one scan performed at any single gestational age per foetus. Therefore while some individuals contributed multiple studies, these were spread across different time points. All included studies were confirmed as normal foetal echocardiograms, either at the foetal cardiac clinic or the foetal medicine clinic, and were subsequently accepted for analysis.

### Disproportion group

The inclusion criteria for the disproportion group focused on individuals presenting to the foetal cardiology clinic at the UHL LRI site with ventricular disproportion, which had been confirmed visually through FE by a cardiac specialist. Only disproportion cases without any additional congenital heart defects were included in the study. Participants were excluded if they demonstrated any of the following exclusion criteria: a maternal age of less than 18 years at the time of booking. Women with multiple pregnancies, or multiple pregnancies but death of one of the twins. Cases with confirmed diagnosis of chromosomal problem or genetic problem. Cases with confirmed foetal diagnosis of a genetic problem. In addition, women who are not capable of giving consent. Studies were also excluded if there was poor image quality from the foetal echocardiogram. This is because poor definition or poor position of the four-chamber view could result in sub-optimal fetal HQ analysis.

### Tachyarrhythmia group

The inclusion criteria for the tachyarrhythmia group focused on individuals presenting to the foetal cardiology clinic at the UHL LRI site with foetal cardiac tachyarrhythmia, which had been confirmed through FE by a cardiac specialist. Only tachyarrhythmia cases without any additional congenital heart defects were included in the study. Each of the ladies were referred to the foetal cardiac clinic at the Leicester Royal Infirmary (LRI) from the university hospitals of Leicester or the surrounding network due to detection or suspicion of a foetal cardiac tachyarrhythmia. A complete foetal echocardiogram was performed in all cases on first presentation following the BCCA foetal cardiology standards (BCCA, 2021) and the Fetal Anomaly Screening Programme (NHS England, 2024). The echocardiogram was performed in order to confirm the cardiac rhythm and to assess for any cardiac structural abnormality. Confirmation of a foetal tachyarrhythmia was confirmed in each case with the use of foetal echocardiography using both M-mode, Doppler and 2D imaging. There was no structural abnormality detected in any of the cases. Follow-up of each patient was then based on clinical findings and treatment indication.

Participants were excluded if they demonstrated any of the following exclusion criteria: a maternal age of less than 18 years at the time of booking. Women with multiple pregnancies, or multiple pregnancies but death of one of the twins. Cases with confirmed diagnosis of chromosomal problem or genetic problem. Cases with confirmed foetal diagnosis of a genetic problem. And women who are not capable of giving consent. Studies were also excluded if there was poor image quality from the foetal echocardiogram. This is because poor definition or poor position of the four-chamber view could result in sub-optimal fetal HQ analysis.

Each case had at least two echocardiograms during the course of the pregnancy and once the heart had reverted back into sinus rhythm they remained frequently monitored via echocardiography and midwife assessment. On the examinations performed where the foetal heart was found to be in sinus rhythm the fetal HQ software was used in order to GSI and GLS of both the left and the right ventricle. Fetal HQ was acquired on at least two studies post tachyarrhythmia for each patient. It was confirmed via echocardiography that each foetus was in sinus rhythm at the time of analysis with foetal heart rate in all cases between 114bpm and 150bpm with a mean heart rate of 136bpm.

## 3.3 – Eligibility Criteria

Pregnant women aged 18 years and over with a singleton viable pregnancy were invited to participate in the study, if they fulfilled all of the study criteria listed below. The inclusion and exclusion criteria are detailed below.

**Inclusion criteria**

Inclusion criteria was set as pregnant women aged 18 years and over who carried a singleton viable pregnancy and were willing and able to consent to be included into one of the following study groups:

- Group I: Normal foetal heart - gestational age matched control
- Group II: foetus with ventricular disproportion
- Group III: foetal arrhythmia requiring therapy

**Exclusion criteria**

- Maternal age less than 18 years at the time of study
- Multiple pregnancies including twins

- Women with multiple pregnancies but death of one of the twins
- Cases with confirmed diagnosis of chromosomal problem
- Cases with confirmed diagnosis of genetic problem
- Women who are not capable of giving consent
- Women with learning disabilities/difficulties
- Prisoners
- Any others deemed to be in the vulnerable group (e.g. mental health condition)
- Poor image quality from the foetal echocardiogram
- Unwilling to consent

**Size of sample:**

The sample size for this study was determined based on a power calculation derived from a previous study by Gozar et al., (2021), assessing GLS in cases of coarctation of the aorta. The study reported an averaged effect size of 0.31 in comparisons between coarctation of the aorta and healthy controls. Assuming a similar effect size a total sample size of 194 was calculated to achieve a statistical power of 95% with an alpha level of 5% across the study groups. This calculation indicated that 32 participants were required in each group. However, due to time constraints and referral limitations, 30 participants were ultimately recruited for each gestational age group for the normal cohort,

- Group I: Normal foetal heart - gestational age matched control (120 subjects) group see table 3.1
- Group II: foetus with ventricular disproportion (30 subjects) – 16 recruited

- Group III: foetal tachyarrhythmia requiring therapy (30 subjects) – 7 recruited

**Table 3.1 – Normal foetal heart – Gestational age groups**

| Group number | Gestational age (weeks) | Study number (n) |
|---|---|---|
| **I** | 19 – 23 | 30 |
| **II** | $23^{+1}$ – 28 | 30 |
| **II** | $28^{+1}$ – 32 | 30 |
| **IV** | $32^{+1}$ – 37 | 30 |

A display of the subdivided groups for the normal cohort (gestational age matched control - group). Sample size was based on a power calculation between coarctation of aorta and healthy controls from Gozar et al., (2021) which revealed an averaged effect size of 0.31. Assuming a similar effect size in this study, a total sample size of 194 will be required to determine an alpha of 5% with 95% power between the 6-study groups .This indicated a sample size of 32 in each group. However, due to time constraints and referral numbers 30 subjects were recruited for each gestational age group.

## 3.4 – Instruments

A Voluson E10 colour Doppler ultrasound system and a Voluson expert 22 colour Doppler ultrasound system (GE Healthcare) equipped with a Foetal HQ quantitative analysis software package were used. Transducer selection was either the GE Healthcare C2-9-D broad-spectrum convex transducer which has a bandwidth of 2.3 – 8.4 MHz or the GE C1-6-D XD clear broad-spectrum convex transducer which has a bandwidth of 1-6 MHz In order to maintain as higher frame rate as possible, the higher frequency transducer was always selected in the first instance and the C1-6-D XD transducer was only selected if image optimisation was not optimal with the C2-9-D transducer.

## 3.5– Fetal Heart Quantification, (Fetal HQ) practical methods.

Fetal heart quantification (fetal HQ) is an advanced diagnostic tool that uses STE to assess the size shape and contractility of the foetal heart from the four-chamber view. Fetal HQ works by obtaining high-resolution 2D ultrasound images of the 4-chamber view of the foetal heart. This view allows detailed assessment of the hearts chambers. One of the key features of fetal HQ is its GSI, which automatically calculates the foetal hearts size and shape. This helps to identify abnormalities in the hearts geometry such as cardiac remodelling or asymmetry that could indicate potential issues such as congenital heart defects. Fetal HQ also evaluates ventricular function of the foetal heart by tracking the movement of the myocardium in end-diastole and end-systole via real-time ultrasound frames. Fetal HQ has the ability to divide the foetal heart into distinct segments for detailed assessment. This allows for a detailed view of individual regions such as the left and right ventricles, this segmented approach enhances the ability to detect regional dysfunction (GE HealthCare, 2020; GE HealthCare, 2020). Use of the fetal HQ quick guide (appendix 1) and the fetal HQ consensus guideline (GE Healthcare, 2020) (appendix 2) were used to ensure accurate acquisition, optimization and quantification of the foetal heart. A guide sheet was created for the purpose of this study and for future use with all the required information condensed into one “how to guide” adapted from the guidelines created by GE HealthCare, 2020 (appendix 3).

### Acquisition of the 4-chamber view

The four-chamber view is obtained via a transverse section of the thorax. It is vital that the correct technique is used for obtaining the four-chamber view before any detailed analysis can be carried out. A round shape to the thorax and one complete

rib in the image demonstrates the correct plane for the four-chamber view. If multiple ribs are seen then the image obtained is oblique. The correct level within heart for assessment is when the four-chamber view shows the crux (centre) of the heart. If the coronary sinus is seen then the level is too low, if the LVOT can be imaged then the level is too high within the heart (Allan et al., 2009). Figure 3.1 illustrates the optimum image required for detailed analysis with fetal HQ.

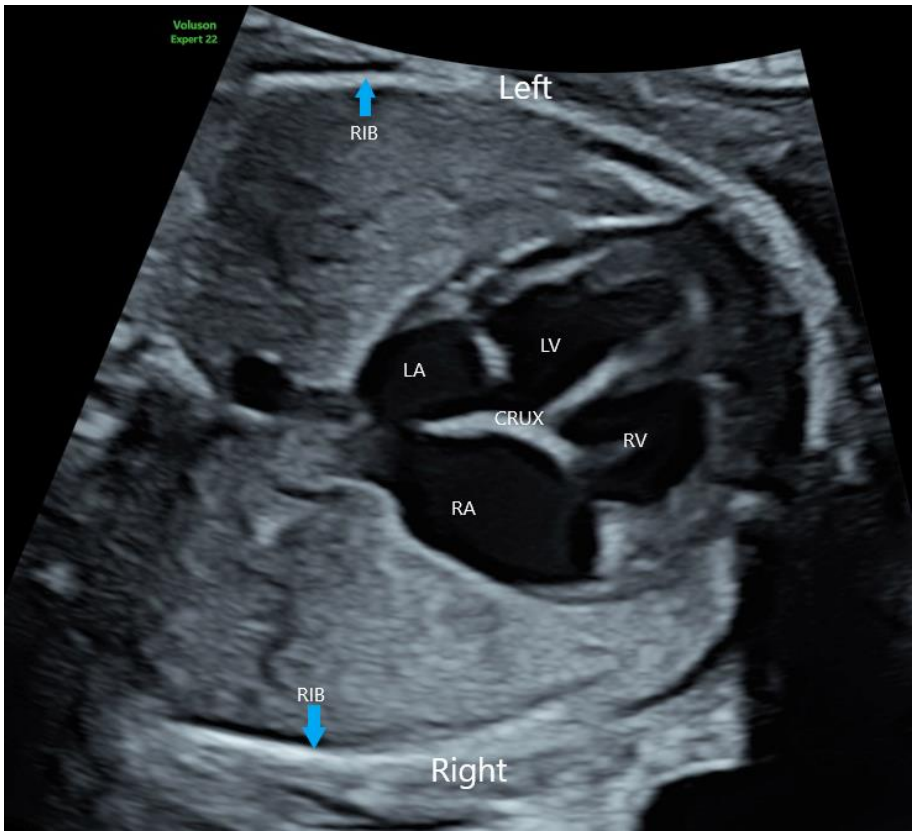


**Figure 3.1**: Correct acquisition of the four-chamber view of the foetal heart, for fetal HQ. This image shows the required four-chamber view. The Left atrium (LA), left ventricle (LV), and the right atrium (RA) and right ventricle (RV) can been clearly identified. The thorax can be seen as a round shape, one rib can be observed both sides demonstrating that the orientation is not oblique and the crux of the heart is clearly visible illustrating that the level of the four-chamber view is correct. (Image obtained with consent)

### Image optimisation

Once the position of the four-chamber view has been confirmed then image optimisation is vital. The use of the cardiac pre-set with the harmonics set to either mid or low is recommended with a narrow angle and low depth selected. A frame rate of ideally above 80Hz is recommended for detailed analysis. The heart should be located centrally within the chest with the septum horizontal either at three or nine o clock position or up to ±45º from horizontal within the green planes as indicated on Figure 3.2 below. A two to three second video clip is proposed for optimal analysis. It is best that images obtained are done so in the absence of foetal and respiratory movements, and the ideal heart orientation is with the left ventricle and the right ventricle in a clockwise position. However, when this was not possible the use of the flip modality can be utilised. Flipping the image to allow for correct orientation does not have an effect on any of the measurement data.

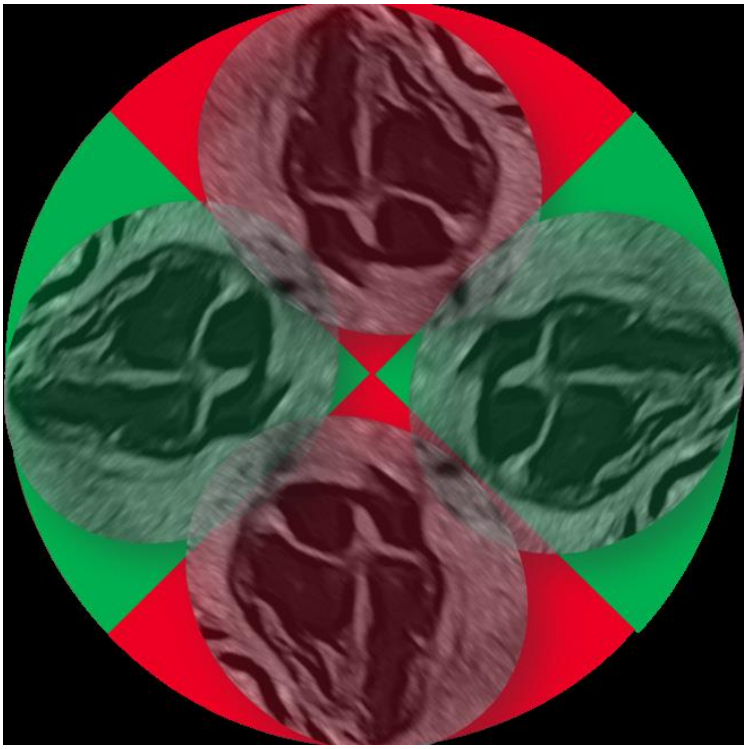

**Figure 3.2**: Example of the 4-chamber view position required for optimal fetal HQ analysis. The image illustrates the optimum position of the four-chamber view required for accurate analysis with use of the fetal HQ software. The orientations marked in green demonstrate the preferred positions required. The orientations marked in red are not ideal for fetal HQ analysis. (GE HealthCare, 2020)

### Global Sphericity Index (GSI) Measurement

Global sphericity index (GSI) is a measurement that is used to evaluate the morphology of the heart. GSI is obtained by dividing the total basal – apical longitudinal length to the transverse width of the four-chamber view at end-diastole. The ratio can then be used as a judgment of the overall deformation and movement of the ventricles and permits an assessment of cardiac shape. If the GSI ratio is lower than 1.1 then overall cardiac shape is considered abnormal (Wang et al., 2021). It is important that precise measurements of the foetal heart be obtained to allow an accurate measurement of the GSI ratio. Once the correct cardiac four-chamber view has been obtained, the clip will then be recalled with the operator

scrolling to the end diastolic frame. Fetal HQ is selected from the touch panel in the measurements section on either the Voluson E10 or the Voluson Expert 22 ultrasound machine. Global size and shape study is chosen on the control panel and measurement of the length and width of the heart is obtained. It is important that this measurement be taken in end-diastole and epicardium to epicardium. The 4-chamber length is obtained via epicardium from apex parallel to the ventricular septum to epicardium between the right and the left atrium, outside of the atrial septum. The transverse width measurement is obtained with points set from epicardium to epicardium on the widest diameter, perpendicular to the septum (GE HealthCare, 2020; GE Healthcare, 2020). Figure 3.3 illustrates the positions required for accurate measurement of GSI.

**A**

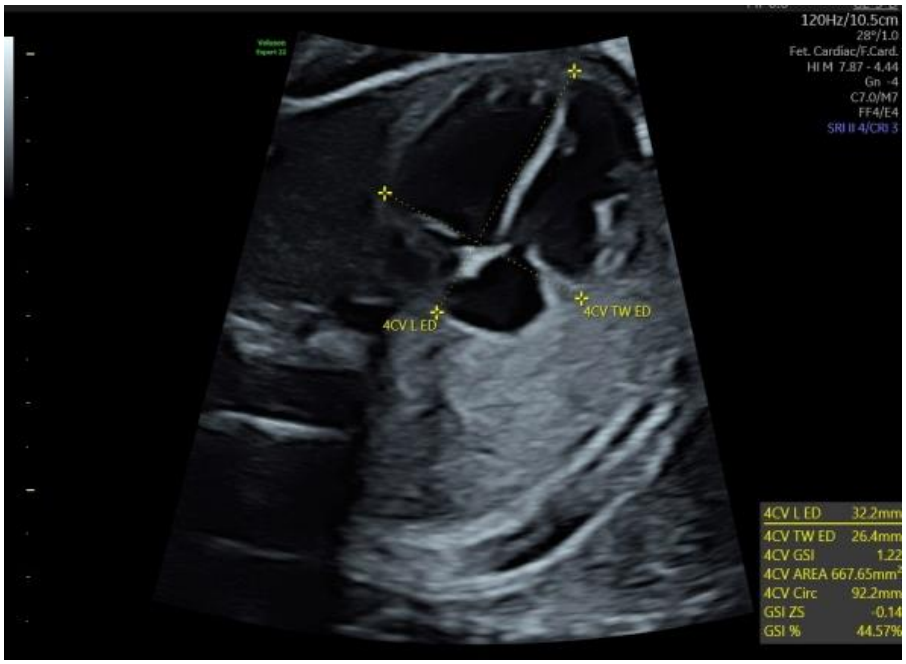


**B**

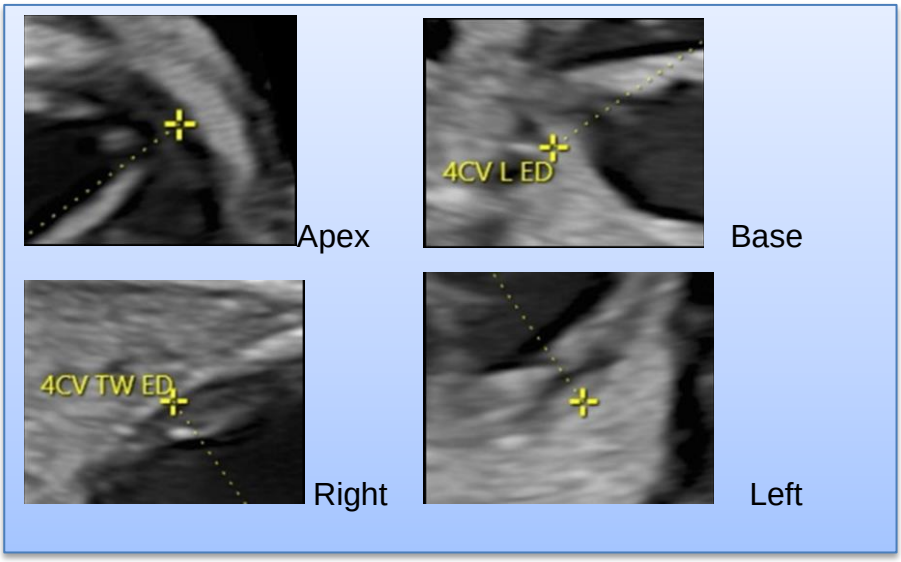


**Figure 3.3**: the images indicate the required positions for accurate measurement of GSI. Image A, shows foetal heart in end diastole where the AV valves are closed. 4CV is measured from epicardium to epicardium in length and width. Image B – indicates the epicardium in all four measurements required for GSI measurement. Image B adapted from GE Guidelines and GE consensus (GE HealthCare, 2020; GE HealthCare, 2020).

## Analysis of ventricular shape and contractility including Global longitudinal Strain (GLS).

### Step 1 – Define orientation

To assess the ventricular shape and contractility of the foetal heart using the fetal HQ software, the ventricles need to be orientated in a specific way. The left ventricle should be on the left if apex is up and the left ventricle should be clockwise before the right ventricle. If not, then the image needs to be flipped using the function on the touch panel. This is demonstrated in Figure 3.4. Correct orientation is important as it allows for the correct display of ventricular graphics at the end of the study. It is also important to note that flipping the image does not result in any impairment to the measurement data

A

B

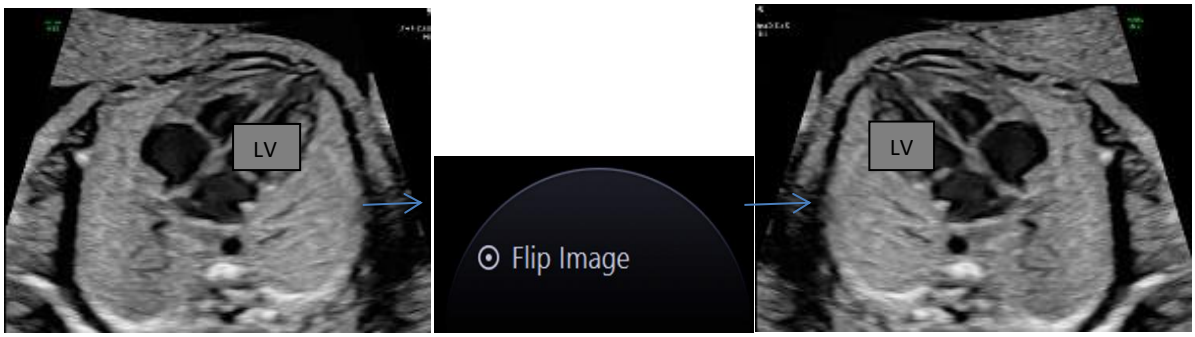


C

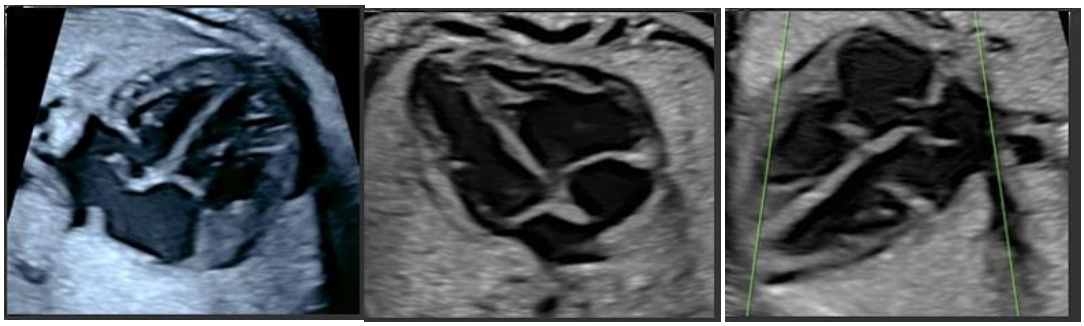

D

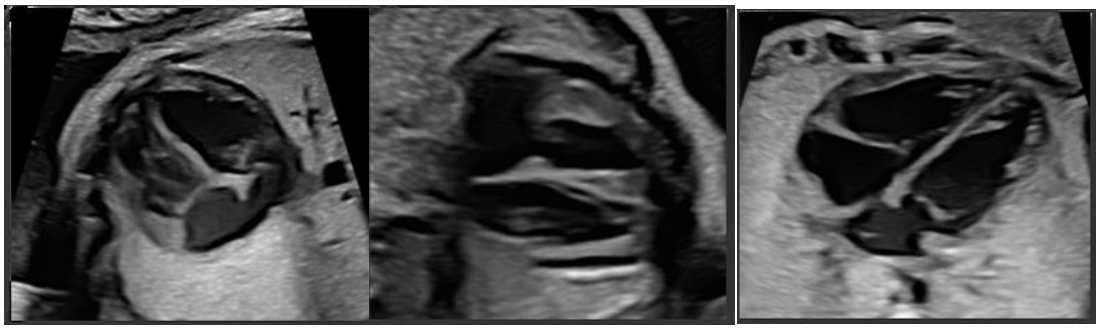

**Figure 3.4**: demonstrates the correct orentation of the left and right ventricles for the assessment of ventricular contractility. Image A shows the LV on the wrong side, the use of the flip button oriantates the LV in a clockwise position to the RV as shown in image B. The correct orentation can been seen in C with D indicating the unaccactable positions. (Adapted from GE HealthCare 2020, and GE HealthCare, 2020)

**Step 2 – Select one cardiac cycle**

Once correct orientation of the heart has been obtained, a complete cardiac cycle will need to be acquired. As there is no foetal electrocardiogram (ECG), the cardiac cycle is determnied via the use of M-mode. The M-mode line is drawn in order to identify end-systolie and end-diastole as shown in Figure 3.5 image A. The M-mode line can be drawn either along the free wall annulus, the centre of the valve or across the ventricles. The main objective is that a clear tracing is attained for the identification of end systole and end diastole. It is important that the M-mode obtained is free from maternal breathing or foetal movement as this will elemenate any drifting of the trace. Figure 3.5 Image B demonstrates the optimal M-mode required for adequate cardiac cycle. An example of drift of the M-mode tracing is illustrated in Figure 3.5 Image C.

A

B

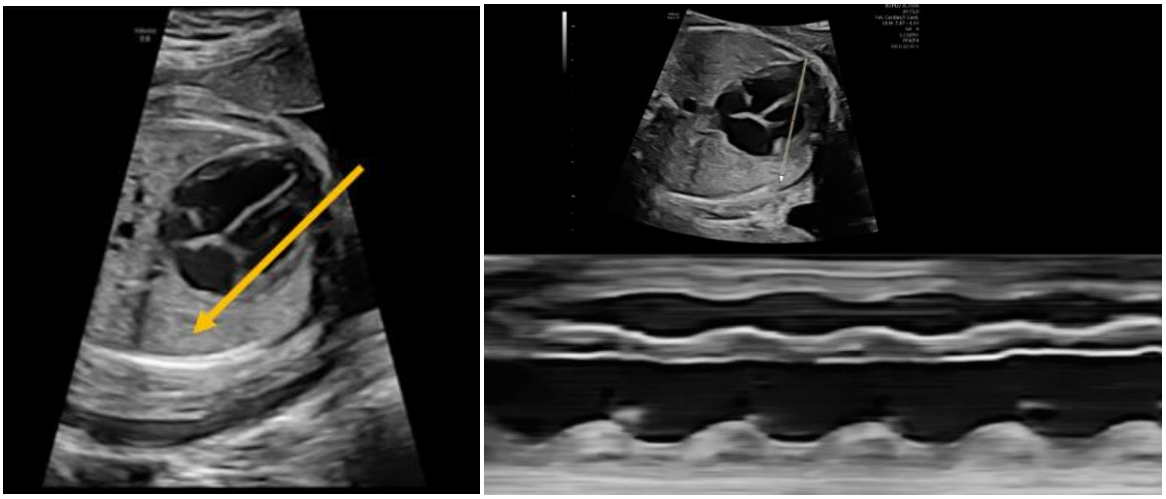

C

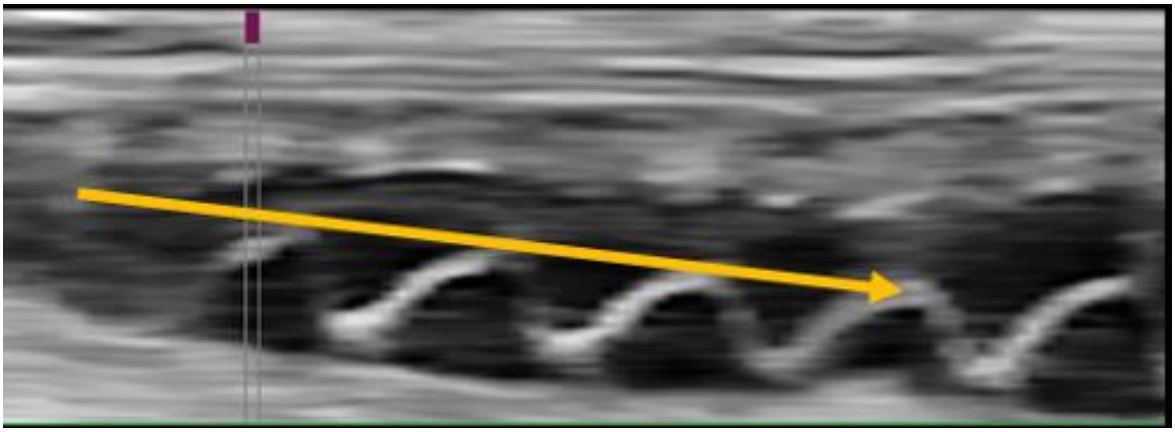

**Figure 3.5**: demonstrates the correct M-mode needed for obtaining the cardiac cycle. Image A indicates the position of the m-mode. It is vital that the m-mode obtained is free from maternal breathing or foetal movements as illustrated in Image B. If there are foetal movements or maternal breathing then the m-mode can drift as shown in image C. (GE HealthCare, 2020).

**Step 3 – Record the cardiac cycle**

Once the correct M-mode recording has been obtained, then the cardiac cycle can be recorded. This is done by selecting end diastole at either end of the cardiac cycle by using the trackball to move along the M-mode trace as shown in Figure 3.6 below. Arrows 1 and 2 on Figure 3.6's panel B demonstrate the points of end-diastole in one cardiac cycle. Once the end-diastole points have been obtained, the selecting of end systole between the two points already made can be obtained as shown in Figure 3.6's panel B illustrated by arrow 3 below. Whist marking out end-diastole and end-systole, it is advisable to watch the 2D image as well as the m-mode to identify accurate positions from the frames.

**A**

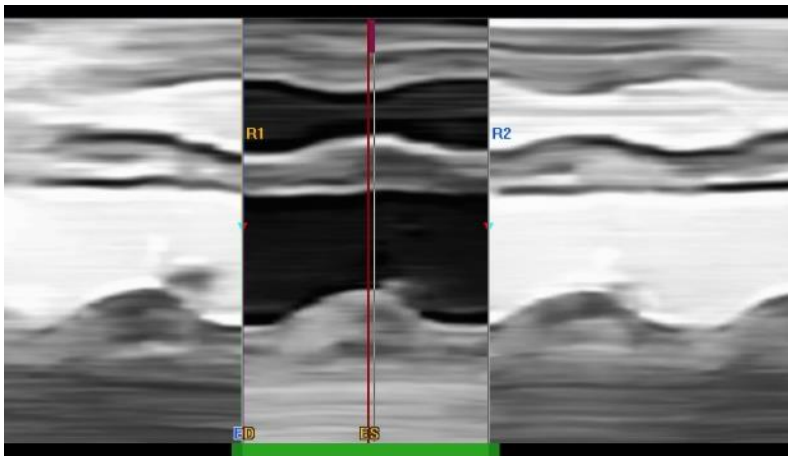


**B**

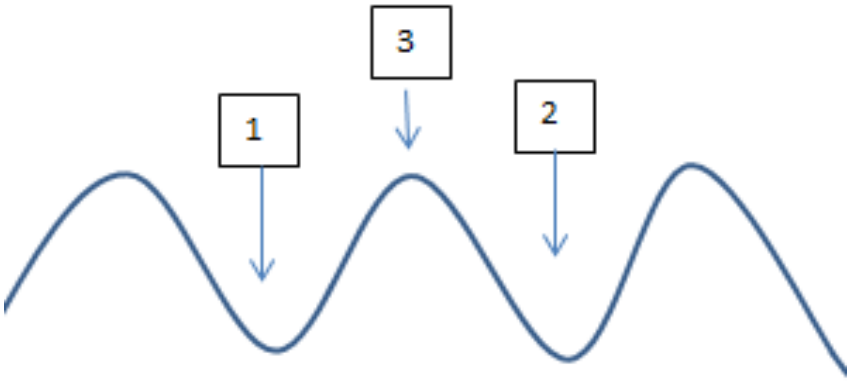


**Figure 3.6**: Correct positions of end-diastole and end-systole to obtain one complete cardiac cycle**.** Image A illustrates the cardiac cycle chosen using m-mode with both end-diastole and end-systole marked. End-diastole is shown via arrows 1 and 2 on image B with end-systole demonstrated via arrow 3. (Image obtained with consent)

**Step 4 – Define end-systolic and end-diastolic endocardial tracing**

Once the cardiac cycle has been selected, the chosen cycle will appear in end-systole. Then the left and the right ventricles can be traced in order to obtain data on the ventricular size and function. In order to accurately trace the left ventricular endocardial border in systole, three initial points must be located. These include the septal mitral valve insertion, the lateral mitral valve insertion and the apex. These points are illustrated in Figure 3.7 represented by the red dots. Once the three anchor points have been selected, then the trace line will appear along the endocardium. This trace line can be adjusted manually to align with the endocardium by either adjusting the anchor points (red dots) or by fine-tuning the trace line (small blue dots). Once the trace has been approved, a proposed trace of the endocardium in end-diastole will appear. This trace can either be confirmed or adjusted as needed. Once the left ventricular endocardial border has been confirmed in both systole and diastole, the tracing can be accepted and the results will be displayed on the results screen as shown in Figure 3.8. The steps can then be repeated for the definition of the endocardial border for the right-ventricle. The initial markers will be in the septal tricuspid valve insertion, the lateral tricuspid valve insertion and at the right ventricle's apex. As with the left ventricle, these points can then be modified to align with the endocardial wall if required. Once the right ventricle has been approved and accepted then the results will also show on the same page as illustrated in Figure 3.8.

**A**

B

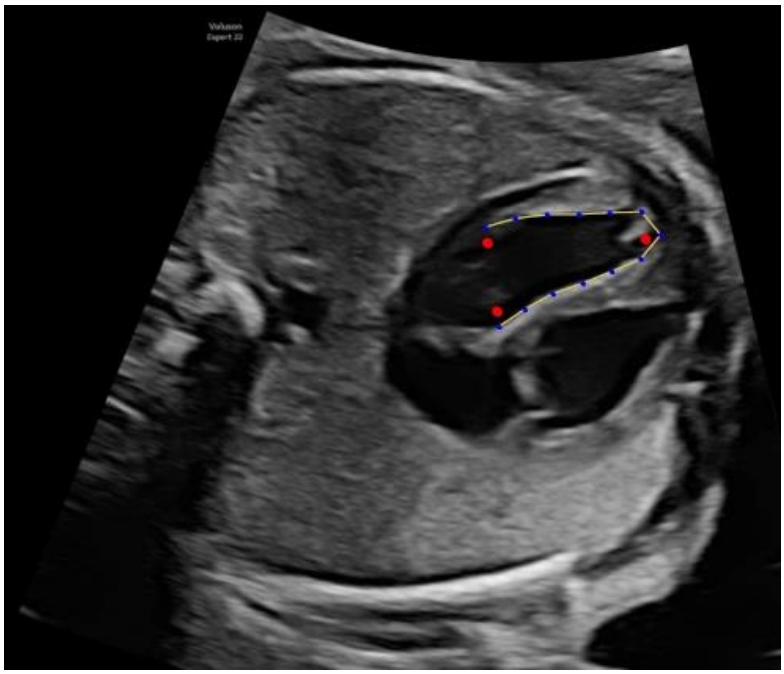

**Figure 3.7**: accurate definition of the LV endocardial tracing in end-systole and end-diastole. Image A illustrates the tracing of the endocardium in systole, the red dots show the three initial markers made in the septal, lateral and apical endocardial wall of the ventricle. Each marker is adjustable to enable accurate definition of the endocardium. Image B shows the automated tracing of the endocardium in diastole. (Image obtained with consent)

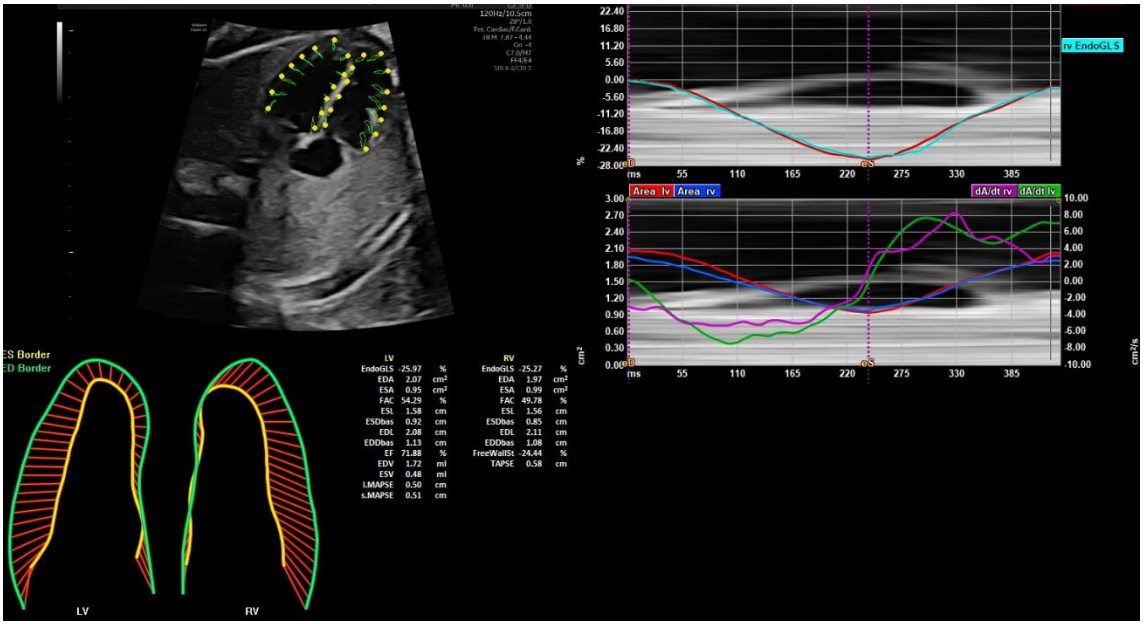


**Figure 3.8**: the fetal HQ results page. The image can be seen in 2D and is recorded as a cine loop. The endocardial tracing can be identified in the lower trace with the green line representing diastole and the yellow line representing systole. The red lines are the 24 segments. The graphs depict LV and RV GLS over time. (Image obtained with consent)

## 3.6– data processing, analysis.

Either a cardiac specialist sonographer, foetal cardiac consultant or a foetal medicine consultant as part of the routine foetal cardiac scan obtained the four-chamber view for the data analysis. A study protocol detailing image optimisation and acquisition was given to all members of the research team highlighting the importance of an optimal four-chamber view. Once the image had been obtained, data analysis was completed using either the Voluson E10 colour Doppler ultrasound system or on the Voluson E22 colour Doppler ultrasound system (GE HealthCare, 2020). Each system is equipped with a fetal HQ quantitative analysis software package. A single specialist foetal cardiac sonographer (CB) with experience in the fetal HQ software performed analysis and who had already performed analysis in over 50 studies.

Once the results were obtained, they are displayed on the ultrasound screen as shown in Figure 3.8. There are numerous measurements that can be obtained from the fetal HQ software. However, for the purpose of this study, the data analysed included GSI and GLS of both the left and the right ventricle. The extrapolated data was given a study number for pseudo-anonymisation and inputted onto a Microsoft Excel 2010 data spreadsheet stored on password protected trust computer.

## 3.7 – statistical analysis

The data and statistical analysis were conducted using Microsoft Excel 2016 and IBM SPSS (version 19).

### Intra-user variability and reproducibility analysis (chapter 4)

In order to assess intra-user variability, fifteen studies were chosen at random from the control group of participants for test (test 1) vs. retest (test 2) comparisons. Gestational age range was 20+3 weeks to 35+6 and maternal age range was 21 years to 36 years with a mean age of 29 years. Data for test 1 and test 2 were collected two weeks apart from the same study by the same examiner for all variables. To assess Inter-user variability and reproducibility, 15 studies were chosen at random and analysis was carried out by two experienced sonographers on the same study at separate occasions. Method error (ME), coefficients of variation (CV), and intra-class correlation (ICC) were calculated to assess intra-user reproducibility. ME, CV and ICC were also calculated for GSI, LV GLS and RV GLS.

### Normative ranges (chapter 4 )

From the 120 scans normal reference ranges were obtained for the entire population with a mean value calculated using the formula mean = $\sum x$ / N (the sum of all data values divided by the number of data values). Standard deviation (SD) for the mean

values was calculated. The data were divided into the four groups of gestational age and was collated for analysis; means were calculated for each group along with SD and 95% confidence intervals. To standardise and compare values within the datasets, individual Z-scores were calculated across the different gestational age groups using Microsoft Excel 2016 as Z-Score = (Data Value – Mean) / SD. Data value is the individual value of the GSI or GLS and mean is the mean value of the entire dataset and the SD is the SD of the data set. In this analysis, Z-scores near +2 or -2 were used as key thresholds. The same formulas and calculation methods were applied in all datasets to ensure consistency.

Spearman's rank correlation analysis was conducted to evaluate the relationship of GSI, LV GLS and RV GLS against gestational age. To compare the LV and RV GLS values across the gestational age range a Shapiro-Wilks test was first conducted to assess distribution of data. Based on the results of data distribution analysis, a Wilcoxon signed rank test was used.

A P-value of < 0.05 was considered statistically significant.

### Ventricular disproportion and Tachyarrhythmia group (chapter 5 and 6)

The data and statistical analysis were conducted using Microsoft Excel 2016 and IBM SPSS (version 19). Descriptive statistics including the mean and SD were used to summarise all data sets. The normality of the data distribution was assessed using the Shapiro-Wilk test. As the data did not meet the assumptions for parametric testing, the Mann-Whitney U test was used to compare differences between groups. A significance level of P < 0.05 was considered statistically significant. Effect size was calculated for the disproportion and the tachyarrhythmia groups compared to the control group using the formula$r = \frac{Z}{\sqrt{\{N\}}}$. Z-scores were calculated for each positive

disproportion and tachyarrhythmia case using the mean and standard deviation of the control group as the reference. The Z-scores were derived using the formula Z-Score = (Data Value – Mean) / SD). To compare the false positive and false negative values within the disproportion group a Shapiro-Wilks test was first conducted to assess distribution of data. Based on the results of data distribution analysis, a Wilcoxon signed rank test was used.

# Chapter 4 – Foetal Speckle Tracking in the clinical setting, feasibility and normal values.

## 4.1 – Introduction

When FE was first introduced, its primary use was for the detection of congenital heart disease (CHD) (Day et al., 2019). However, with functional echocardiographic techniques being adapted from postnatal and adult scanning and ultrasound machines and software improving, the assessment of foetal cardiac function has become an integral part of the foetal heart examination (Day et al., 2019; Rocha et al., 2019 and Crispi and Gratacos, 2012). The accurate assessment of foetal cardiac function has become increasingly important in the diagnosis and prognosis of not just cardiac conditions but also non-cardiac diseases such as foetal growth restriction or maternal diabetes (Van Ostrum et al., 2022). Information from foetal heart functional assessments can also be extremely useful for the clinical management of pregnant women with foetal cardiac conditions such as foetal arrhythmias and/or congenital heart disease (Rocha et al., 2019). As discussed in Chapter 2, there are many techniques available to assess the function of the foetal heart such as 2-Dimensional imaging (2D), m-mode imaging and Doppler derived techniques. Yet there is still no consensus on the preferred method to be used in the evaluation of cardiac function despite its importance in the foetal heart examination (Rocha et al., 2019). This is in part due to the challenging nature of the assessment of foetal cardiac function. Functional assessment of the foetal heart is difficult due to the small size of the foetal heart and the highly mobile foetus. Foetal position can also be unpredictable which makes optimal image acquisition difficult (Day et al., 2019 and Crispi & Gratacos, 2012).

Foetal cardiac function is expected to change during pregnancy due to the physiological growth and development of the heart and the changes in loading conditions with advancing gestation (Germanakis et al., 2012); therefore, reference

ranges require adjustment for gestational age or size (Day et al., 2019.) Numerous studies have assessed these established techniques within the clinical setting (Simpson, 2004; DeVore, 2005; Godfrey et al., 2012 and Rocha et al., 2019) and many papers have produced normal values and reference ranges for the differing conventional modalities of assessing the function of the foetal heart (Carvalho et al., 2001; Koestenberger et al., 2009, Cruz-Martinez et al., 2012 and Peixoto et al., 2020). However, these conventional techniques remain variable and limited, due to being angle dependent and therefore reliant on suitable foetal lie and skill of the sonographer (Day et al., 2019). An additional challenge to the assessment is that dysfunction of the foetal heart is essentially a sub-clinical finding (Hatem et al., 2008). Clinical indication of cardiac failure, such as with hydrops or valvular regurgitation although being rare, is often associated with a poor prognosis for the foetus. Early indication of cardiac dysfunction therefore could potentially aid in the management and prognosis of the foetus.

Over recent years, STE has emerged as a promising tool in the assessment of cardiac function. It is a relatively new technique first described in the adult population by Leitman et al (2004). Global longitudinal strain is obtained via STE. It obtains information on heart contractility by measuring the change in the length of the heart's muscle (deformation) during one cardiac cycle (Day et al., 2019). GLS strain rate is gained by measuring the maximal shortening of the myocardium longitudinal length during systole and is compared to the resting longitudinal length in diastole. It has been stated that STE has advantages over alternative methods of functional assessment. It has been considered less angle dependent than conventional methods, allowing a more flexible approach to image acquisition than m-mode or Doppler derived techniques (Barker et al., 2009). Such an approach if accurate

presents significant advantages in determining foetal cardiac dysfunction in a clinical setting. However, a recent study by Semmler et al (2020) argued that GLS was not angle-independent and that the angle of insonantion did in fact alter the GLS significantly. This study concluded that consideration must be taken when comparing studies with different acquisition protocols when forming normal values for GLS.

Over the years, there has been contradicting data from studies performed in the assessment of normal reference values for GLS with the use of speckle-tracking echocardiography. Van Oostrium et al., (2020) comprised a table illustrating the results found from twenty-three studies over an 8-year period between 2011 and 2019. The results of this review showed highly variable results between the different studies for the normal reference ranges for GLS. It was concluded that more data collected in a standardised manner was needed across gestational ages to produce reliable reference ranges for foetal GLS.

The fetal HQ software also allows the calculation of the global sphericity index (GSI). GSI is a ratio used to quantify the sphericity or the overall shape of the foetal heart. GSI of the four-chamber view is calculated by dividing the end-diastolic basal-apical length by the end-diastolic transverse width. (DeVore et al., 2017; Devi et al., 2023). In foetal echocardiography, the GSI is used to evaluate the shape of the foetal heart. A perfectly spherical shape would have a GSI value of 0 whereas deviations from that would indicate a more elliptical shape or abnormal shape. A lower GSI would suggest the remodelling of the heart from an elliptical to a spheroidal shape, which could be an indication of the dilatation of the whole foetal heart. (Li et al., 2024). Changes in cardiac sphericity may be an indicator of sub-clinical cardiac dysfunction (Sehgal et al., 2016). Limited studies have been performed in this field. However, previous studies investigating the use of GSI in both cardiac and non-cardiac

conditions have revealed abnormal cardiac sphericity conditions (Crispi et al., 2008; Perez-Cruz et al., 2015; DeVore et al., 2020). Nevertheless, small cohort numbers has limited these studies. Additionally, most studies have not adequately accounted for gestational age, a critical factor that may influence foetal cardiac shape and function. To date, no research has systematically evaluated or established normal reference values for GSI in relation to gestational ages.

## 4.2 – Aims and Objectives

The aim of this study is to assess the feasibility, reliability and reproducibility of STE in the clinical setting. Fetal HQ software can be used for the assessment of foetal cardiac size using the global sphericity index (GSI). Cardiac function can also be assessed with the use of left ventricular and right ventricular global longitudinal strain (GLS). The purpose of this study was to investigate the applicability of the fetal HQ software in the clinical setting and to examine reproducibility and reliability of measures. Study's further aim was to produce reference values for foetal cardiac size (GSI) and foetal cardiac contractility (GLS) of both the left and right ventricles in healthy foetuses across gestational age groups 19 weeks – 37 weeks.

## 4.3 – Materials and Methods

The methods and materials underpinning the analysis presented in this chapter are detailed in Chapter 3. This includes information on ethics, patient selection and recruitment, instruments used, data acquisition and STE echocardiography technique for the fetalHQ software. Information on data and statistical analysis is detailed in chapter 3.7.

## 4.4 – Results

Maternal age range was between 18 to 43 years with a mean maternal age of 30.4 years (SD ± 6.3 years). Figure 4.5 demonstrates the distribution of maternal age across the entire normal population (n 72).

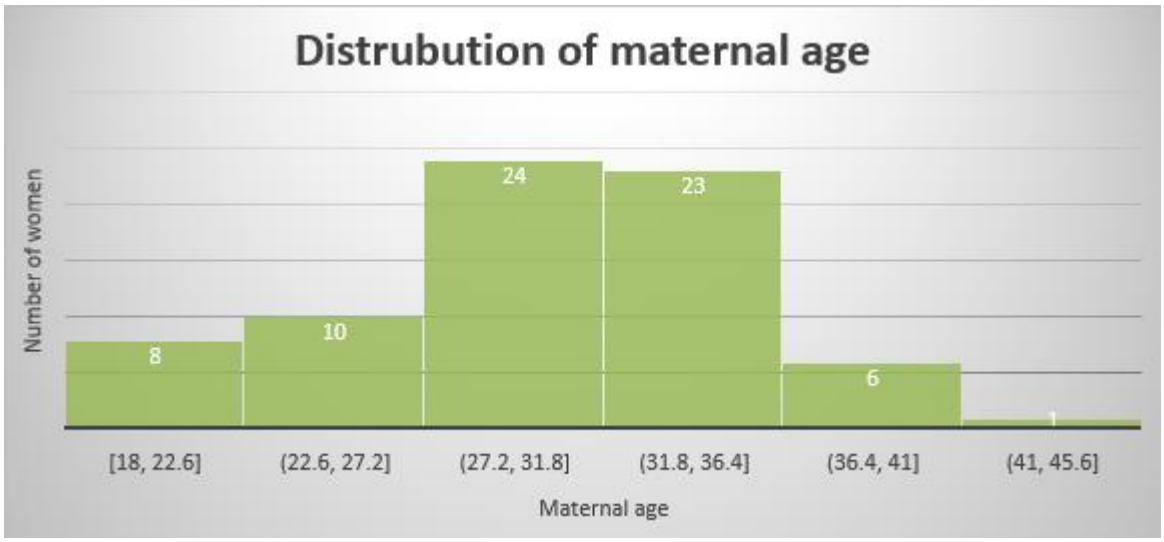


**Figure 4.1:** Histogram showing the distribution of maternal age among all study participants (n 72). The mean maternal age was 30.4years with SD ±6.3years. Age groups are displayed in 5-year intervals.

Of the seventy-two study participants recruited, 77.8% of the Women recruited were White British (n 56), 9.7% were White Other (n 7), Indian and Asian each made up 5.6% (n 4) of the total population, with 1.3% (n 1) being classified as other ethnicity. (Figure 4.2)

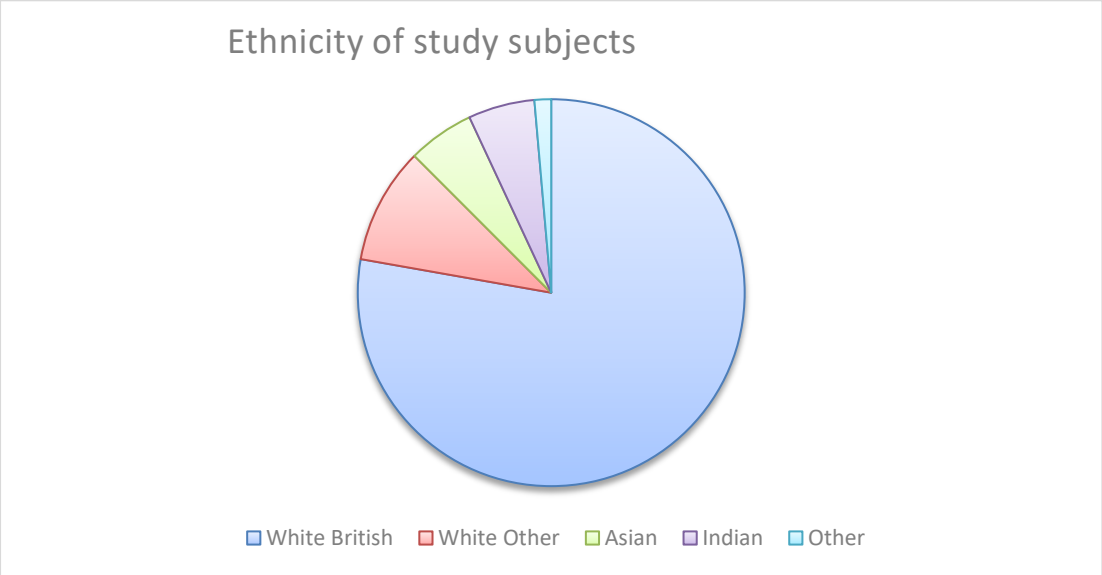


**Figure 4.2:** Pie chart illustrating the ethnicity distribution of study participants (n=72). The majority were white British (77.8%), followed by white other (9.7%), Indian (5.6%), Asian (5.6%) and other ethnicity (1.3%).

The gestational age ranged between 19 weeks and $36^{+2}$ weeks. Study population was then subdivided into four gestational age groups consisting of thirty studies per sub-group: group one consisted of gestational age range of 19 weeks to 23 weeks, group two was gestational age of $23^{+1}$ to 28 weeks, group three consisted of gestational age range of $28^{+1}$ weeks – 32 weeks and the final group was gestational age range of $32^{+1}$ weeks – 37 weeks. The mean and SD of each GA subgroup are presented in Table 4.1.

**Table 4.1 –** Mean and SD GA for control group

| Gestational Age range (weeks) (n=30) | Mean (weeks + Days) | SD (weeks) |
|---|---|---|
| **19 – 23** | 21+3 | ± 0.94 |
| **23.1 – 28** | 25+5 | ± 1.4 |
| **28.1 – 32** | 30+1 | ± 1.24 |
| **32.1 – 38** | 34+1 | ± 1.2 |

Summary of gestational age subgroups in the control population (n=120). Participants were divided into four GA groups, each comprising 30 studies. The table presents the GA range for each group, alongside the corresponding mean GA (in weeks + days) and SD.

Table 4.2 presents the data obtained from the measurements conducted to assess the reliability and reproducibility of GSI and LV and RV GLS values. The GSI values showed minimal variation between Test 1 and Test 2. Mean values were calculated for each test: GSI test 1 mean was 1.24 ±0.09 and test 2 being 1.25 ± 0.09. Similarly, the LV GLS values demonstrated small variations between repeated measurements. Mean values for LV GLS were: test 1 -30.70% ± 4.90 and test 2 -29.57% ± 4.50. Likewise, the RV GLS values followed a similar trend with a mean for test 1 of -30.68% ± 4.31 and -29.97% ± 4.90 for test 2.

**Table 4.2 –** Intra-user variability of GSI and LV and RV GLS.

| Study | Global Sphericity Index - ratio | | LV Global Longitudinal strain - % | | RV Global Longitudinal strain - % | |
|---|---|---|---|---|---|---|
| | Test 1 | Test 2 | Test 1 | Test 2 | Test 1 | Test 2 |
| **1** | 1.10 | 1.13 | -36.94 | -35.21 | -38.55 | -36.54 |
| **2** | 1.35 | 1.40 | -28.40 | -32.10 | -28.81 | -31.65 |
| **3** | 1.26 | 1.23 | -25.79 | -22.41 | -26.96 | -27.24 |
| **4** | 1.25 | 1.33 | -21.22 | -27.79 | -18.91 | -17.92 |
| **5** | 1.29 | 1.34 | -22.26 | -21.58 | -24.22 | -20.58 |
| **6** | 1.16 | 1.21 | -27.12 | -23.83 | -35.89 | -32.57 |
| **7** | 1.21 | 1.23 | -33.74 | -36.27 | -35.53 | -33.70 |
| **8** | 1.24 | 1.31 | -33.96 | -32.74 | -24.26 | -23.07 |
| **9** | 1.33 | 1.30 | -39.51 | -36.90 | -39.61 | -24.78 |
| **10** | 1.15 | 1.20 | -28.00 | -26.89 | -31.32 | -29.61 |
| **11** | 1.30 | 1.27 | -39.04 | -36.17 | -38.35 | -36.24 |
| **12** | 1.16 | 1.20 | -27.16 | -24.83 | -28.27 | -25.11 |
| **13** | 1.43 | 1.38 | -27.15 | -25.05 | -26.91 | -24.08 |
| **14** | 1.20 | 1.18 | -32.46 | -35.34 | -34.25 | -35.61 |
| **15** | 1.17 | 1.17 | -28.48 | -25.45 | -29.49 | -33.39 |

Data to show intra-user variability GSI, LV GLS and RV GLS. Test and re-test data can be seen. The same examiner (CB) carried out test 1 and test 2 on the same patient two weeks apart to assess for reliability and reproducibility.

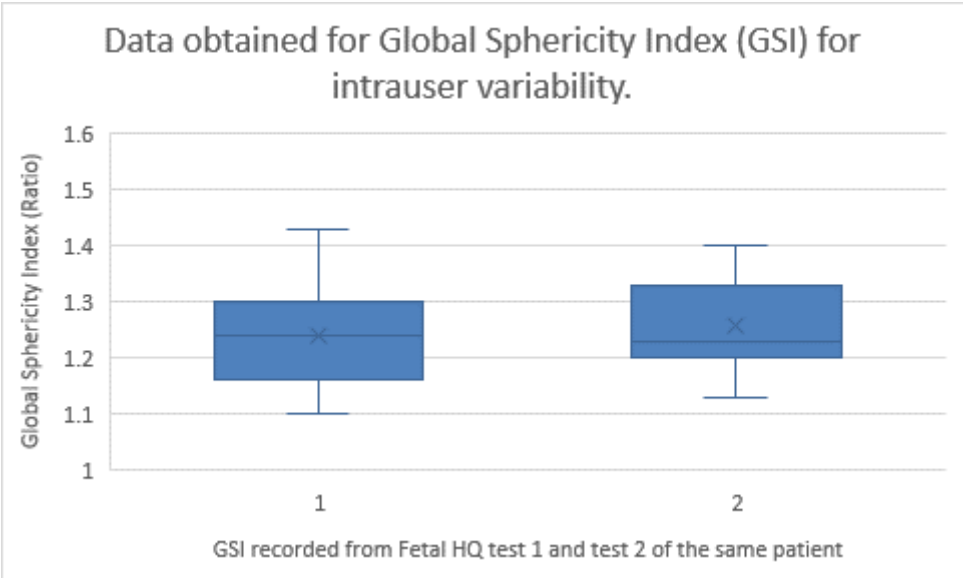


**Figure 4.3:** Median and Inter-quartile ranges of tests one and two for GSI. The box chart summarises the distribution of data and outliers for GSI when assessing for reproducibility and reliability. The same examiner (CB) on the same patients performed test 1 and test 2. The GSI median value is represented via the black line within the box and can be seen in each data set. The max and minimum GSI values can been identified via the whiskers. The mean for each data set is represented via the X. there are no outliers within either dataset.

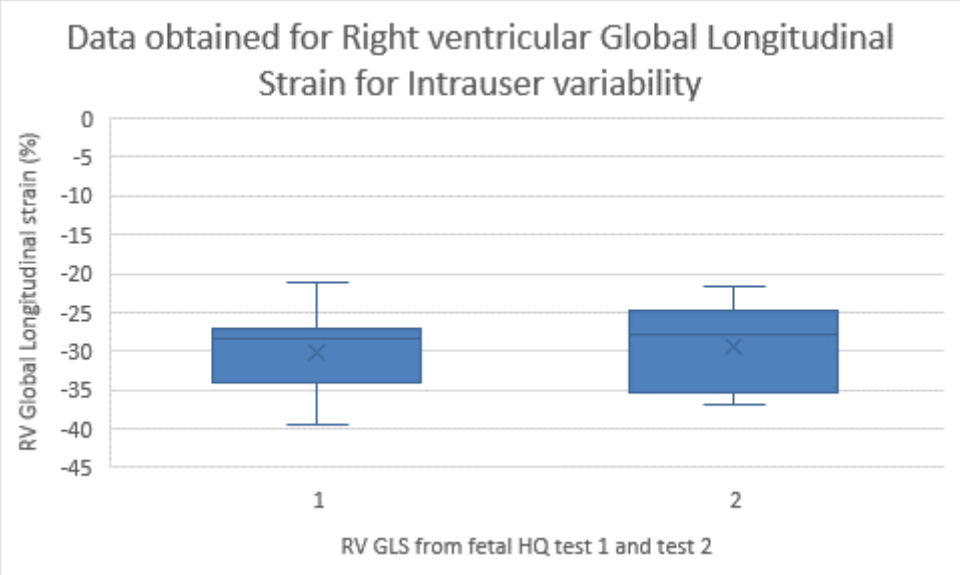


**Figure 4.4:** Median and Inter-quartile ranges of tests one and two for RV GLS. The box chart summarises the distribution of data and outliers for RV GLS when assessing for reproducibility and reliability. The same examiner (CB) on the same patients performed test 1 and test 2. The median value can be seen as the black line in each data set with the max and minimum RV GLS values represented via the whiskers. The mean RV GLS value for each data set is shown as the X. All values can been seen as being similar for each series of data. There were no outliers for either dataset.

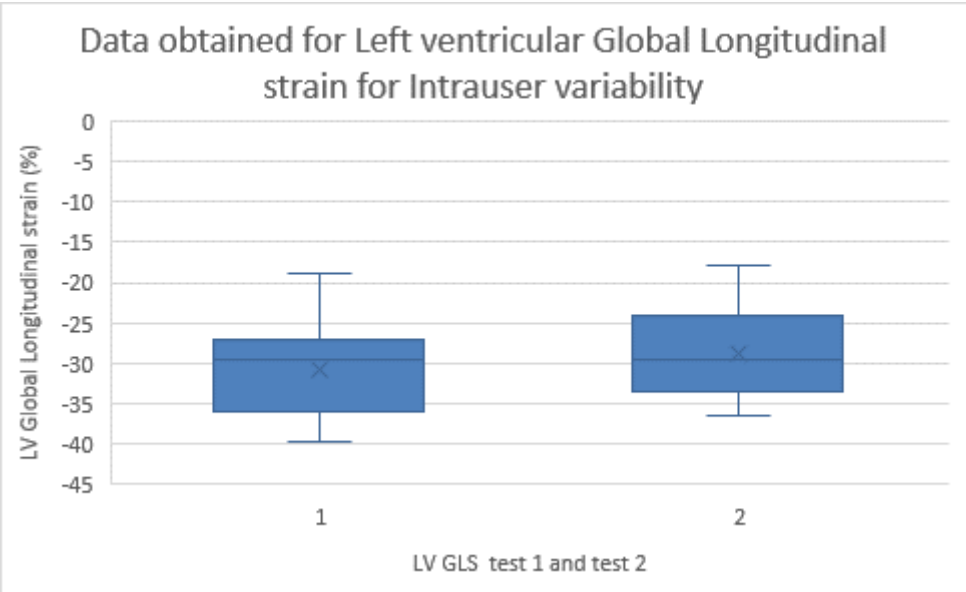


**Figure 4.5:** Median and Inter-quartile ranges of tests one and two for LV GLS reproducibility. The box chart summarises the distribution of data for LV GLS when assessing for reproducibility and reliability. The same examiner (CB) on the same patients performed test 1 and test 2. The median value can be seen as the black line within the box in each data set with the max and minimum values shown as whiskers and being similar for each series of data. The mean LV GLS value for each data set is shown as the X. All values can been seen as being similar for each series of data. There were no outliers for either dataset.

The ICC was calculated for each group to assess measurement reliability for inter and intra-user. The GSI demonstrated excellent reliability with an ICC of 0.93 for intra and 0.94 for inter, along with a low ME (0.03) and (0.02) and a CV (2.41%, (2.52) indicating high reproducibility. Although LV GLS and RV GLS showed slightly greater variability, both maintained good reliability. The ICC for LV GLS was 0.92, while RV GLS had an ICC of 0.84. ME and CV for LV and RV GLS were also calculated to assess for consistency and are presented in table 4.3.

**Table 4.3 –** Statistical analysis for intra-user and inter-user variability

| Parameter | Intra ICC | Inter ICC | Intra Method Error | Inter Method Error | Intra CV (%) | Inter CV (%) |
|---|---|---|---|---|---|---|
| **GSI** | 0.93 | 0.94 | 0.03 | 0.02 | 2.41 | 2.52 |
| **LV GLS** | 0.92 | 0.76 | 2.15 | 1.33 | 7.21 | 8.06 |
| **RV GLS** | 0.84 | 0.77 | 2.97 | 1.87 | 9.97 | 11.03 |

Statistical analysis of intra-observer and inter-observer variability for GSI, LV GLS and RV GLS. Results include intraclass correlation coefficients (ICC), method error and coefficient of variation (CV %) for both intra- and inter- user measurements. High ICC values indicate good reproducibility, with GSI demonstrating the highest intra and inter-user agreement.

### Values and reference range for global sphericity index.

Reference ranges for each gestational age group are shown in Table 4.4. Normal ranges of GSI of the 120 studies across the GA were between 1.1 and 1.38 with a mean of 1.22 ± 0.07 (SD). GSI for all normal cohorts was above 1.1. The GSI was not significantly associated with GA (figure 4.6). Gestational age and global sphericity index yielded a weak negative association with correlation coefficient of –0.102 with a P-value of 0.45, this indicates no significant relationship between GSI and GA. Table 4.4 and Figure 4.6 presents the data in the GSI with increasing gestational age.

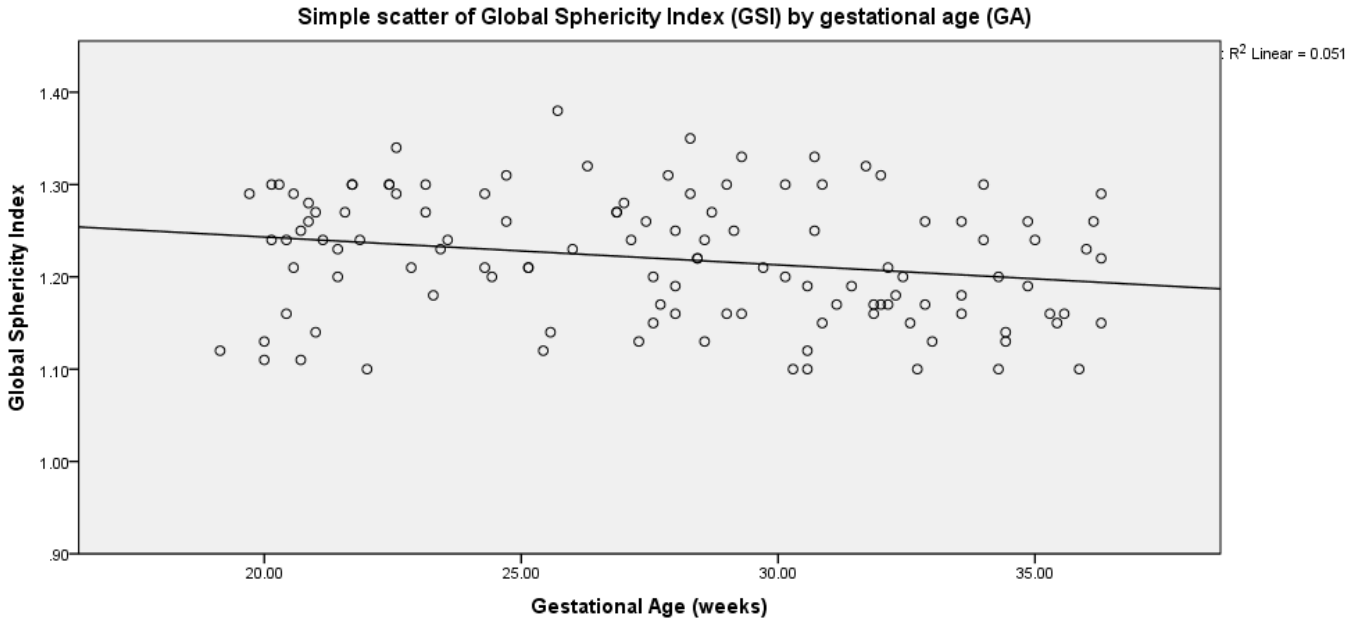


**Figure 4.6:** the scatter graph shows the distribution of GSI across GA groups of all 120 examinations. The chart illustrates the normal reference range obtained from this study for foetal GSI between 19-38 weeks is between 1.1 and 1.38

**Table – 4.4 -** descriptive statistics for GSI for healthy control cohort.

| GA (weeks) | Range (ratio) | Mean (ratio) | SD | 5% | 95% |
|---|---|---|---|---|---|
| **19 - 23** | 1.11 – 1.34 | 1.23 | 0.069 | 1.11 | 1.35 |
| **23+1 – 28** | 1.13 – 1.35 | 1.23 | 0.060 | 1.13 | 1.33 |
| **28+1 – 32** | 1.1 – 1.35 | 1.22 | 0.074 | 1.09 | 1.344 |
| **32+1 – 37** | 1.1 – 1.3 | 1.18 | 0.056 | 1.09 | 1.28 |

Descriptive statistics for GSI across GA groups in the healthy control cohort. The table presents the GSI range, mean and SD, and 5$^{th}$ and 95$^{th}$ percentile values for each GA subgroup. The data indicate that GSI remains relatively stable throughout gestation, with narrow variability across the examined time points.

The Z-score analysis for each data observation across each gestational age group for GSI can be seen in Table 4.5. Overall, the data suggests that the GSI values are relatively stable across the gestational age groups, as indicated by the Z-scores predominately staying within ±2 SD from the mean.

**Table – 4.5 -** GSI Z-scores across gestational age groups for healthy control cohort.

| 19 – 23 weeks | | | 23+1 – 28 weeks | | | 28+1 – 32 weeks | | | 32 + 1 – 37 weeks | | |
|---|---|---|---|---|---|---|---|---|---|---|---|
| **GA** | GSI | Z-score | **GA** | GSI | Z-score | **GA** | GSI | Z-score | **GA** | GSI | Z-score |
| **19+1** | 1.12 | -1.630 | **23+1** | 1.27 | 0.597 | **28+2** | 1.29 | 0.915 | **32+1** | 1.17 | -0.349 |
| **19+5** | 1.29 | 0.801 | **23+1** | 1.3 | 1.076 | **28+2** | 1.35 | 1.722 | **32+1** | 1.21 | 0.360 |
| **20+0** | 1.13 | -1.488 | **23+2** | 1.18 | -0.842 | **28+3** | 1.22 | -0.027 | **32+2** | 1.18 | -0.171 |
| **20+0** | 1.11 | -1.773 | **23+3** | 1.23 | -0.042 | **28+3** | 1.22 | -0.027 | **32+3** | 1.2 | 0.183 |
| **20+1** | 1.24 | 0.086 | **23+4** | 1.24 | 0.117 | **28+4** | 1.13 | -1.238 | **32+4** | 1.15 | -0.703 |
| **20+1** | 1.3 | 0.944 | **24+2** | 1.29 | 0.916 | **28+4** | 1.24 | 0.242 | **32+5** | 1.1 | -1.589 |
| **20+2** | 1.3 | 0.944 | **24+2** | 1.21 | -0.362 | **28+5** | 1.27 | 0.646 | **32+6** | 1.17 | -0.349 |
| **20+3** | 1.16 | -1.059 | **24+3** | 1.2 | -0.522 | **29+0** | 1.16 | -0.834 | **32+6** | 1.26 | 1.247 |
| **20+3** | 1.24 | 0.086 | **24+5** | 1.31 | 1.236 | **29+0** | 1.3 | 1.049 | **33+0** | 1.13 | -1.058 |
| **20+4** | 1.29 | 0.801 | **24+5** | 1.26 | 0.437 | **29+1** | 1.25 | 0.377 | **33+4** | 1.18 | -0.171 |
| **20+4** | 1.21 | -0.343 | **25+1** | 1.21 | -0.362 | **29+2** | 1.16 | -0.834 | **33+4** | 1.16 | -0.526 |
| **20+5** | 1.11 | -1.774 | **25+1** | 1.21 | -0.362 | **29+2** | 1.33 | 1.453 | **33+4** | 1.26 | 1.247 |
| **20+5** | 1.25 | 0.229 | **25+3** | 1.12 | -1.800 | **29+5** | 1.21 | -0.161 | **34+0** | 1.3 | 1.956 |
| **20+6** | 1.26 | 0.372 | **25+4** | 1.14 | -1.481 | **30+1** | 1.2 | -0.296 | **34+0** | 1.24 | 0.892 |
| **20+6** | 1.28 | 0.658 | **25+5** | 1.38 | 2.354 | **30+1** | 1.3 | 1.049 | **34+2** | 1.1 | -1.589 |
| **21+0** | 1.27 | 0.515 | **26+0** | 1.23 | -0.043 | **30+2** | 1.1 | -1.641 | **34+2** | 1.2 | 0.183 |
| **21+0** | 1.14 | -1.345 | **26+2** | 1.32 | 1.395 | **30+4** | 1.12 | -1.372 | **34+3** | 1.13 | -1.058 |
| **21+1** | 1.24 | 0.086 | **26+6** | 1.27 | 0.597 | **30+4** | 1.1 | -1.641 | **34+3** | 1.14 | -0.880 |
| **21+3** | 1.2 | -0.486 | **26+6** | 1.27 | 0.597 | **30+4** | 1.19 | -0.430 | **34+6** | 1.26 | 1.247 |
| **21+3** | 1.23 | -0.057 | **27+0** | 1.28 | 0.756 | **30+5** | 1.25 | 0.377 | **34+6** | 1.19 | 0.006 |
| **21+4** | 1.27 | 0.515 | **27+1** | 1.24 | 0.117 | **30+5** | 1.33 | 1.453 | **35+0** | 1.24 | 0.892 |
| **21+5** | 1.3 | 0.944 | **27+2** | 1.13 | -1.640 | **30+6** | 1.3 | 1.049 | **35+2** | 1.16 | -0.526 |
| **21+5** | 1.3 | 0.944 | **27+3** | 1.26 | 0.437 | **30+6** | 1.15 | -0.968 | **35+3** | 1.15 | -0.703 |
| **21+6** | 1.24 | 0.086 | **27+4** | 1.2 | -0.522 | **31+1** | 1.17 | -0.699 | **35+4** | 1.16 | -0.526 |
| **22+0** | 1.1 | -1.917 | **27+4** | 1.15 | -1.321 | **31+3** | 1.19 | -0.430 | **35+6** | 1.1 | -1.589 |
| **22+3** | 1.3 | 0.944 | **27+5** | 1.17 | -1.001 | **31+5** | 1.32 | 1.318 | **36+0** | 1.23 | 0.715 |
| **22+3** | 1.3 | 0.944 | **27+6** | 1.31 | 1.236 | **31+6** | 1.17 | -0.699 | **36+1** | 1.26 | 1.247 |
| **22+4** | 1.29 | 0.801 | **28+0** | 1.19 | -0.682 | **31+6** | 1.16 | -0.834 | **36+2** | 1.22 | 0.538 |
| **22+4** | 1.34 | 1.516 | **28+0** | 1.16 | -1.161 | **32+0** | 1.31 | 1.184 | **36+2** | 1.29 | 1.778 |
| **22+6** | 1.21 | -0.343 | **28+0** | 1.25 | 0.277 | **32+0** | 1.17 | -0.699 | **36+2** | 1.15 | -0.703 |

Z-scores for GSI across GA groups for the healthy control cohort. The table presents individual GSI values and their corresponding Z-scores for each foetus, grouped by gestational age. Z-scores were calculated using the formula: Z= (observed value – group mean) / Standard deviation (SD), Based on normative reference data from table 4.4 This analysis indicates how many SD each GSI value deviates from the group mean. Z-scores within ±2 were considered within normal range. This data support the use of Z-scores as a standardised method for identifying outliers and interpreting GSI in a clinically meaningful way.

### Values and reference range for LV GLS

Spearman rank correlation conducted between LV GLS and GA yielded $r_s$ = 0.194 with a p-value of 0.034. The mean LV GLS across the GA groups was found to be -25.46% with a SD of ±2.58%. The mean and SD was calculated for each gestational age group and can be seen in table 4.6. As gestational age increases the mean value for LV GLS shows a slight increase (less negative). These results suggest trends of decreasing LV GLS values with advancing gestational age. The narrowing of the range and the SD can also be seen in later gestational age groups which indicate a more consistent LV GLS with advancing gestation.

**Table 4.6 -** LV GLS mean SD and gestational age for healthy control cohort

| GA (weeks) | Range (%) | Mean (%) | SD (%) | 5% | 95% |
|---|---|---|---|---|---|
| **19 - 23** | -21.18 to -32.74 | -26.55 | 3.39 | -32.13 | -20.97 |
| **23+1 – 28** | -20.1 to -30.45 | -25.05 | 2.49 | -29.15 | -20.95 |
| **28+1 – 32** | -22.23 to -30.16 | -25.52 | 2.05 | -28.89 | -22.15 |
| **32+1 – 37** | -21.37 to -28.36 | -24.61 | 1.71 | -27.42 | -21.80 |

Descriptive statistics for LV GLS across GA groups in the healthy control cohort. The table presents the LV GLS range, mean and SD, and 5$^{th}$ and 95$^{th}$ percentile values for each GA subgroup. The data indicate that mean LV GLS becomes slightly less negative with advancing gestation, suggesting a modest reduction in strain as the foetal heart matures.

Table 4.7 presents the calculated Z-scores for LV GLS across the gestational age groups. This enabled standardised data and to account for variations due to foetal growth. Z-scores were calculated from 19 weeks gestation up to 36$^{+2}$ weeks gestation.

**Table 4.7 -** LV GLS individual Z -scores across gestational age groups for healthy control cohort.

| 19 – 23 weeks | | | 23+1 – 28 weeks | | | 28+1 – 32 weeks | | | 32 + 1 – 37 weeks | | |
|---|---|---|---|---|---|---|---|---|---|---|---|
| **GA** | LV GLS | Z-score | **GA** | LV GLS | Z-score | **GA** | LV GLS | Z-score | **GA** | LV GLS | Z-score |
| **19+1** | -28.45 | -0.561 | **23+1** | -24.68 | 0.148 | **28+2** | -27.03 | -0.733 | **32+1** | -24.14 | 0.273 |
| **19+5** | -30.68 | -1.219 | **23+1** | -23.71 | 0.538 | **28+2** | -28.42 | -1.408 | **32+1** | -21.37 | 1.884 |
| **20+0** | -27.54 | -0.293 | **23+2** | -23.36 | 0.678 | **28+3** | -22.23 | 1.598 | **32+2** | -26.62 | -1.169 |
| **20+0** | -26.60 | -0.016 | **23+3** | -23.50 | 0.622 | **28+3** | -27.05 | -0.743 | **32+3** | -22.35 | 1.314 |
| **20+1** | -28.07 | -0.449 | **23+4** | -27.77 | -1.092 | **28+4** | -27.06 | -0.748 | **32+4** | -22.19 | 1.407 |
| **20+1** | -23.67 | 0.848 | **24+2** | -30.45 | -2.167 | **28+4** | -26.62 | -0.534 | **32+5** | -22.55 | 1.198 |
| **20+2** | -23.25 | 0.972 | **24+2** | -22.69 | 0.947 | **28+5** | -27.31 | -0.869 | **32+6** | -25.28 | -0.390 |
| **20+3** | -29.82 | -0.965 | **24+3** | -20.11 | 1.987 | **29+0** | -22.36 | 1.535 | **32+6** | -25.42 | -0.472 |
| **20+3** | -32.74 | -1.826 | **24+5** | -24.19 | 0.345 | **29+0** | -26.81 | -0.626 | **33+0** | -25.74 | -0.658 |
| **20+4** | -22.26 | 1.264 | **24+5** | -25.58 | -0.213 | **29+1** | -25.44 | 0.039 | **33+4** | -23.78 | 0.482 |
| **20+4** | -27.16 | -0.181 | **25+1** | -22.53 | 1.011 | **29+2** | -24.88 | 0.311 | **33+4** | -25.66 | -0.611 |
| **20+5** | -29.36 | -0.829 | **25+1** | -23.45 | 0.642 | **29+2** | -22.48 | 1.477 | **33+4** | -23.77 | 0.488 |
| **20+5** | -27.78 | -0.363 | **25+3** | -27.56 | -1.007 | **29+5** | -25.92 | -0.194 | **34+0** | -26.12 | -0.879 |
| **20+6** | -22.41 | 1.219 | **25+4** | -28.41 | -1.344 | **30+1** | -29.25 | -1.812 | **34+0** | -23.35 | 0.732 |
| **20+6** | -24.75 | 0.529 | **25+5** | -24.29 | 0.305 | **30+1** | -24.11 | 0.689 | **34+2** | -24.30 | 0.179 |
| **21+0** | -26.75 | -0.059 | **26+0** | -27.66 | -1.047 | **30+2** | -26.93 | -0.685 | **34+2** | -26.55 | -1.129 |
| **21+0** | -22.00 | 1.341 | **26+2** | -27.82 | -1.112 | **30+4** | -22.11 | 1.656 | **34+3** | -25.39 | -0.454 |
| **21+1** | -25.61 | 0.276 | **26+6** | -24.43 | 0.249 | **30+4** | -25.73 | -0.102 | **34+3** | -23.69 | 0.5347 |
| **21+3** | -22.46 | 1.205 | **26+6** | -22.35 | 1.084 | **30+4** | -25.84 | -0.155 | **34+6** | -25.14 | -0.309 |
| **21+3** | -24.45 | 0.618 | **27+0** | -21.74 | 1.328 | **30+5** | -30.16 | -2.257 | **34+6** | -26.21 | -0.925 |
| **21+4** | -25.29 | 0.371 | **27+1** | -24.60 | 0.181 | **30+5** | -24.69 | 0.403 | **35+0** | -23.31 | 0.756 |
| **21+5** | -36.09 | -2.814 | **27+2** | -28.57 | -1.413 | **30+6** | -25.77 | -0.121 | **35+2** | -26.56 | -1.135 |
| **21+5** | -28.07 | -0.449 | **27+3** | -26.69 | -0.658 | **30+6** | -24.46 | 0.515 | **35+3** | -23.31 | 0.756 |
| **21+6** | -21.18 | 1.583 | **27+4** | -24.14 | 0.365 | **31+1** | -26.44 | -0.447 | **35+4** | -22.61 | 1.163 |
| **22+0** | -30.09 | -1.045 | **27+4** | -26.89 | -0.738 | **31+3** | -24.79 | 0.355 | **35+6** | -28.36 | -2.182 |
| **22+3** | -25.59 | 0.282 | **27+5** | -25.79 | -0.297 | **31+5** | -25.97 | -0.218 | **36+0** | -26.70 | -1.216 |
| **22+3** | -28.16 | -0.476 | **27+6** | -27.89 | -1.139 | **31+6** | -25.50 | 0.001 | **36+1** | -24.01 | 0.349 |
| **22+4** | -23.56 | 0.881 | **28+0** | -25.75 | -0.281 | **31+6** | -24.68 | 0.408 | **36+2** | -24.42 | 0.110 |
| **22+4** | -27.06 | -0.151 | **28+0** | -23.70 | 0.542 | **32+0** | -23.30 | 1.078 | **36+2** | -22.59 | 1.175 |
| **22+6** | -25.52 | 0.303 | **28+0** | -21.22 | 1.537 | **32+0** | -22.28 | 1.574 | **36+2** | -26.80 | -1.274 |

Z-scores for LV GLS across GA groups for the healthy control cohort. The table presents individual LV GLS values and their corresponding Z-scores for each foetus, grouped by gestational age. Z-scores were calculated using the formula: Z= (observed value – group mean) / Standard deviation (SD), Based on normative reference data from table 4.6 This analysis indicates how many SD each LV GLS value deviates from the group mean. Z-scores within ±2 were considered within normal range.

### Values and reference range for RV GLS

Spearman rank correlation conducted between RV GLS and GA yielded $r_s$ = 0.285 with a p-value of 0.002. The mean RV GLS across the entire gestational range was -26.79% with a SD of ±3.40%.

Table 4.8 presents the descriptive statistics for RV GLS across different gestational age groups. The table includes the range, mean and SD with the 5% and 95% confidence intervals for RV GLS at each gestational age range. The confidence intervals provide an estimate of the expected variability in RV GLS measurements helping to assess the distribution of the data can be seen in Table 4.8.

**Table 4.8 -** descriptive statistics for RV GLS, across the gestational age ranges, for healthy control cohort.

| GA (weeks) | Range (%) | Mean (%) | SD (%) | 5% | 95% |
|---|---|---|---|---|---|
| **19 - 23** | -20.58 to -31.32 | -28.14 | 3.81 | -34.41 | -21.87 |
| **23+1 – 28** | -20.65 to -34.56 | -27.09 | 3.04 | -32.09 | -22.09 |
| **28+1 – 32** | -19.99 to -35.96 | -26.66 | 3.70 | -32.75 | -20.57 |
| **32+1 – 37** | -19.34 to -30.42 | -25.54 | 2.60 | -29.82 | -21.26 |

Descriptive statistics for RV GLS across GA groups in the healthy control cohort. The table presents the RV GLS range, mean and SD, and 5$^{th}$ and 95$^{th}$ percentile values for each GA subgroup. The data indicate that mean RV GLS becomes slightly less negative with advancing gestation, suggesting a reduction in strain as the foetal heart matures.

Z-scores for RV GLS across the different gestational age groups from 19 weeks to 37 weeks gestation were calculated. The Z-scores provided standardise the data and account for any variation due to foetal growth these calculations are presented in table 4.9.

**Table 4.9:** Individual Z-scores for RV GLS across the gestational age groups.

| 19 – 23 weeks | | | 23+1 – 28 weeks | | | 28+1 – 32 weeks | | | 32 + 1 – 37 weeks | | |
|---|---|---|---|---|---|---|---|---|---|---|---|
| **GA** | RV GLS | Z-score | **GA** | RV GLS | Z-score | **GA** | RV GLS | Z-score | **GA** | RV GLS | Z-score |
| **19+1** | -31.32 | -0.83408 | **23+1** | -25.31 | 0.58673 | **28+2** | -24 | 0.70290 | **32+1** | -28.39 | -1.09158 |
| **19+5** | -35.45 | -1.91802 | **23+1** | -27.35 | -0.08244 | **28+2** | -28.8 | -0.5635 | **32+1** | -24.3 | 0.47971 |
| **20+0** | -28.33 | -0.04934 | **23+2** | -24.69 | 0.79011 | **28+3** | -22.98 | 0.97204 | **32+2** | -25.35 | 0.07632 |
| **20+0** | -27.53 | 0.16062 | **23+3** | -24.67 | 0.79667 | **28+3** | -25.27 | 0.36781 | **32+3** | -25 | 0.21078 |
| **20+1** | -29.61 | -0.38528 | **23+4** | -28.11 | -0.33174 | **28+4** | -28.83 | -0.57150 | **32+4** | -27.61 | -0.79192 |
| **20+1** | -25.14 | 0.78789 | **24+2** | -31.69 | -1.50608 | **28+4** | -28.86 | -0.57942 | **32+5** | -26.96 | -0.54220 |
| **20+2** | -26.32 | 0.47819 | **24+2** | -26.56 | 0.17669 | **28+5** | -25.9 | 0.20158 | **32+6** | -27.08 | -0.58831 |
| **20+3** | -24.78 | 0.88237 | **24+3** | -28.1 | -0.3284 | **29+0** | -25.11 | 0.41003 | **32+6** | -22.36 | 1.22502 |
| **20+3** | -23.07 | 1.33117 | **24+5** | -27.23 | -0.04308 | **29+0** | -25.41 | 0.33087 | **33+0** | -23.51 | 0.78321 |
| **20+4** | -20.58 | 1.98469 | **24+5** | -26.17 | 0.30462 | **29+1** | -26.43 | 0.06174 | **33+4** | -26.75 | -0.46153 |
| **20+4** | -29.32 | -0.3091 | **25+1** | -29.61 | -0.82378 | **29+2** | -25.01 | 0.43641 | **33+4** | -30.03 | -1.72164 |
| **20+5** | -28.43 | -0.07558 | **25+1** | -25.43 | 0.54737 | **29+2** | -35.96 | -2.45279 | **33+4** | -27.33 | -0.68435 |
| **20+5** | -23.55 | 1.205 | **25+3** | -27.61 | -0.16773 | **29+5** | -25.49 | 0.30976 | **34+0** | -25.4 | 0.05711 |
| **20+6** | -26.96 | 0.31022 | **25+4** | -28.84 | -0.57120 | **30+1** | -27.77 | -0.29182 | **34+0** | -24.35 | 0.46050 |
| **20+6** | -25.49 | 0.69603 | **25+5** | -26.38 | 0.23574 | **30+1** | -24.64 | 0.53404 | **34+2** | -28.11 | -0.98401 |
| **21+0** | -28.6 | -0.12020 | **26+0** | -25.39 | 0.560 | **30+2** | -23.07 | 0.94829 | **34+2** | -25.99 | -0.16955 |
| **21+0** | -28.36 | -0.05721 | **26+2** | -28.2 | -0.36126 | **30+4** | -19.99 | 1.76096 | **34+3** | -22.14 | 1.30954 |
| **21+1** | -28.84 | -0.18319 | **26+6** | -34.56 | -2.44753 | **30+4** | -27.36 | -0.18364 | **34+3** | -19.34 | 2.38525 |
| **21+3** | -24.25 | 1.02147 | **26+6** | -25.6 | 0.49160 | **30+4** | -25.28 | 0.36517 | **34+6** | -25.56 | -0.0043 |
| **21+3** | -27.39 | 0.19736 | **27+0** | -26.87 | 0.07500 | **30+5** | -25.49 | 0.30976 | **34+6** | -28.22 | -1.02627 |
| **21+4** | -26.54 | 0.42045 | **27+1** | -24.89 | 0.72450 | **30+5** | -24.03 | 0.69499 | **35+0** | -25.2 | 0.13395 |
| **21+5** | -37.32 | -2.40882 | **27+2** | -33.41 | -2.07029 | **30+6** | -29.53 | -0.75620 | **35+2** | -26.12 | -0.21949 |
| **21+5** | -27 | 0.29972 | **27+3** | -24.06 | 0.99676 | **30+6** | -32.46 | -1.52930 | **35+3** | -24.57 | 0.37598 |
| **21+6** | -23.97 | 1.09496 | **27+4** | -32 | -1.60777 | **31+1** | -27.85 | -0.31293 | **35+4** | -24.54 | 0.38751 |
| **22+0** | -35.63 | -1.96527 | **27+4** | -29.61 | -0.82378 | **31+3** | -38.71 | -3.17839 | **35+6** | -29.28 | -1.43351 |
| **22+3** | -27.01 | 0.29710 | **27+5** | -27.44 | -0.11196 | **31+5** | -27.82 | -0.30501 | **36+0** | -30.42 | -1.87147 |
| **22+3** | -31.73 | -0.94169 | **27+6** | -25.6 | 0.49160 | **31+6** | -24.57 | 0.55251 | **36+1** | -25.67 | -0.04661 |
| **22+4** | -32.49 | -1.14115 | **28+0** | -20.65 | 2.11534 | **31+6** | -25.17 | 0.39419 | **36+2** | -21.33 | 1.6207 |
| **22+4** | -30.6 | -0.64511 | **28+0** | -24.03 | 1.00661 | **32+0** | -24.91 | 0.46280 | **36+2** | -23.01 | 0.97530 |
| **22+6** | -28.65 | -0.13332 | **28+0** | -22.9 | 1.37728 | **32+0** | -23.22 | 0.90871 | **36+2** | -22.54 | 1.1558 |

Z-scores for RV GLS across GA groups for the healthy control cohort. The table presents individual RV GLS values and their corresponding Z-scores for each foetus, grouped by gestational age. Z-scores were calculated using the formula: Z= (observed value – group mean) / Standard deviation (SD), Based on normative reference data from table 4.8 This analysis indicates how many SD each RV GLS value deviates from the group mean. Z-scores within ±2 were considered within normal range.

### Comparison of left ventricular and right ventricular values for GLS

The GLS of both the left and the right ventricle were compared against each other across the entire population.

Table 4.10 presents the mean values and SD for LV and RV GLS. The mean LV GLS was -25.46 with a SD of 2.58 while the mean RV GLS was -26.79% with a SD 3.40. These values provide an overview of the central tendency and variability of LV and RV GLS within the study population (table 4.10).

The data of the entire population indicated that there was a statistically significant difference between the LV and RV GLS with the RV GLS being generally more negative than the LV GLS ($p<0.001$).

**Table 4.10** – LV and RV GLS mean SD

| | | Mean % | SD % |
|---|---|---|---|
| **Left ventricle (LV)** | | -25.46 | 2.58 |
| **Right Ventricle (RV)** | | -26.79 | 3.40 |

The descriptive statistics and P value for LV and RV GLS values. The mean and SD were calculated with the Shapiro-Wilk test being conducted to assess distribution of the data.

Table 4.11 shows the mean, SD and P-values when comparing LV and RV GLS across the gestational age groups. The mean values seen for RV GLS are higher in the gestational age groups 19-23 weeks (-26.54% ± 3.39) and $23^{+1}$-28 (-25.05 ± 2.49) when compared to the RV GLS which was -28.14 ± 3.81 and -27.09 ± 3.04 respectively. P values suggested a statistically significant difference between the LV GLS and the RV GLS, P = 0.02 for 19-23 weeks and P <0.01 for $23^{+1}$-28 weeks. Conversely from 28 weeks to 37 weeks there is no statistically significant difference between the two groups however the mean values for GLS in the later gestational age groups ($28^{+1}$-32 and $32^{+1}$-37) were higher in the RV compared to the LV.

**Table 4.11:** LV and RV mean SD and p-value across gestational age groups

| Gestational Age group | LV GLS % (Mean ± SD) | RV GLS % (mean ± SD) | P-Value |
|---|---|---|---|
| **19 - 23** | -26.54 ± 3.39 | -28.14 ± 3.81 | 0.02 |
| **23+1 – 28** | -25.05 ± 2.49 | -27.09 ± 3.04 | <0.01 |
| **28+1 – 32** | -25.52 ± 2.05 | -26.66 ± 3.70 | 0.30 |
| **32+1 – 37** | -24.60 ± 1.72 | -25.54 ± 2.60 | 0.07 |

The mean, SD and P values for each gestational age group can be seen for LV and RV GLS measurements obtained.

## 4.5 – Discussion

This study aimed to assess the feasibility, reliability and reproducibility of STE using fetal HQ software within a routine clinical setting. The findings support that GSI and GLS can be successfully obtained in healthy foetuses and demonstrate good to excellent intra and inter user reproducibility. These results are consistent with previous research supporting the clinical application of foetal speckle tracking (Di Salvo et al., 2008; Krause et al., 2017; Huntley et al., 2021). Over recent years there have been increasing studies that have investigated the normal values for GSI and GLS in the foetal heart. Nevertheless, the results from these studies differ with regards to normal values obtained, and the relationship of advancing GA on STE (Kapusta et al., 2013; Lee-Tannock et al., 2020; Ohira et al., 2020; Van Oostrum et al., 2022).

Foetal echocardiography is a widely used tool in the diagnosis of congenital heart disease before birth. With ever-advancing techniques and improved ultrasound technology, foetal echocardiography's importance continues to increase. 2D foetal STE analysis in the assessment of strain and strain rate has become increasingly popular over the recent years. The development of advanced software and semi-automated analysis has made this technique more desirable within the clinical setting.

Reproducibility and Feasibility

This study has detailed that GSI and GLS are achievable within the clinical setting with good reliability and reproducibility. ICC indicated good to excellent reliability, with intra user values of 0.93 for GSI and 0.92 for LV GLS and inter-user values of 0.94 for GSI and 0.76 for LV GLS indicating a good degree of agreement and

consistency. The ICC of RV GLS showed slightly lower reproducibility of intra-user (0.84) and inter-user (0.77) however the range still falls within good reproducibility and indicates consistency with minor variability. These results show that the measurement processes used were highly consistent, and support the idea of acquiring reproducible data in future use. The CV was lowest for GSI (Intra- 2.41%, Inter-2.52%) further supporting its reliability, indicating minimal variability relative to the mean and therefore a high consistency in the measurements within the clinical setting. While CV values for LV GLS and RV GLS showed higher variability ( Intra- 7.21%, Inter- 8.06) and Intra -9.97%, Inter- 11.03%) respectively indicating a moderate level of variability from the mean. While this level may generally be accepted; it suggests that there is some degree of measurement fluctuation, particularly for RV. This does highlight areas where measurement consistency could be improved. Importantly, both ICC and CV for RV GLS showed the highest levels of variation compared to LV. This does align with previous concerns about measurement challenges (Krause et al., 2017) and could be due to the morphology of the RV and to the difficulty in distinguishing between the moderator band, the RV trabeculations and the endocardial wall, leading to challenges in accurate tracing. These findings highlight the need for adequate training and operator experience, particularly when assessing the RV. The values indicate that there were varying degrees of consistency across the measurements. However, all of the measurements according to commonly accepted thresholds do indicate good to excellent reliability. These results show that the measurement processes used in this study were highly consistent, and supports the reproducibility of the findings. Statistical analysis revealed that there was good reproducibility across the three groups. Statistical analysis detailed in Table 4.3 presented no statistically significant

difference between the two measurements made on each group. This study's findings aligns with previous research, which have also shown that STE is feasible and reproducible in the assessment of foetal cardiac shape and function (Di Salvo et al., 2008; Krause et al., 2017; Huntley et al., 2021).

STE for GSI and GLS is a measurement that is easily obtained in foetal life, it is a non-invasive technique with the semi-automated software already available on many ultrasound machines. It can be easily performed from early gestation with no stress on the mother or the foetus and can be easily incorporated into a routine FE. It is proved to have good reliability and reproducibility aiding in its potential benefit within the clinical setting.

Normal reference ranges

There have been previous studies published on the normal reference ranges and values for GSI and GLS of the foetal heart (Ohira et al., 2020; Van Oostrum et al., 2022). However, of the studies performed there have been widely varying valuations on the normal ranges, with studies consisting of low cohort numbers and only very few looking at the difference across the GA groups (DeVore et al., 2016; Ohira et al., 2020). Van Oostrum et al, (2020) summarised the data from these studies in his paper, which concluded that there was considerable variability between the normal values produced in these studies and that there needed to be further work looking at normal GLS values and the relationship between GA and GLS.

There have been limited studies researching the normal values for GSI across the GA ranges (DeVore et al., 2016; Anuwutnavin et al., 2021; Huntley et al., 2021; Van Oostrum et al., 2022). The GSI is calculated as the ratio of the hearts basal to apical length, divided by its transverse width in diastole from epicardium to epicardium

(DeVore et al., 2016). A GSI close to 0 in the foetal heart would suggest a perfectly spherical shape of the heart. In a study conducted by Anuwutnavin et al, (2021) it was determined that normal morphology of the foetal heart produces a GSI of above 1.1. Consistent with Anuwutnavin et al, (2021) this study also determined that the normal range for GSI across 19 to 38 weeks of gestation was above 1.1. The sample size used in this study was greater than that of Anuwutnavin et al (2021) who analysed 79 four-chamber views compared with the 120 analysed in this study.

The results revealed stable GSI values across gestation (mean 1.22 ± 0.07), with no significant correlation between GSI and gestational age. This is consistent with earlier studies (DeVore et al., 2016; Anuwutnavin et al., 2021) and suggests that GSI may remain relatively constant throughout foetal development in normal uncomplicated pregnancies. Although the cohort size was modest, this reinforces the potential value of GSI as a standardised index of foetal cardiac geometry.

The Results from this study also confirmed the findings on normal GSI values from previous studies conducted (Huntley et al., 2021; Van Oostrum et al., 2022). As found in previous studies, it was revealed that there was no significant change in the GSI ratio across the gestational age ranges. From the data obtained Z-scores were calculated for GSI across the gestational age groups. The use of Z-scores in evaluating the GSI provides a standardised framework to assess deviations in cardiac morphology which could be the result of a congenital heart defect or extra cardiac conditions.

The GSI ratio is easily achievable and reproducible within the clinical setting, as it only requires two measurements to be made, the basal to apical length and the transverse width of the foetal heart which is obtained from the four-chamber view.

GSI may be beneficial in the diagnosis and management of congenital heart disease and non-cardiac conditions, where the remodelling of the foetal heart suggested buy an abnormal GSI value may be the first indication of cardiac dysfunction. However, due to the large spectrum of anomalies for congenital heart disease and the difficulties in detection of CHD during foetal life, more research is required to investigate the effect of congenital heart disease on GSI. Nonetheless, GSI could potentially be used as another indicator in the diagnosis and prognosis of congenital heart disease when compared to the normal foetal heart. This could potentially aid in the counselling, management of the foetus and the parental information available.

In contrast, both LV and RV GLS demonstrated a significant trend with advancing gestation. A weak positive correlation was identified between LV GLS and GA (rs =0.194, p=0.034), suggesting a subtle decrease in LV contractility (i.e., less negative strain) as gestation progresses. RV GLS exhibited a moderate correlation with GA (rs= 0.285, p=0.002), supporting previous findings by Huntley et al. (2021) and Ohira et al (2020) that RV strain declines with maturation. These gestational trends could reflect physiological adaption to changing preload and afterload conditions in utero. It is important to understand the relationship between GA and GLS as it allows for differentiation of normal developmental changes from pathological abnormalities.

In this study statistical tests revealed that there was a weak positive correlation between LV GLS and gestational age. This data suggests that foetal LV GLS in the normal population is higher at lower gestational age and as gestational age increases the GLS reduces. On the contrary, previous studies conducted, assessing GA and LV GLS indicated that there was no correlation between advancing GA and reduced GLS values, (Kapustra et al., 2013; Ohira et al., 2020;). These studies consisted of smaller sample sizes compared with this study (n-44 and n-98

respectively). However, findings from this study were consistent with much larger study conducted by Van Oostrum et al., (n-592) where they concluded that there was a significant correlation in LV GLS and GA.

As the data from this study showed a weak correlation in lower GLS values at increased GA, it would be beneficial to conduct further research with larger cohort numbers to confidently conclude whether there is a useful link with increasing gestational age and LV GLS.

The link between RV GLS and GA showed a much stronger link with a moderate correlation identified between RV GLS and advancing gestational age. This correlation was statistically significant indicating that the correlation seen is likely due to the relationship between the two variables. Previous research has provided contradicting results. Lee-Tannock et al., (2021) findings suggested that as GA increased there was no change in the RV GLS values. However, studies by Huntley et al., (2021) and by Ohira et al, (2020) concurred that, as GA increased there was a significant decrease in RV GLS values. The findings from this study agreed with both Huntley et al, (2021) and Ohira et al, (2020) and revealed there was stronger evidence to suggest that there is a relationship with reduction in RV GLS values and advancing GA.

Understanding the changes in GLS throughout gestational age could potentially aid in the diagnosis and management of congenital heart disease. It is known that GLS can detect subclinical changes in myocardial function before any changes in fractional shortening or ejection fraction when assessing for early signs of cardiac dysfunction. This is due to GLS measuring myocardial deformation directly enabling it to detect subtle changes in the heart's contractility (Adamo et al., 2017).

Comparison of LV and RV GLS in the normal population

The study investigated the differences in LV GLS and RV GLS across varying gestational ages revealing a gestational age dependent variation in strain values. In this study, RV GLS was consistently more negative than LV GLS in earlier gestation (19-28 weeks), LV GLS and RV GLS differed significantly. The results of the data suggest that the RV has higher contractility at this gestation with a greater myocardial strain (more negative) compared to the left ventricle. However, in later gestation from 28 weeks no statistical difference was observed.

This aligns with the known physiological dominance of the right ventricle in foetal circulation due to its role in supplying the systemic and placental circuits via the ductus arteriosus, the increased RV preload, coupled with higher pulmonary vascular resistance, may explain the greater GLS seen in the RV compared to the LV during early gestation (Zhu et al., 2023).

As gestation advances, pulmonary vascular resistance gradually decreases, and the LV begins to take on a greater proportion of systemic output. This transition may explain the narrowing difference in GLS values between the ventricles. Furthermore the increased myocardial compaction and maturation of the LV over gestation may contribute to a more uniformed contractility between the terms by full term (Dominguez-Gallardo et al., 2022).

Other studies have reported similar findings. Huntley et al. (2021) and Ohira et al. (2020) found that RV strain was more negative than LV strain in mid-gestation. In contrast, studies with smaller sample sizes or using different software (e.g. strain calculated via TomTec or EchoPac) reported conflicting patterns (Lee-Tannock et al., 2020). These discrepancies may be due to vendor –specific algorithms, differences

in frame rate, or regional tracking differences, all of which can affect absolute GLS values.

## 4.6 – Limitations

Although this study looked at a relatively large overall normal cohort of 120 studies, once divided into gestational age related subgroups, it meant that each subgroup had a relatively low sample size of thirty studies per gestational age group. This sample size was two short of the target calculated during power analysis. While the study findings remain valid, the slight shortfall in sample size could marginally reduce the statistical power. To enable Z-scores and normal reference ranges that are more robust, a larger cohort of studies in each gestational age group would be required. A further limitation to this study was that a single examiner did not acquire the four-chamber views used for analysis. These images were obtained during routine clinical FE. This introduces potential variability in image acquisition and optimisation. However to mitigate this variability, a detailed how-to guide for standardised image acquisition was developed and disseminated to all examiners involved. This guide aimed to ensure consistency and reliability across the images collected. Nonetheless, the possibility of residual variability such as framerate cannot be excluded. Additionally due to the morphology of the RV and its differing structures compared to the LV, STE in the RV may prove more challenging. Adequate training would be required in order to accurately identify structures such as the moderator band to enable precise and exact tracing of the endocardial border. Finally, this study was conducted using the fetal HQ software. Alternative vendors offering other STE analysis may result in varying normal values when compared to this study and this should be explored (de Waal and Phad, 2018).

To strengthen the clinical relevance of these findings, future research should aim to validate the observed trends in larger, multicentre cohorts that allow for the generation of robust normative data and z-scores across gestational ages. Standardising image acquisition across multiple examiners and centres will also be essential to ensure reproducibility, particularly in structures prone to variability such as the right ventricle. Additionally given the dependency on vendor-specific software, comparative studies across different platforms are warranted to assess the consistency of GSI and GLS measurements. These steps would not only enhance the generalisability of foetal speckle tracking but also support its integration into clinical practice by defining clinical thresholds for early cardiac dysfunction.

## 4.7 – Conclusion

Assessment of foetal heart shape GSI and GLS with the use of STE is easily performed within the clinical setting. There is good reproducibility and reliability of both GSI and GLS. Normal values have revealed that there is a potential negative correlational relationship in decreasing GLS in advancing GA. However, more research is required with a larger population to confirm these findings. GSI and GLS in the clinical setting could prove to be useful in the diagnosis and management of foetus presenting with CHD. Reference ranges for GSI and LV GLS and RV GLS were produced.

# Chapter 5 – Can foetal Speckle tracking be a useful tool in cases of ventricular disproportion?

## 5.1 – Introduction

Ventricular disproportion is characterised by an asymmetry in the size of the heart's ventricles. This condition is assessed through FE and is subjectively defined as a visual discrepancy in the size of the left and the right ventricles of the heart. Disproportion of the ventricles is an indicator for an obstruction within the foetal heart. Most commonly, ventricular disproportion presents as a smaller LV relative to the RV (Figure 5.1 and 5.2), suggesting the potential presence of left heart obstruction. Ventricular disproportion identified during foetal life is a leading marker for the suspicion of coarctation of the aorta (CoA), (Hornberger et al., 1994; Matsui et al., 2008). CoA is a congenital cardiovascular malformation and is defined as a discrete narrowing of the aortic arch most commonly located at the isthmic region, at the ductus arteriosus (2016 Allan et al., 2009; Abuhamad and Chaoui), which then becomes the ligamentum arteriosum after birth and is typically just distal to the left subclavian artery as shown in Figure 5.3. Coarctation however, can be discrete, long or complex and often involves the aortic arch or the isthmus. The underlying theory for coarctation of the aorta is not well understood, but there are two important mechanisms proposed: the ductal tissue theory and the reduced flow theory (Buyens et al., 2012). The ductal tissue theory suggests that during foetal development, tissue from the ductus arteriosus extends into the adjacent wall of the aortic isthmus. The ductus arteriosus remains patent in utero due to high levels of circulating prostaglandin E2, but following birth, prostaglandin levels fall and the ductus begins to close (Yokoyama et al., 2017). If ductal tissue is present within the aortic wall, its contraction during ductal closure may lead to secondary narrowing of the aorta at this site. (Buyens et al., 2012). This theory helps to explain why CoA often only becomes clinically apparent after birth, when the ductus closes due to the systemic

circulation being ductus-dependent. In this context prostaglandin infusion can be used to maintain ductal patency, providing an alternative route for systemic blood flow until surgical intervention can be performed. The alternative widely proposed mechanism for the development of CoA is the reduced flow theory (Schneider et al., 2008; Yuan et al., 2015). This theory suggests that diminished antegrade blood flow through the left heart and aortic arch during foetal life results in underdevelopment, or hypoplasia, of these structures (Yokoyama et al., 2017). In normal foetal circulation, most of the right ventricular output bypasses the lungs via the ductus arteriosus, and only a portion of the left ventricular output passes through the ascending aorta and aortic isthmus, when there is a left sided obstruction, ventricular dysfunction, or a hemodynamic imbalance favouring right heart dominance, the reduced flow through the aortic arch may impair its growth and remodelling, leading to structural narrowing postnatally (Schneider et al., 2008; Hornberger and Sahn, 2007; Yuan, 2015). This theory highlights the relationship between foetal heart flow dynamics and aortic arch morphology, it also supports the importance of assessing ventricular symmetry and aortic dimensions during foetal echocardiography.

CoA accounts for between 4 and 8% of all congenital heart disease (Rosenthal et al., 2005; Van Nisselrooij et al., 2018). However, the diagnosis of foetal CoA is complex, as it primarily relies on visual detection of ventricular disproportion – specifically, a reduced width of the LV compared to the RV (Figure 5.1 and Figure 5.2).

Unlike hyperplastic left heart syndrome, where the left ventricle is underdeveloped, in CoA, the left ventricle remains apex forming and the mitral valve remains patent.

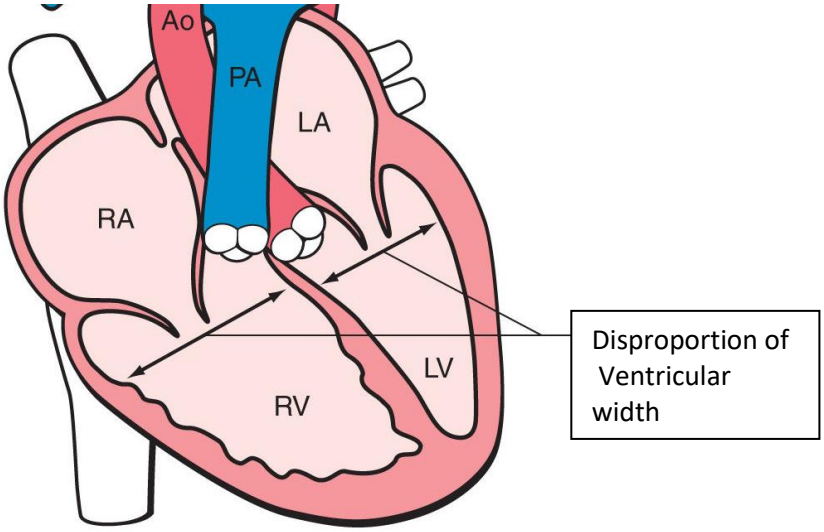


**Figure 5.1**: schematic illustration demonstrating ventricular disproportion in the fetal four-chamber view. The LV appears reduced in width when compared to the RV.A finding that is commonly associated with CoA. (Image adapted from https://obgynkey.com/coarctation-of-the-aorta-and-interrupted-aortic-arch/ Accessed 14/01/2025).

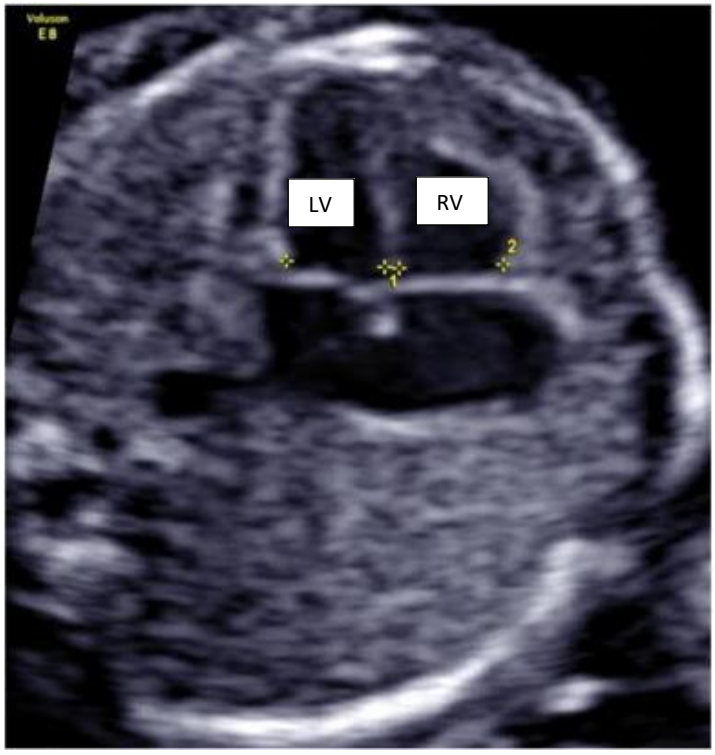


**Figure 5.2**: Echocardiographic four-chamber view demonstrating foetal ventricular disproportion in a foetus with suspected CoA. The LV appears subjectively narrower in width compared with the RV. (Image obtained with consent).

Arterial disproportion may also be observed with CoA; however, this is not always the case (Vigneswaran et al., 2020). Accurately identifying foetuses that will develop CoA postnatally remains challenging, with false positive rates exceeding 50% in cases (Head et al., 2005; Matasui et al., 2008 and Vigneswaran et al., 2020). It is known ventricular disproportion can occur as a normal variant during late pregnancy. Generally a discrepancy in ventricular size increases the likelihood of CoA. Nonetheless, significant size differences can still be associated with normal outcomes, while CoA may occur even in the presence of minimal ventricular disproportion (Allan et al., 2009).

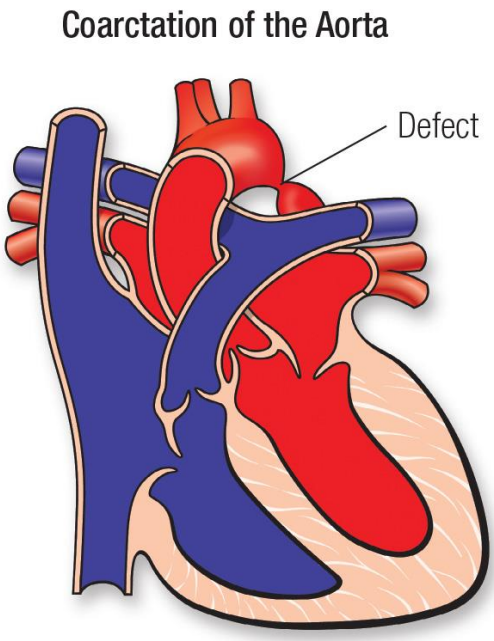


**Figure 5.3**: The illustration depicts CoA, the congenital narrowing can be seen (Defect) in the descending aorta. This narrowing would restrict blood to the foetal body. (Image adapted from https://www.heart.org/en/health-topics/congenital-heart-defects/about-congenital-heart-defects/coarctation-of-the-aorta-coa. Accessed 14/01/2025).

CoA occurs more frequently in males at around a ratio of 2.6:1 (Simpson et al., 2018). In critical or duct dependent CoA swift identification and treatment is vital to avoid long-term morbidity or death (Lloyd et al., 2021). Postnatal management for CoA involves the monitoring via serial echocardiograms as constriction of the arterial duct confirms its diagnosis. Should CoA be confirmed, this warrants and enables prompt action, which causes high anxiety for the parents, and increases service delivery demands on the neonatal and paediatric cardiology services (Lloyd et al., 2021).

Despite advances in technology and experience, prenatal diagnosis of CoA remains challenging with many cases not detected until the postnatal period (Beattie et al., 2017 and Hede et al., 2019). Diagnosis and interventions to correct CoA postnatally do not always carry as positive an outcome as those detected in the antenatal period (Brown et al., 2006 and Singh et al., 2015).

Functional assessment in suspected CoA during foetal life remains challenging. Traditional parameters such as ventricular size disproportion, Doppler flow across the aortic isthmus, and subjective assessment of ventricular function are limited in sensitivity and are prone to inter-operator variability (Hornberger and Sahn, 2007; Schneider et al., 2008). Moreover these methods often fail to detect subtle subclinical myocardial dysfunction that may precede overt structural changes. STE offers a relatively angle –independent, quantitative analysis of myocardial deformation and can provide early insight into global and regional function through parameters such as GLS and GSI (Devore et al., 2021). These parameters may be particularly useful in foetuses with suspected CoA, where altered haemodynamics and increased afterload can impair LV performance before significant anatomical narrowing is evident (Yuan, 2015).

STE in foetuses exhibiting ventricular disproportion could potentially assist in the diagnosis of CoA. However, limited and inconclusive research exists on this specific foetal cardiac condition in relation to speckle tracking. Miranda et al (2017) conducted a retrospective case-control study involving foetuses with confirmed CoA. The study included 12 cases of CoA and 12 gestational aged-matched controls; Due to the rarity of CoA as a congenital heart disease, sample sizes are typically small. Compared to earlier studies such as Germanakis et al (2012) which only included two CoA cases, Miranda et al, in their 2017 study offers more robust data. Interestingly, Germanakis et al (2012) found no significant difference in LV strain between with their two cases and normal controls. In contrast, Miranda et al (2017) found that foetuses with CoA had a reduced LV longitudinal strain when compared to age-matched controls.

DeVore et al (2020) investigated the size, shape (GSI) and function of the foetal heart with confirmed CoA in a retrospective study involving a larger cohort of 50 confirmed CoA cases and 200 controls. Their findings revealed that when compared to gestational aged-matched controls foetuses with CoA had decreased longitudinal and transverse strain. Additionally, DeVore et al (2020) discovered that the size and shape (GSI) of the heart in foetuses with CoA were differed from those of the control group. DeVore et al (2020) proposed that incorporating these measurements into prospective studies could potentially enhance the examiners ability to diagnose CoA effectively. DeVore et al (2021) investigated the use of STE on the last examination prior to delivery in foetuses with confirmed CoA. This retrospective study included 54 confirmed cases of CoA against 54 false positive. All foetuses had presented in the antenatal period with ventricular disproportion and were suspected cases of CoA. They found that confirmed cases of CoA had a greater number of abnormalities in

the size, shape (GSI) and function of the LV then those with a false positive. However, they did not find a significant difference in the percent of ventricular disproportion between the two groups. This study concluded that abnormalities noted in ventricular size, shape and function from STE could assist in the antenatal diagnosis of CoA.

## 5.2 – Aims and Objectives

The aim of the study was to determine if STE to obtain GSI and GLS could aid in the diagnosis of obstructive lesions such as CoA, in women presenting with foetal cardiac ventricular disproportion. The normal values developed from the control group (healthy foetal hearts; presented previously in Chapter 4), were used for comparison with the cases presenting with ventricular disproportion and those positive for an obstructive lesion.

## 5.3 – Materials and Methods

The methods and materials underpinning the analysis presented in this chapter are detailed in Chapter 3. This includes information on ethics, patient selection and recruitment, instruments used, data acquisition and STE echocardiography technique for the fetal HQ software. Information on data and statistical analysis is detailed in chapter 3.7.

## 5.4 – Results

### Patient selection

#### Ventricular disproportion group

Sixteen women were recruited between February 2023 and August 2024 after presenting at the university hospitals of Leicester antenatal foetal cardiology clinic with suspected ventricular disproportion. Gestational age at presentation was between $21^{+0}$ and $34^{+1}$ weeks with a mean gestational age of $26^{+6}$ weeks, SD ± 5.2 weeks. Maternal age at the time of presentation was between 18 years and 41 years with a mean maternal age of 29.1 years, SD ± 6.0 years. Thirteen of the sixteen women (81%) were White British with three ladies (19%) of Asian ethnicity. One participant was excluded from the study due to intrauterine foetal demise.

#### Control Group

A control group comprising of foetuses from normal low risk pregnancies were recruited to establish baseline values. Maternal age range was between 18 to 43 years with a mean maternal age of 30.4 years (SD ± 6.3 years). Of the seventy-two study participants recruited for the control group 56 (77.8%) were White British, 7 participants (9.7%) were White Other. 4 participants (5.6%) were Indian, 4 (5.6%) were Asian and 1 participant (1.3%) being classified as other ethnicity.

### Disproportion raw data

Table 5.1 presents the individual GSI and GLS values for the disproportion group, derived from 22 studies involving 15 participants. The mean values and SD for each group can be seen in table 5.2. The GSI ratio for this group ranged from 0.98 to 1.43 (mean 1.15 ± 0.10). The LV GLS values varied between -13.88% and -29.24% (mean -21.40% ± 3.60%), while the RV GLS values ranged from -29.94% to -30.11%

(mean – 26.79% ± 3.41%). these results are displayed in chronological order based on GA.

**Table 5.1 –** GSI and GLS values for disproportion group

| GA (weeks) | GSI (ratio) | LV GLS (%) | RVGLS (%) |
|---|---|---|---|
| **20+1** | 1.21 | -24.92 | -24.96 |
| **21** | 1.43 | -21.11 | -29.06 |
| **21** | 1.30 | -29.24 | -30.11 |
| **21+3** | 1.29 | -27.42 | -26.38 |
| **21+4** | 1.12 | -21.83 | -24.34 |
| **22** | 1.11 | -23.22 | -24.36 |
| **23+4** | 1.10 | -20.15 | -25.58 |
| **23+5** | 1.10 | -24.67 | -27.69 |
| **24+4** | 1.20 | -21.66 | -22.52 |
| **27+6** | 1.06 | -18.53 | -23.99 |
| **28+6** | 1.04 | -17.73 | -22.13 |
| **29+1** | 1.22 | -20.95 | -26.64 |
| **30+3** | 1.30 | -26.72 | -24.90 |
| **31+2** | 0.98 | -16.37 | -27.01 |
| **31+5** | 1.20 | -20.86 | -24.81 |
| **31+6** | 1.09 | -19.45 | -26.13 |
| **32+2** | 1.03 | -20.18 | -25.3 |
| **32+3** | 1.16 | -13.88 | -24.83 |
| **32+5** | 1.13 | -19.90 | -27.13 |
| **34** | 1.10 | -21.47 | -26.92 |
| **34+1** | 1.23 | -21.87 | -21.94 |
| **37** | 1.10 | -18.77 | -28.47 |

Table shows the values for GSI and LV and RV GLS for the disproportion group. The data is displayed in GA chronological order. This table illustrates the entire ventricular disproportion group irrespective of those who were positive for an obstructive legion.

### GSI and GLS in Ventricular disproportion

The mean and SD of the disproportion group were calculated and compared to those of the entire control group to assess variability and central tendencies, the results can be seen in Table 5.2.

The statistical results for the entire disproportion group are presented in table 5.2. There was a statistically significant difference identified between the LV GLS in the disproportion group compared to the control. Due to the difference in sample size between the control group (n=120) and the disproportion group (n=22) effect size was calculated to quantify the differences between the two groups, which indicated a moderate effect size of $r$ = 0.33. P values for GSI and RV GLS suggest that there was no statistically significant difference between the disproportion and control group.

**Table 5.2 –** Descriptive statistics including mean, SD and P-values for disproportion group compared to the control population.

| | GSI | | | LV GLS | | | | RV GLS | | |
|---|---|---|---|---|---|---|---|---|---|---|
| | Mean | SD | P-Value | Mean | SD | P-Value | Effect Size | Mean | SD | P-Value |
| **Disproportion** | 1.15 | 0.10 | 0.263 | -21.40 | 3.60 | <0.001 | 0.33 | -25.69 | 2.13 | 0.341 |
| **Control** | 1.22 | 0.07 | | -26.79 | 3.41 | | | -25.46 | 2.58 | |

Descriptive statistics for ventricular disproportion and control groups, including mean, SD, and P-values for GSI, LV GLS and RV GLS. The table presents mean values and SD for each parameter in the disproportion and the control groups. P-values indicate the statistical significance of group differences, and Cohen's d effect size is included for LV GLS. Data represents the combined population regardless of the presence of an obstructive lesion. The disproportion group demonstrated lower mean values for both GSI and LV GLS compared to controls, with a statistically significant reduction observed in LV GLS ($p<0.001$). No significant differences were found for RV GLS between groups. An effect size is included for LV GLS to reflect the magnitude of difference between groups.

The dataset of the ventricular disproportion group was divided based on GA and descriptive statistics for GSI, LV GLS and RV GLS were computed. These were then compared to the control group with matching GA. For each GA group P values were determined. Effect size was calculated for those found to have a statistically significant difference due to small cohort numbers for the disproportion group. The findings are presented in tables 5.3 to 5.5. The mean GSI (Table 5.3) remained relatively stable across the gestational age groups when compared to the control group. However, there was a variable degree of statistical significance across the GA groups. The P value indicated a statistically significant difference between the disproportion and control group in the $32^{+1}$ to 37 week population (P - 0.03) with a small to moderate effect size of 0.36. The LV GLS in the disproportion group compared to the control (table 5.4) exhibited noticeable variation across the GA groups. P values indicated significant differences in GA groups 23+1 weeks to 37 weeks (P values 0.03 and <0.01) with a moderate to large effect size. There was no statistically significant difference noted between the disproportion and the control group for RV GLS (table 5.5). This is evidenced with higher P values (ranging from 0.15-0.83) and lower effect sizes (0.04 to 0.14).

**Table 5.3 –** Statistics of disproportion for GSI, compared to control group across the GA groups

| GA - weeks | Disproportion (n) | GSI ventricular disproportion, mean (SD) ratio | Control (n) | GSI control, mean (SD) ratio | P Value | Effect size *r* |
|---|---|---|---|---|---|---|
| **19 - 23** | 6 | 1.24 ± 0.12 | 30 | 1.23 ± 0.06 | 0.93 | 0.01 |
| **23+1 - 28** | 4 | 1.15 ± 0.05 | 30 | 1.23 ± 0.06 | 0.06 | 0.47 |
| **28+1 – 32** | 6 | 1.13 ± 0.12 | 30 | 1.22 ± 0.07 | 0.12 | 0.26 |
| **32+1 – 37** | 6 | 1.12 ± 0.07 | 30 | 1.18 ± 0.05 | 0.03 | 0.36 |

Descriptive statistics, p-values and effect sizes for GSI in ventricular disproportion and control groups, analysed across GA subgroups. Mean GSI values ± SD are presented for each group. P-values reflect the statistical comparison between the disproportion and control groups, and the effect size (r) quantifies the magnitude of group differences. The analysis was performed irrespective of the presence of an obstructive lesion. While the largest effect size was observed in the 23+1 to 28 week group (r=0.47), statistical significance was only reached in the 32+1 to 37 week subgroup (p=0.03).

**Table 5.4 –** Statistics of disproportion group for LV GLS, compared to control group across the GA groups

| GA - weeks | Disproportion (n) | LV GLS ventricular disproportion, mean (SD) % | Control (n) | LV GLS control, mean (SD) % | P Value | Effect Size *r* |
|---|---|---|---|---|---|---|
| **19 - 23** | 6 | -23.79 ± 4.15 | 30 | -26.62 ± 3.20 | 0.17 | 0.22 |
| **23+1 - 28** | 4 | -21.25 ± 2.61 | 30 | -25.05 ± 2.49 | 0.03 | 0.38 |
| **28+1 – 32** | 6 | -20.34 ± 3.59 | 30 | -25.52 ± 2.05 | <0.01 | 0.49 |
| **32+1 – 37** | 6 | -19.34 ± 2.90 | 30 | -24.60 ± 1.72 | <0.01 | 0.62 |

Descriptive statistics, p-values and effect sizes for LV GLS in ventricular disproportion and control groups, analysed across GA subgroups. Mean LV GLS values ± SD are presented for each group. P-values reflect the statistical comparison between the disproportion and control groups, and the effect size (r) quantifies the magnitude of group differences. The analysis was performed irrespective of the presence of an obstructive lesion. Statistically significant differences were observed from 28 weeks onwards, with the largest effect size seen in the 32+1 to 37 week sub-group (r= 0.62, p<0.01), indicating a marked reduction in LV GLS in the disproportion group during later gestation.

**Table 5.5 –** Statistics of disproportion group for RV GLS, compared to control group across the GA groups.

| GA - weeks | Disproportion | RV GLS ventricular disproportion, mean (SD) % | Control (n) | RV GLS control, mean (SD) % | P Value | Effect Size *r* |
|---|---|---|---|---|---|---|
| **19 - 23** | 6 | -26.54 ± 2.50 | 30 | -28.54 ± 3.81 | 0.37 | 0.14 |
| **23+1 - 28** | 4 | -24.94 ± 2.21 | 30 | -27.09 ± 3.04 | 0.15 | 0.25 |
| **28+1 – 32** | 6 | -25.27 ± 1.79 | 30 | -26.67 ± 3.79 | 0.61 | 0.09 |
| **32+1 – 37** | 6 | -25.77 ± 2.29 | 30 | -25.54 ± 2.60 | 0.83 | 0.04 |

Descriptive statistics, p-values and effect sizes for RV GLS in ventricular disproportion and control groups, analysed across GA subgroups. Mean RV GLS values ± SD are presented for each group. P-values reflect the statistical comparison between the disproportion and control groups, and the effect size (r) quantifies the magnitude of group differences. The analysis was performed irrespective of the presence of an obstructive lesion. In contrast to LV GLS, RV GLS values demonstrated no statistically significant differences across GA groups, suggesting preserved RV function in the disproportion cohort.

### Cases found positive for Obstructive lesion

The investigation into ventricular disproportion post-delivery revealed that seven out of the fifteen participants were diagnosed with obstructive lesions. Among these cases, six were identified with CoA (85.71%) while one had mitral stenosis (14.29%). Parameters analysed included GA, GSI and RV and LV GLS, with corresponding Z-scores for each. Clinical data can be seen in table 5.6. GA of the affected cases were from $27^{+6}$ weeks to 37 weeks, highlighting that the condition was identified across a wide GA range. Due to this variation, 3 patients (30%) required an additional scan before delivery. The GSI values ranged from 0.98 to 1.23 with Z-scores varying from -3.15 to 0.69. 40% (n=4) of the GSI Z-scores were below the expected range of -2 indicating a lower GSI value than the norm. LV GLS values ranged from -16.37% to -23.22%. Z-scores were outside of the normal range in 80% of these cases indicating a lower GLS (less negative) compared to the norm. RV

GLS values ranged between -22.13% and -27.13% with all Z-scores (100%) seen within the normal range.

**Table 5.6 –** Data obtained for disproportion cases found positive for obstructive lesions

| patient | GA (wks) | GSI | Z-score | LV GLS % | Z-score | RV GLS % | Z-score |
|---|---|---|---|---|---|---|---|
| **1** | 32+5 | 1.13 | -1.02 | -19.9 | 2.65 | -27.13 | -0.58 |
| | 22+0 | 1.11 | -1.71 | -23.22 | 0.94 | -24.36 | 1.97 |
| **2** | 34+1 | 1.23 | 0.69 | -21.87 | 1.54 | -21.94 | 1.34 |
| | 37+0 | 1.1 | -1.53 | -18.77 | 3.28 | -28.47 | -1.09 |
| **3** | 32+3 | 1.16 | -0.50 | -13.88 | 6.03 | -24.83 | 0.26 |
| **4** | 31+6 | 1.09 | -1.71 | -19.45 | 2.85 | -26.13 | 0.14 |
| | 27+6 | 1.06 | -2.66 | -18.53 | 2.53 | -23.99 | 0.98 |
| **5** | 28+6 | 1.04 | -2.36 | -17.73 | 2.84 | -22.13 | 1.58 |
| **6** | 32+2 | 1.03 | -2.7 | -20.18 | 2.49 | -25.3 | 0.09 |
| **7** | 31+2 | 0.98 | -3.15 | -16.37 | 4.30 | -27.01 | -0.09 |

Individual patient data for GA, GSI and LV and RV GLS for the subgroup identified as disproportion which were positive for an obstructive lesion. Z-scores were calculated for each examination performed.

To further analyse the impact of ventricular disproportion on GSI and GLS, mean values and SD were calculated for each group (GSI, LV GLS, and RV GLS). These values were then compared to a gestational age-matched control group ($28^{+1}$-37 weeks, n=60). The findings are summarised in Table 5.7. The mean GSI for obstructive lesion cases was 1.09 which was lower than the control group of 1.21. LV GLS mean value was also lower (less negative) at -18.99% when compared to the control -24.46% indicting a reduced GLS in cases diagnosed with an obstructive lesion. RV GLS mean value of the obstructive lesion group (-25.13%) was less pronounced when compared to the control group (-26.79%). The group positive for an obstructive lesion was statistically compared to a gestational age-matched control group ($28^{+1}$-37 weeks) using appropriate statistical methods to assess significant differences whilst controlling for gestational age. GSI in the obstruction group

differed significantly compared to the age – matched controls (p = 0.001) with a moderate to large effect (r = 0.422, N = 70). LV GLS in the obstructive lesion group also revealed a statistically significant difference when compared to gestational age-matched controls, with a p value of < 0.001 and an effect size of r = 0.577 (N = 70) indicating a robust relationship between the groups. Statistical analysis revealed no significant difference between the RV GLS of the obstructive group compared with gestational age-matched controls, p value = 0.365.

**Table 5.7 –** Mean and SD for disproportion cases positive for an obstructive lesion.

| Parameter | Mean | SD | Range | P value | Effect size |
|---|---|---|---|---|---|
| **Obstructive lesion GSI** | 1.09 | 0.07 | 0.98-1.23 | 0.001 | 0.42 |
| **Control group GSI** | 1.21 | 0.06 | 1.1 – 1.35 | - | - |
| **Obstructive lesion LV GLS %** | -18.99% | 2.66% | -17.73 to -23.22 | <0.001 | 0.58 |
| **Control LV GLS %** | -24.46% | 2.5% | -21.37 to -30.16 | - | - |
| **Obstructive lesion RV GLS %** | -25.13% | 1.13% | -21.94 to -28.47 | 0.365 | - |
| **Control RV GLS %** | -26.79% | 2.5% | -19.37 to -38.71 | - | - |

Table summarises the mean, SD and range for the GSI, LV GLS and RV GLS values in both the disproportion positive subgroup and the control group. The data highlights differences in GSI and GLS values between the two groups

Comparison of GSI and GLS between true positive and false positive cases of ventricular disproportion with an obstructive lesion demonstrated significant differences in GSI and LV GLS (table 5.8, figures 5.4 and 5.5). The true positive group had a lower mean GSI (1.09 ± 0.07) compared to the false positive group (1.21 ± 0.10), with a statistically significant difference (p=0.009, r = 0.56). Similarly, LV GLS was significantly reduced in the true positive group (-18.99 ± 2.65) relative to the false positives (-23.41 ± 3.05), indicating impaired left ventricular deformation

(p=0.003, r = 0.63). There was no statistically significant difference observed in RV GLS between the two groups, (table 5.9).

**Table 5.8** – Comparison of mean, SD, p-values and effect sizes for GSI and GLS between true and false positive cases of ventricular disproportion.

| Parameter | Group | Mean ± SD | P-value | Effect Size |
|---|---|---|---|---|
| **GSI** | True Positive | 1.09 ± 0.07 | 0.009 | 0.56 |
| | False Positive | 1.21 ± 1.10 | | |
| **LV GLS %** | True Positive | -18.99 ± 2.65 | 0.003 | 0.63 |
| | False Positive | -23.41 ± 3.05 | | |
| **RV GLS %** | True Positive | -25.12 ± 2.13 | 0.323 | 0.21 |

The table presents the mean values ± SD for GSI and GLS comparing true positive cases (postnatal confirmed obstruction) and false positive cases (no postnatal obstruction) identified antenatally with ventricular disproportion. P values were calculated and effect size is reported to reflect the magnitude of difference between groups. Significant differences were observed for GSI and LV GLS, with lower values in the true positive group, indicating altered ventricular geometry and impaired myocardial deformation. No significant difference was observed in RV GLS

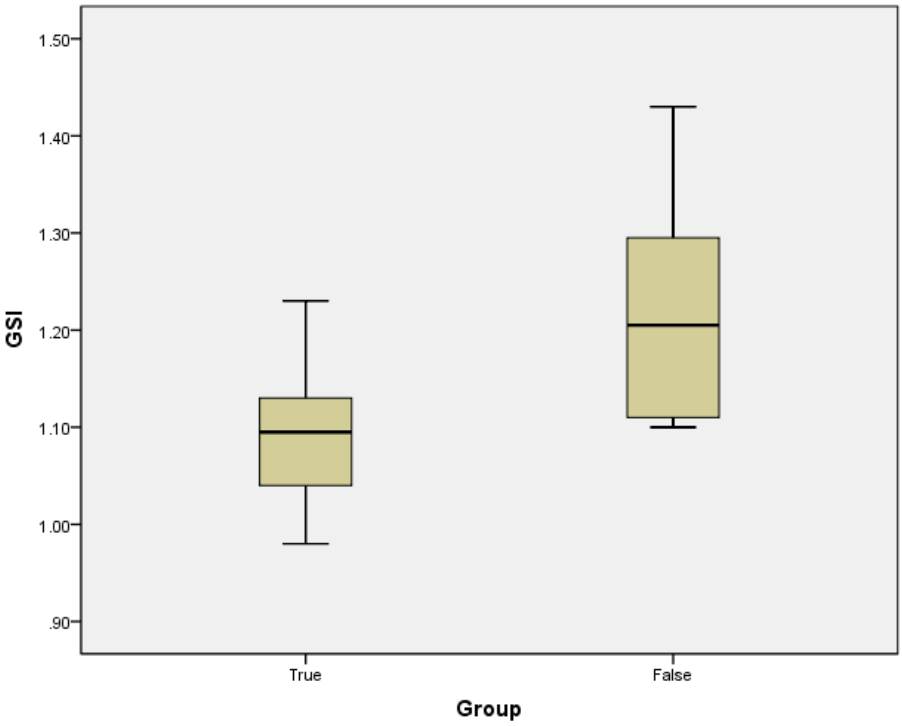


**Figure 5.4:** Boxplot comparing GSI values between true positive and false positive cases of ventricular disproportion. This boxplot illustrates the distribution of GSI measurements in foetuses classified as true positive and false positive, following prenatal identification of ventricular disproportion. The true positive group demonstrated consistently lower GSI values, with a narrower

interquartile range and a lower median compared to the false positive group. The median interquartile range (box), and minimum/maximum values are displayed for each group.

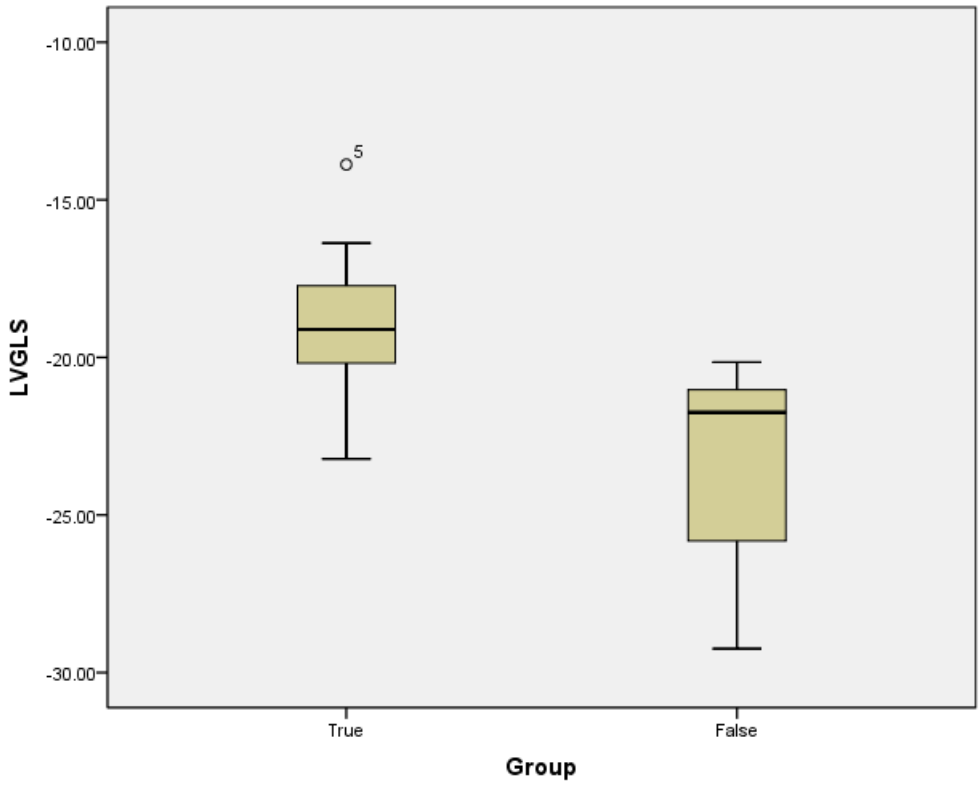


**Figure 5.5:** Boxplot comparing LV GLS values between true positive and false positive cases of ventricular disproportion. This boxplot displays the distribution of LV GLS in true positive and false positive foetal cases identified antenatlly with ventricular disproportion. The true positive group showed significantly reduced LV GLS (less negative values), consistent with impaired myocardial deformation. In contrast, the false positive group had more negative GLS values, reflecting preserved LV function. The plot demonstrates a clear separation between groups, with the true positive cohort clustering closer to the -20% range, and includes an outlier. Median, interquartile ranges, and full data spread are illustrated for both groups.

## 5.5 – Discussion

The purpose of this study was to investigate whether the shape and function of the foetal heart plays a role in the development of ventricular disproportion which is associated with an obstructive cardiac lesion such as COA. Some advantages of this study are that the images required for quantitative analysis are simple and only require the acquisition of the four-chamber view. The use of a high quality four-chamber view was consistent throughout as this is a standard view used in clinical practice.

The use of STE of the foetal heart has been investigated previously. Yet, it is not currently part of the standard FE in the detection of congenital heart disease. In recent years, further studies on the clinical application of foetal STE in the detection of obstructive disorders have emerged. However, these studies have been few and have revealed conflicting outcomes, such as RV dysfunction and abnormal GSI values compared to normal population, particularly in cases of ventricular disproportion with confirmed CoA. (Germanakis et al., 2012; Miranda et al., 2017; DeVore et al., 2021; Liu et al., 2022; Yang et al., 2024). Previous studies conducted to investigate the application of STE in foetuses with ventricular disproportion and CoA have been predominantly retrospective, meaning that there is the limitation of selection bias and inconsistent data. The early studies investigating CoA during foetal life included very low cohort numbers of CoA (Germanakis et al., 2012; Willruth et al., 2012). These studies only included two and three CoA cases respectively. In both of these studies the LV GLS was found not differ when compared with normal controls. More recent studies however have included larger cohort numbers (Miranda et al., 2017; DeVore et al., 2021; Liu et al., 2022) and were

found to have a reduced LV GLS in foetus' confirmed with CoA when compared to the control group.

The diagnosis of an obstructive lesion, such as CoA in foetal life is largely reliant on the accurate measurement of the relative size of the foetal ventricles and/or the great vessels (Pasquini et al., 2007; Matsui et al., 2008; Buyens et al., 2012). Despite advancements in FE, the detection of CoA during foetal life remains one of the most challenging, with high false positive rates (30% - 80%) which can result in increased parental stress and anxiety (Familiari et al., 2017; Lloyd et al., 2021). In this study 8 of the 15 cases proved negative for an obstructive lesion (53%), evidencing the difficulty in accurate diagnosis from FE alone. Further analysis with the use of STE in these cases revealed reduced GSI values and lower LV GLS.

The results from this study align with the findings from previous research by DeVore et al, (2021) and Miranda et al, (2017). The outcomes demonstrate a positive correlation between abnormal GSI and a reduced LV GLS in foetuses that were diagnosed with obstructive lesions, when compared to gestational age-matched controls. In the cases of disproportion that were confirmed as having an obstructive lesion, both the LV GLS and GSI showed statistically significant differences from controls. Z-scores were also abnormal for GSI in 40% of the cases (n = 4) and LV GLS Z-scores were abnormal in 80% (n =8) in confirmed cases of obstruction when compared to the control group.

Statistical analysis of LV GLS was also conducted for the disproportion group irrespective of confirmed obstruction and this revealed that there was a statistically significant difference in LV GLS values between the disproportion group and the control group. When assessed as a combined cohort (Table 5.2), the disproportion

group demonstrated significantly reduced LV GLS compared to the control, Indicative of subclinical myocardial dysfunction. This does align with previous work suggesting that reductions in GLS may reflect early changes in myocardial contractility before overt dysfunction becomes apparent (Arduini et al., 2017; Moon-Grady et al., 2021). Although the GSI was lower in the disproportion group, this did not reach statistical significance, possibly due to subtle geometric changes that may become more pronounced with advancing gestation. The mean rank values indicated that LV GLS values were also significantly reduced in the disproportion group (less negative) compared to the control group. The calculated effect size for LV GLS indicated a moderate effect size. Although 53% of these cases were false positive the small sample size and moderate effect size could account for the significant difference in LV GLS found in the cases that were confirmed as having an obstructive lesion and the small sample size of the disproportion group.

The results obtained from this study are consistent with previous research conducted by DeVore et al., 2021 and Miranda et al., 2017. Their findings also demonstrated strong correlation between abnormal GSI values and reduced LV GLS in foetuses with suspected obstructive lesions. These observations suggest that incorporating STE into FE assessments in ventricular disproportion cases may enhance the reliability of CoA detection, potentially reducing the rate of false positive cases.

In this study, the mean values of GSI and LV GLS were observed to be lower in the ventricular disproportion group when compared to the control groups. This could suggest that foetuses with disproportion could exhibit reduced myocardial deformation. However, despite the observed findings in lower GSI values, statistical analysis revealed no significant difference in these values between the disproportion group and the control group; this was irrespective of any obstructive lesion.

There have been inconsistent results in studies assessing RV GLS in cases of CoA when compared with a control population (DeVore et al., 2012; Miranda et al., 2017; Liu et al., 2022). Largely the studies showed that RV GLS was similar in cases of CoA and the control groups (Miranda et al., 2017; Liu et al., 2022). The results of this investigation confirm that there is no difference in the RV GLS in the disproportion group or those confirmed with an obstructive lesion when compared to the gestational age matched controls. The findings did not demonstrate any statistically significant differences in the RV GLS of the disproportion group or those confirmed with an obstructive lesion when compared to the control group. These findings differ from those of DeVore et al, (2021) where they found that there was a statistically significance difference in RV GLS compared to age-matched control group. The difference in these findings may be attributed to differences in ultrasound machines or software, or the techniques used in the assessment of RV GLS.

Normal GSI of the foetal heart is classified as being greater than 1.1 (GE HealthCare, 2020). The findings of this study suggest that foetuses presenting with disproportion and confirmed obstruction such as CoA have a lower GSI value when compared to the normal population. 40% of the confirmed cases demonstrated abnormal Z-scores and 50% of the cases had a GSI of below 1.1 with the remaining 50% being within the normal range. This indicates that the foetal heart in these cases is more spherical in shape with an increased width and decreased length when compared to the control group. This finding could be a result of ventricular remodelling in the presence of subclinical ventricular dysfunction due to an obstruction such as CoA (Crispi et al., 2020). These findings are consistent with the findings by DeVore et al, (2021) and that of Yang et al, (2024) where they found that there were changes in cardiac shape and function among foetuses with CoA.

Comparison between true and false positive case of ventricular disproportion revealed that GSI and LV GLS offer potential value in distinguishing foetuses with true underlying left-sided obstructive lesions. The true positive group demonstrated significantly lower GSI and more impaired LV GLS compared to the false positive group, with large effect sizes for both parameters (r=0.56 and 0.63 respectively). These findings align with previous studies reporting that altered LV geometry and reduced myocardial deformation are common in foetuses with CoA (Pasquini et al., 2007; Gardiner, 2009; Donofrio et al., 2014).

While ventricular disproportion remains a commonly used prenatal marker, it is limited by its high false positive rate. The integration of quantitative functional parameters such as GLS and GSI may enhance risk stratification by identifying subtle but clinically relevant changes in myocardial performance and shape. Notably, RV GLS remained comparable between the two groups, consistent with prior evidence suggesting that the RV is less affected in early left-sided obstruction due to its dominance in foetal circulation (Li et al., 2019).

These results support the potential for speckle tracking derived indices, particularly LV GLS, to improve prenatal diagnostic accuracy and reduce parental anxiety in cases of ventricular disproportion.

The study successfully met its objective of assessing the feasibility and clinical utility of STE in this cohort. The ability to detect functional differences in foetuses with disproportion – prior to overt haemodynamic compromise- indicates that STE may offer added diagnostic value beyond conventional morphological assessment. In particular, reductions in LV GLS could reflect impaired longitudinal fibre shortening

due to increased resistance distal to the aortic arch, as seen in CoA morphology (Opie et al., 2006).

## 5.6 – Limitations

Several limitations must be acknowledges, each of which may impact the reliability and generalisability of the findings presented in this chapter. Firstly, although this was a prospective study with well-defined inclusion criteria, a key limitation of this study was the small sample size within the disproportion group due to referral patterns and case availability. Based on power calculations, a sample size of 32 participants was required to ensure adequate statistical power. However as only 15 participants were available with a total of 22 sets of data in this group, this discrepancy may have limited the study's ability to detect statistically significant effects. While the findings achieved statistical significance in several comparisons, the relatively small cohort may limit the statistical power. This was exacerbated as the subgroup was divided further into gestational age groups; this resulted in between only 4 and 6 sets of data per gestational age group. Because of the small sample size for disproportion cases this resulted in a reduced sample size of those confirmed as having an obstructive lesion, increasing the risk of error and reducing the robustness of the subgroup analysis. This would also affect the ability to generalise findings across the broader antenatal population. However, this study is ongoing and the recruitment of ventricular disproportion participants is continuing. This should enable future research to recruit larger, more representative samples in both the disproportion group and the confirmed obstructive cases to address this limitation and improve statistical reliability. A further limitation to this study was that the four-chamber views used for analysis were not acquired by a single examiner.

These images were obtained during routine clinical FE. This introduces potential variability in image acquisition and optimisation. Poor acoustic windows or foetal motion could compromise STE image acquisition and tracking quality. Having multiple examiners acquiring the image may have introduced variability into GSI and GLS measurements. However, to mitigate this variability, a detailed how-to guide for standardised image acquisition was developed by CB and disseminated and explained to all examiners involved. This guide (appendix 3) aimed to ensure consistency and reliability across the images collected. Nonetheless, the possibility of residual variability such as framerate cannot be excluded and STE remains sensitive to minor tracking errors, especially in the foetal heart where standardisation is more difficult than in postnatal echocardiography (Simpson et al., 2018). Finally STE software and methodology variations may arise due to the use of different vendors and comparisons with other published studies should be made cautiously, as each may have their own algorithm within their commercial software and differences in frame rate, segmentation algorithms and operator training can all influence strain outputs. These factors highlight the need for standardisation and validation across platforms if STE is to be adopted as a routine tool in prenatal cardiac assessment. (de Waal and Phad, 2018).

## 5.7 – Conclusion

Despite the limitations of sample size, the findings suggest that foetuses with an obstructive lesion have an abnormal GSI and reduced LV GLS when compared to gestational age-matched controls. The observed statistical difference in both GSI and LV GLS measurements between foetuses presenting with ventricular disproportion plus obstructive lesion and the control group suggest that STE analysis

may be a useful tool in the assessment of this population and may have value in the prediction of an obstructive lesion such as CoA. Further research with larger cohorts will be essential to validate these initial findings and refine clinical application of STE in foetal cardiology.

# Chapter 6 – Foetal heart Global Sphericity Index and Global Longitudinal Strain after a foetal tachyarrhythmia– A case series

## 6.1 – Introduction

Cardiac rhythm abnormalities are detected in antenatal life due to the advancements in ultrasound imagining. However, if left untreated or not adequately controlled, are associated with increased morbidity and mortality (Abuhmad and Chaoui, 2022). Factors, which lead to mortality, include the development of foetal congestive heart failure, hydrops foetalis or presence of simultaneous congenital heart disease such as Ebsteins anomaly of the tricuspid valve (Yuan, 2019).

The normal foetal heart rate is faster than that of postnatal life with the average foetal heart rate being between 110 and 180 beats per minute (bpm). The typical average heart rate is related to gestational age; as the gestational age increases, the heart rate of the foetus reduces (Simpson, 2018). During the first 10 weeks of life, foetal heart rate can reach up to 180 bpm. It then falls to between 110 and 160 by 14 weeks gestation. Rates outside of this range could indicate a foetal heart arrhythmia (Archer and Manning, 2018). Foetal cardiac rhythm abnormalities are encountered in about 1% to 2% of pregnancies (Abuhamad and Chaoui, 2022). Irregular foetal cardiac rhythm is the leading cause for referral to foetal echocardiography centres for rhythm disturbances; however, the majority of these cases are benign atrial ectopic beats (Abuhamad and Chaoui, 2022). Suspected foetal tachyarrhythmia or bradyarrhythmia, which are associated with an increase in foetal morbidity and mortality account for less than 10% of referrals for foetal rhythm disturbance (Reed, 1989).

Classification of cardiac arrhythmias postnatally is aided by established criteria on electrocardiogram findings. However as such technology is not available antenatally, a more practical approach is required, which relies on existing FE modalities such as

M-mode and Doppler techniques to aid diagnosis. Foetal arrhythmias are classified into three main groups:

1. **Irregular foetal heart rhythms** – This is the most common, often a benign rhythm and generally a result of atrial ectopic beats.
2. **Foetal Tachycardia** – Heart Rate >180 bpm
3. **Foetal Bradycardia** – Heart Rate < 100 bpm

(Abuhamad and Chaoui, 2022)

Foetal tachyarrhythmia is defined by a sustained foetal heart rate of greater than 180 bpm (Sharland, 2013). SVT is an umbrella term that refers to a group of fast heart rhythm disorders originating at or above the atrioventricular (AV) node (Patti et al., 2023). However, during foetal life the term supraventricular tachycardia is classically applied to pathological tachycardia where 1:1 AV conduction is seen with rates above 180bpm (Sharland, 2013; Simpson et al., 2018; Abuhamad and Chaoui, 2022). However a variety of different types of tachycardia can have 1:1 AV conduction, therefore the differentiating of the mechanisms is important as it may affect the type of drug therapy chosen (Simpson et al., 2018). Types of tachyarrhythmia include:

1. **Re-entry tachycardia (short or long AV time)**
2. **Atrial Flutter**
3. **Atrial Fibrillation**
4. **Ventricular tachycardia**

Irregular foetal heart rhythms including foetal tachyarrhythmia and foetal bradycardia do require investigation and management (Archer and Manning, 2018). BCCA

guideline (2021) state that the aim of the foetal cardiac service is to make an accurate diagnosis and initiate treatment, when required for foetal arrhythmias. This case series will focus on foetal tachyarrhythmia classified as having 1:1 AV conduction of a rate above 180bpm including atrial flutter. In many cases atrial flutter and 1:1 conduction tachycardia can be successfully reverted into sinus rhythm once treatment has been initiated. Unlike foetal bradycardias where the heart rhythm rarely reverts to sinus rhythm throughout foetal life (Archer and Manning, 2018).

Understanding the basic principles of the conduction system is important in the assessment of a foetal cardiac arrhythmia. The mechanisms of foetal arrhythmias depend on the generation and the propagation of the electoral impulses of the heart (Yuan, 2019; Allan et al., 2009). The normal conduction system of the heart is when the electrical impulse is initiated from the sinoatrial (SA) node situated in the wall of the right atrium and the impulse spreads throughout the atria causing them to contract. The impulse will then trigger the atrioventricular (AV) node and is then conducted through the bundle of His and the bundle branches into the Purkinje fibres to the right and left ventricles which results in the contraction of the ventricles (Ventricular systole) (Allan et al., 2009).

In postnatal life, an electrocardiogram is recorded to assess for normal sinus rhythm. In foetal cardiology however, echocardiography is used inform the electrocardiogram findings by providing information on muscle contraction (M-mode) and / or on blood flow (Doppler techniques) (Archer and Manning, 2018).

**A** **B**

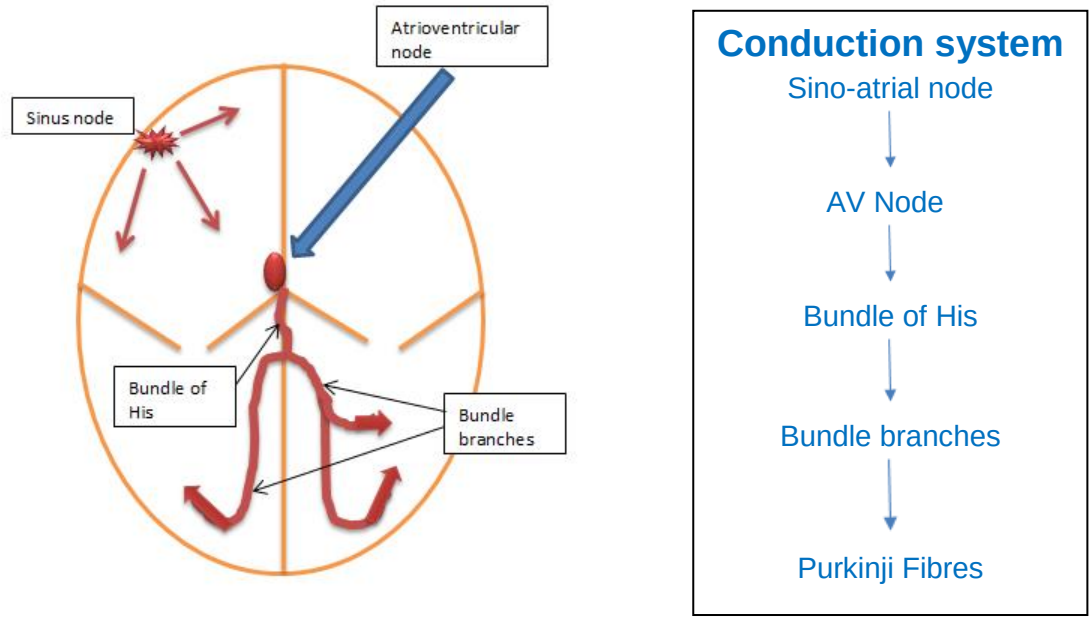


**Figure 6.1**: Image **A** is a simple diagram of the conduction system through the heart. The SA node lies in the right atrium with the AV node seen on the right atrial side of the AV junction. **B** is illustrating the direction of the impulses that originate in the right atrium from the SA node. The impulses from the SA node spread throughout the left and the right atrium it then travels to the atrioventricular node (AV Node) to the bundle of his, the bundle branches and then from purkinje fibres into the left and right ventricles which in turn causes them to contract. (Image adapted from Allan et al., 2009)

### M-mode Echocardiography

M-mode echocardiography is not only a useful tool in the assessment of cardiac function; it is also a useful tool in the assessment of foetal arrhythmias. In normal sinus rhythm, every atrial contraction that is initiated by the SA node is followed by a ventricular contraction and every ventricular contraction is preceded by an atrial contraction. M-mode echocardiography permits simultaneous imaging of the atrial and ventricular contractions (Sharland, 2013).

To enable the accurate assessment of foetal cardiac rhythm accurate measurements of the heart rate and the time intervals between specific events is required. Particular

attention should be paid to the relationship between the atrial and ventricular contractions. M-mode echocardiography in foetal life is a valuable method that can be utilised when assessing for foetal cardiac rhythm as it allows atrial and ventricular activity to be recorded simultaneously. For this to be done, the cursor on the imaging plane needs to be positioned so that the atrial and ventricular activity can be recorded simultaneously. This is usually with the cursor positioned through the free wall of one or other of the atrium at an angle that can give a clear M-mode trace. The cursor must also be positioned either through the ventricular wall or through the aortic valve. (Archer and Manning, 2018; Allan et al., 2009).

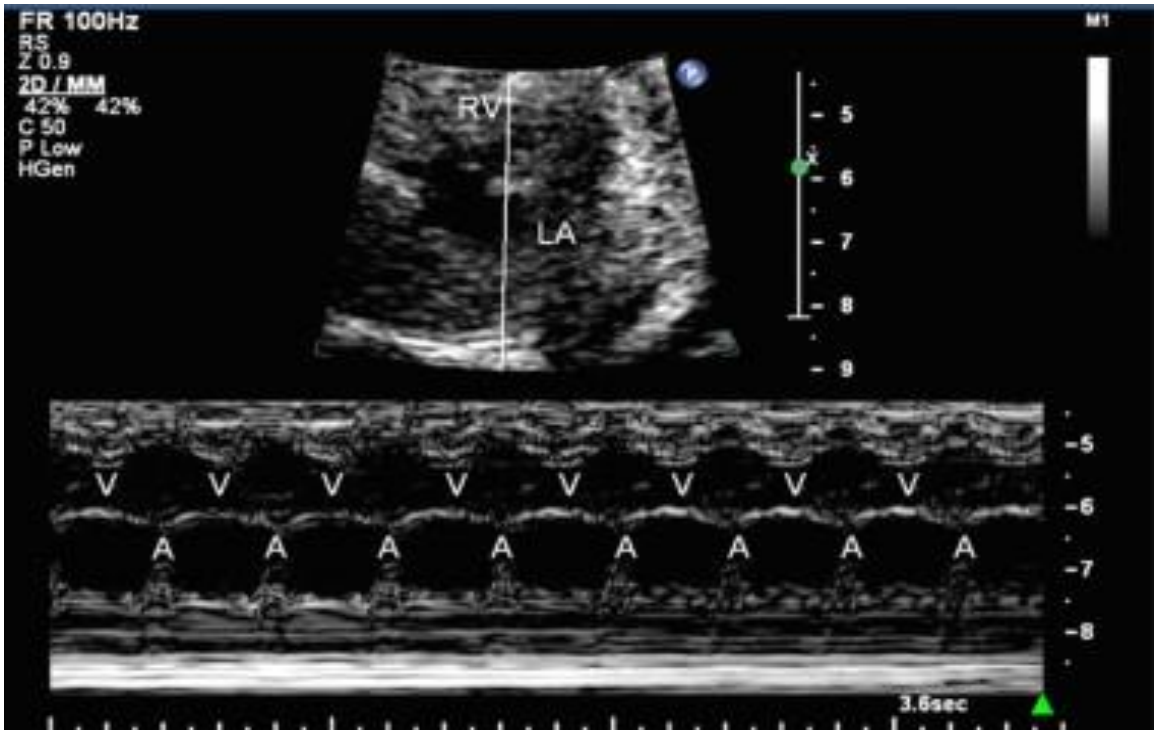


**Figure 6.2:** M-mode recording showing normal sinus rhythm. Ventricular (V) and atrial contraction (A) can be seen with the cursor positioned through the RV and LA wall. There is 1:1 conduction with each ventricular contraction preceded by an atrial contraction (Weber et al., 2011).

### Doppler Techniques

Pulsed wave Doppler can be used to assess the foetal heart rate, confirm sinus rhythm and to assist in the diagnosis of some types of foetal arrhythmia such as

foetal tachycardia and bradycardia. In order to determine rhythm, the cursor is positioned so that it is simultaneously sampling the inflow and outflow of the foetal heart. Either this can be through the left ventricular outflow tract (LVOT) and Mitral valve (MV) (Figure 6.3) or alternately it can be recorded with the cursor positioned through the pulmonary artery and the pulmonary vein. This Doppler imaging technique is used more commonly in the presence of a foetal tachycardia as at higher heart rates, the E:A (E- early diastolic filling: A-Atrial contraction) of the mitral valve inflow will fuse, making accurate assessment of the type of SVT significantly challenging.

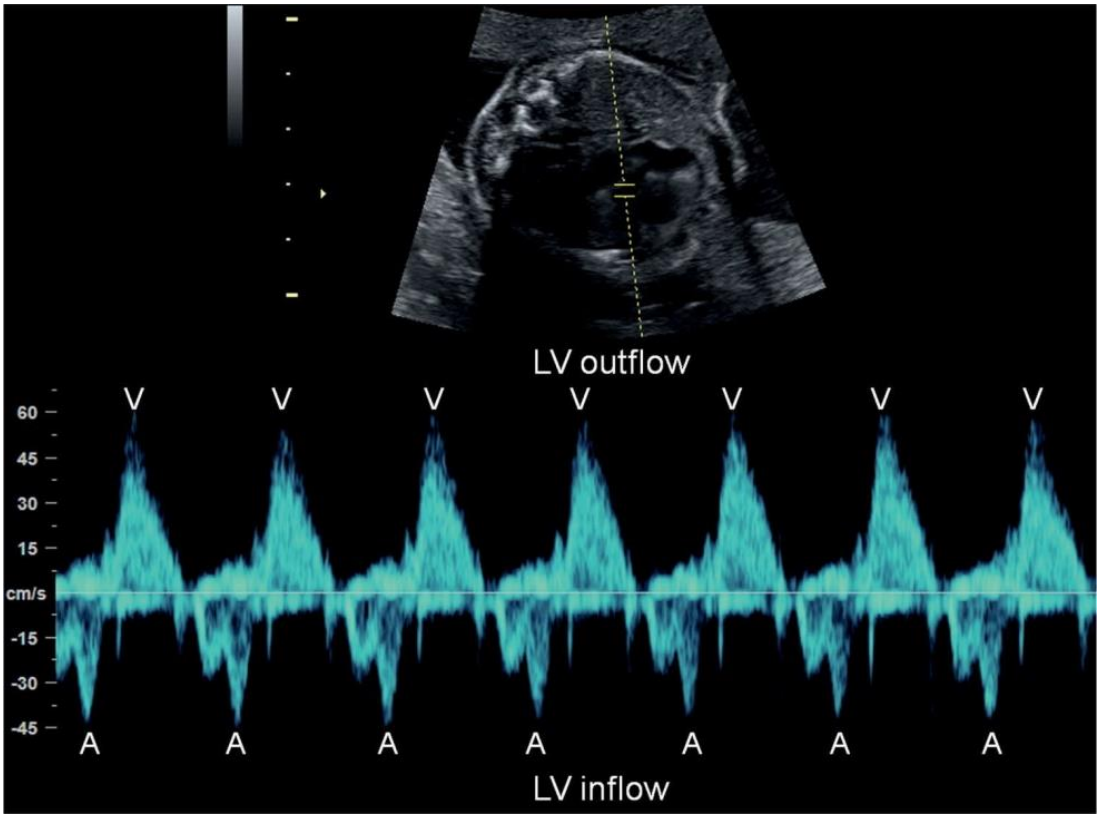


**Figure 6.3**: Pulsed wave Doppler positioned through the left ventricular (LV) outflow tract and the mitral valve demonstrating normal sinus rhythm. The mitral valve inflow waveform represents atrial contraction (A) with ventricular contraction represented by the outflow through the left ventricular outflow tract (V). 1:1 conduction can be seen representing normal sinus rhythm (Weber et al., 2011).

### Foetal Tachycardia

Foetal tachycardia is defined by a foetal heart rate above 180bpm or those normal for gestational age range as stated previously. A significant tachycardia is usually defined as a heat rate above 200bpm (Allan et al., 2009 and Simpson et al., 2018). Foetal tachycardia can be divided into two groups, ventricular tachycardia and supraventricular tachycardia (Allan et al., 2009).

Re-entry tachycardia the most common cause of foetal tachyarrhythmia (Abuhamad and Chaoui, 2022), followed by less common atrial tachycardia such as due to atrial flutter or even more rarely by atrial fibrillation (Archer and Manning, 2018). Foetal tachyarrhythmia is a treatable arrhythmia. However, if left untreated, it can lead to a reduction in cardiac function, foetal hydrops with a significant risk of foetal demise (Simpson, 2018).

### Re-entry Tachycardia

In a re-entry tachycardia there is 1:1 ratio of atrial and ventricular contractions with a heart rate typically >200 beats per minute (Figure 6.4). This can be documented via M-mode or Doppler echocardiography (Bravo-Valenzuela et al., 2018). Differentiation of the different types of tachycardia can be made by examining the time intervals between the atrial and ventricular contractions.

The most common form is the short interval between the ventricular and atrial contractions (short VA tachycardia). This tachycardia is conduction re-entry via an accessory pathway and generally has a heart rate of around 240 bpm. If the mechanism is an ectopic atrial tachycardia or a junctional reciprocating tachycardia then the ventricular and atrial interval will be long (long VA tachycardia). These are

rarer forms of tachyarrhythmia and heart rate is commonly around 200-220 bpm (Bravo-Valenzuela et al., 2018)

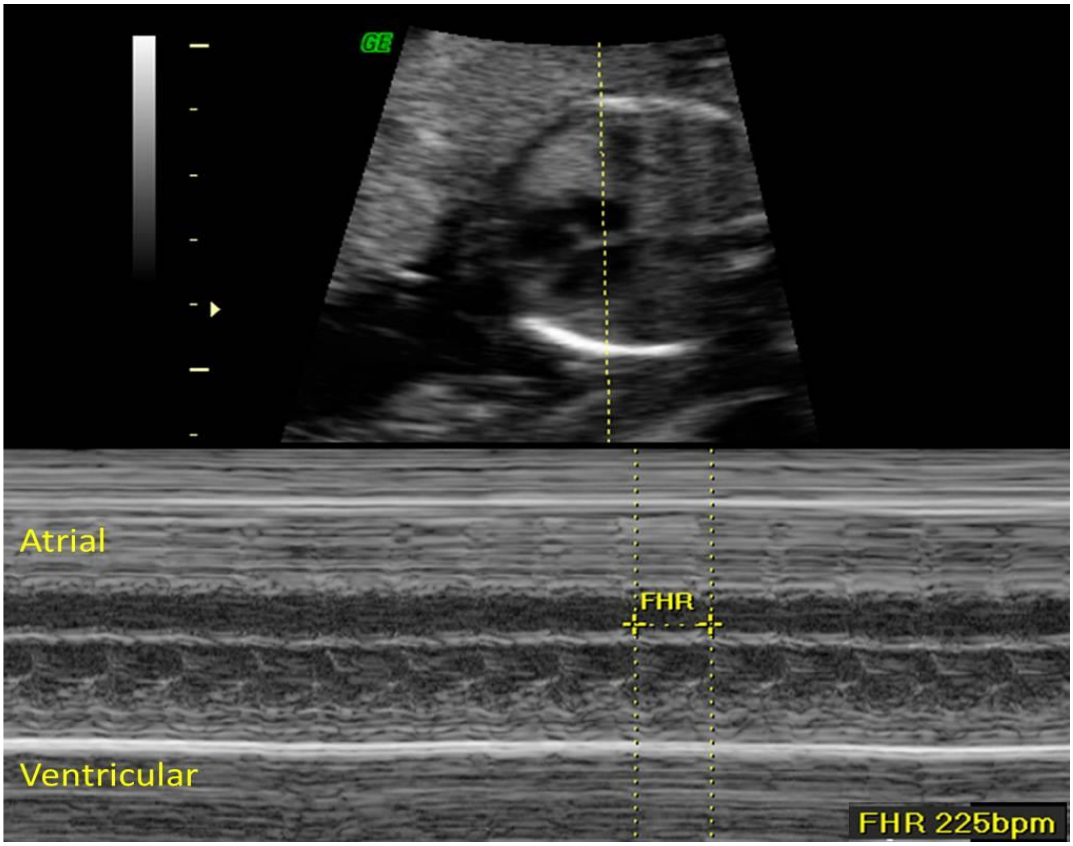


**Figure 6.4** – M-mode demonstrating foetal tachyarrhythmia with 1:1 conduction at a rate of 225bpm (Weber et al., 2011) atrial wall contraction is illustrated along the top wall, with ventricular contraction noted along the bottom of the M-mode trace

### Atrial Flutter

Foetal atrial flutter is categorised by a rapid regular atrial contraction (300-600 bpm). This often much faster atrial rate means the ventricles are unable to respond to this rapid speed in a 1:1 pattern, as the AV node is unable to conduct at such high rates leading to varying atrioventricular (AV) block. Typically, alternate flutter beats will be blocked, leading to a ventricular rate of half the atrial rate of approximately 240-250 bpm. The proposed underlying mechanism causing foetal atrial flutter is the re-

entrant circuit causing premature atrial impulses (Archer and Manning, 2018; Sharland, 2013, and Allan et al., 2009).

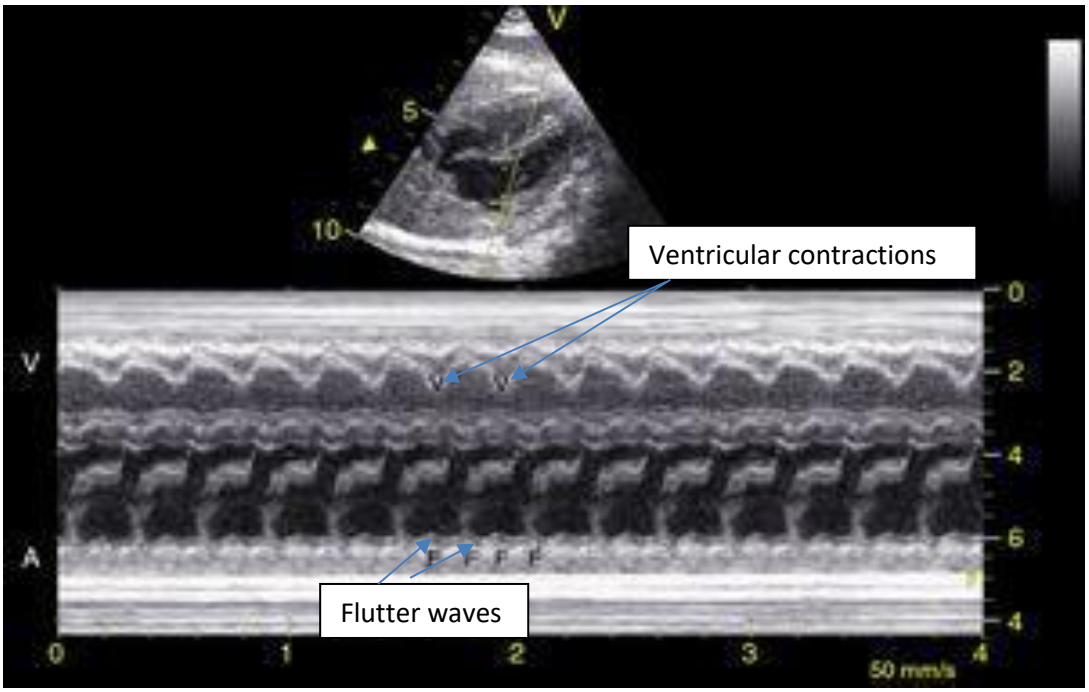


**Figure 6.5** - M-mode demonstrating foetal atrial flutter with 2:1 AV block (Weber et al., 2011)

### Fetal Heart Quantification (fetal HQ) and Speckle Tracking Echocardiography (STE)

Speckle tracking echocardiography (STE) was first introduced for adult cardiac imagining in 2004 (Leitman et al., 2004). It is an advanced technique used to assess cardiac function, particularly myocardial movement and deformation. This method utilises specialised software to track “speckles” which are natural acoustic markers within the myocardium, over a chosen timeframe (Cameli, 2022). Myocardial strain refers to the amount of deformation observed as the myocardium contracts and relaxes during each cardiac cycle, while strain rate measures the speed at which this occurs (Geyer et al., 2010). Fetal HQ is a specialised software tool used in FE to assess and quantify the size shape and function of the foetal heart using STE. The Global Sphericity Index (GSI) is a measurement obtained via echocardiography that evaluates how closely the heart resembles a sphere. It is calculated with the use of

the fetal HQ software by determining the ratio of the hearts length to the width of the epicardium. Fetal HQ assess cardiac function is via ventricular strain and strain rate.

With ongoing research and advances in foetal echocardiography there has been an increasing interest in the use of STE for the evaluation of cardiac function and deformation of the foetal myocardium (Simpson et al., 2018). Small size of the foetal heart and the movement of the foetus makes assessment of foetal cardiac function challenging (Van Oostrum et al., 2022). STE however has been found to be relatively angle independent compared with conventional methods to assess foetal cardiac function. Further, with its semi-automated technology, it has been found to have good reliability and reproducibility (Germanakis and Gardiner, 2018).

### Foetal tachyarrhythmia and Cardiac Function

Although usually well tolerated, in utero persistent or uncontrolled foetal tachycardia can lead to haemodynamic compromise with a reduction in cardiac function due to impaired ventricular filling, reduced contractility and venous congestion (weber et al., 2011). Persistent tachyarrhythmia eventually leads to impaired diastolic filling and reduced myocardial compliance. As a result, ventricular relaxation is compromised, leading to elevated central venous and filling pressures. This increased cardiac workload places significant stress on the foetal circulation and if left unmanaged can progress to foetal heart failure. (Resnik et al., 2008). Ultimately, this could lead to more serious complications such as reduced cardiac output and foetal hydrops (Weber et al., 2011 and Yuan, 2019). Foetal hydrops is a consequence of high-output cardiac failure and is characterised by the abnormal accumulation of fluid in at least two or more foetal compartments. These include ascites, pleural effusion, pericardial effusion, and skin oedema (Resnik et al., 2008). If left untreated,

progressive fluid accumulation can compromise organ function and placental perfusion, ultimately leading to intrauterine foetal demise (Dempsey et al., 2020).

The treatment goal for foetal arrhythmias is to prevent or reverse hydrops and ventricular dysfunction, as well as to control the cardiac rhythm (Purkayastha et al., 2022). However, management of foetal arrhythmia is complex, which can include antiarrhythmic drug therapy, observation with no treatment, or delivery (Weber et al., 2011). Each centre often has its own protocols. For continued assessment and treatment observation, assessment of foetal cardiac function once the rhythm has been successfully reverted into sinus rhythm is vital. There is currently a dearth of information in relation to foetal cardiac function for foetuses found to have a tachyarrhythmia that have been successfully reverted into sinus rhythm. M-mode and Doppler techniques can be used; however, these have their limitations such as foetal position, foetal movement and maternal habitus (Day et al., 2019). Though foetal STE is becoming more recognised, it remains a relatively new technique (Day et al., 2019) and is not routinely used in foetal cardiology clinics. However, due to its ability to assess early sub-clinical changes in foetal heart deformation, it could be a useful tool in assessing cardiac function in foetuses post arrhythmia. Several studies have assessed the feasibility of foetal cardiac STE with good inter and intra observer reproducibility (Crispi et al., 2012 and Maskatia et al., 2016). Fetal HQ software uses STE to assess the size, shape and function of the foetal heart (GE HealthCare 2020). GSI is a simple measurement evaluates the shape of the foetal heart. The GSI ratio is calculated by dividing the heart's basal-apical length by its transverse width at end diastole. An abnormal GSI could precede changes in cardiac function by detecting early morphological adaptions before functional abnormalities are seen (DeVore. 2016). As it is known that uncontrolled or sustained foetal tachyarrhythmia

can potentially cause significant morbidity and mortality due to cardiac dysfunction (Abuhamad and Chaoui, 2022), these changes in cardiac morphology could provide further information to aid in the management of these cases. The use of STE in the context of foetal tachyarrhythmia may offer distinct advantages over conventional functional imagining methods such as M-mode, Pulsed Doppler and MPI. Traditional methods often lack sensitivity to detect subtle myocardial dysfunction before overt clinical symptoms occur (Simpson, 2004; DeVore, 2005). STE also allows for a more angle-independent analysis of cardiac function when compared to traditional methods and therefore can help to overcome the highly variable foetal position (Simpson et al., 2018; Ohira et al., 2020). This allows for more sensitive detection of changes in cardiac function, which may persist even after arrhythmia resolution. Additionally, STE is the only modality available to assess cardiac deformation. In cases of foetal tachyarrhythmia, where cardiac function recovery may lag behind electrical stabilisation, STE could provide a valuable tool to assess myocardial function beyond what conventional imaging can detect. Reduced GLS in the foetal heart could precede clinical indications such as atrio-ventricular valve regurgitation, cardiac failure and hydrops. Given the limited existing literature addressing post foetal tachyarrhythmia myocardial function, the use of STE for GSI and GLS could provide a quantitative assessment of cardiac shape and function in this cohort and addresses a knowledge gap by evaluating the potential of this modality to serve as an additional diagnostic tool in post tachyarrhythmia surveillance.

## 6.2 – Aims and objectives

The primary aim of this case series is to evaluate the effectiveness of STE in assessing foetal cardiac morphology and function in cases of foetal tachyarrhythmia.

Specifically this study seeks to determine whether any structural or functional changes persist after restoration of sinus rhythm in affected foetuses.

The null hypothesis states that STE will detect no significant changes in foetal cardiac shape or function following the reversion to sinus rhythm in foetuses treated for tachyarrhythmia.

The objective of this case series is to establish whether STE can serve as an effective quantitative diagnostic tool for monitoring post-arrhythmic cardiac function, potentially contributing to improved perinatal and postnatal management and outcomes.

## 6.3 – Materials and Methods

The methods and materials underpinning the analysis presented in this chapter are detailed in Chapter 3. This includes information on ethics, patient selection and recruitment, instruments used, data acquisition and STE echocardiography technique for the fetal HQ software. Information on data and statistical analysis is detailed in chapter 3.7.

## 6.4 – Results

### Patient selection

**Tachyarrhythmia Group**

Seven women were recruited between February 2023 and August 2024 after presenting at the university hospitals of Leicester antenatal foetal cardiology clinic with foetal cardiac arrhythmia. GA at presentation was between $25^{+3}$ and $32^{+6}$ weeks with a mean gestational age of $31^{+4}$ weeks. Maternal age at the time of presentation was between 22 years and 33 years with a mean age of 28.1 (SD ±3.5 years SD) years. Six of the seven women (85.7%) were White British with one woman (14.3%) of Indian ethnicity.

On echocardiographic examination of the seven cases of foetal tachyarrhythmia, six cases (85%) were confirmed as having a tachyarrhythmia with 1:1 AV conduction at initial presentation, with one case (15%) presenting in atrial flutter at the first scan, however one case also altered to atrial flutter on subsequent examinations. All cases were found to have structurally normal heart with no indication of congenital heart disease. Fifteen scans were performed from the seven participants recruited. Of the 15 scans performed 80% (n-12) were within the gestational age of $32^{+1}$ – 37 weeks with 20% (n-3) with a gestational age from 26 weeks to 32 weeks.

**Control Group**

The control group is presented in detail in chapter 4. Seventy-two women were recruited, resulting in one hundred and twenty studies obtained. Maternal age range was between 18 to 43 years with a mean maternal age of 30.4 years (± 6.3 years SD). Of the seventy-two study participants recruited for the control group, 77.8% of the Women recruited were White British (n 56) 9.7% were White Other (n 7), Indian and Asian ethnicities each made up 5.6% (n 4) of the total study population, with

1.3% (n 1) being classified as other ethnicity. For the purpose of this case series the Control group used for comparison included GA $32^{+1}$-37 weeks gestation due to GA at presentation of the tachyarrhythmia group.

Medication management

In 86% (n=6) of Cases presenting with tachyarrhythmia with 1:1 conduction treatment with flecainide 100mg three times a day was initiated. In five of these six cases flecainide was successfully restored the foetal heart rhythm to sinus rhythm, as confirmed echocardiography. Medication remained unchanged in these five cases and all cases maintained sinus rhythm until delivery.

In one case, flecainide was initially successful in restoring sinus rhythm. However, throughout the pregnancy the foetus experienced recurrent episodes of tachyarrhythmia, including atrial flutter as well as episodes of sinus rhythm. Consequently, the patient was started on metoprolol in addition to flecainide. At time of delivery, the foetal heart was in atrial flutter with a controlled heart rate of 180bpm.

Another case involved atrial flutter presenting at $29^{+6}$ weeks GA. The patient was started on metoprolol, but the condition proved resistant to metoprolol alone. As a result, flecainide was introduced which lead to successful medical management with the foetal heart remaining in sinus rhythm until delivery.

### Control group data

The control group raw data and Z-scores are presented in Table 6.1. This data was obtained from a normal cohort between $32^{+1}$ and $36^{+2}$ weeks of gestation. The GSI ranged from 1.1 to 1.3, LV GLS varied from -22.59 to -28.61 and RV GLS ranged from -19.34 to -30.42. All Z-scores, except two, were within the normal range of -2 to 2, suggesting that observed variations were within expected norms. The range, mean values and SD were calculated for the GSI and the LV and RV GLS for the normal control group are also presented in table 6.1. Mean GSI was 1.18 (SD ±0.06), LV GLS mean value was -24.61 (±1.71) and the RV GLS mean value was calculated at -25.54 (±2.60).

**Table 6.1** – GSI and GLS data and Z-scores in control foetuses between $32^{+1}$ and $36^{+2}$ weeks gestation

| GA | GSI | Z-score | LV GLS % | Z-score | RV GLS % | Z-score |
|---|---|---|---|---|---|---|
| **32+1** | 1.17 | -0.35 | -24.14 | 0.27 | -28.39 | -1.09 |
| **32+1** | 1.21 | 0.36 | -21.37 | 1.89 | -24.3 | 0.48 |
| **32+2** | 1.18 | -0.17 | -26.62 | -1.17 | -25.35 | 0.08 |
| **32+3** | 1.2 | 0.18 | -22.35 | 1.31 | -25 | 0.21 |
| **32+4** | 1.15 | -0.7 | -22.19 | 1.41 | -27.61 | -0.79 |
| **32+5** | 1.1 | -1.58 | -22.55 | 1.2 | -26.96 | -0.54 |
| **32+6** | 1.17 | -0.35 | -25.28 | -0.39 | -27.08 | -0.59 |
| **32+6** | 1.26 | 1.25 | -25.42 | -0.47 | -22.36 | 1.23 |
| **33+0** | 1.13 | -1.06 | -25.74 | -0.66 | -23.51 | 0.78 |
| **33+4** | 1.18 | -0.17 | -23.78 | 0.48 | -26.75 | -0.46 |
| **33+4** | 1.16 | -0.53 | -25.66 | -0.61 | -30.03 | -1.72 |
| **33+4** | 1.26 | 1.25 | -23.77 | 0.49 | -27.33 | -0.68 |
| **34+0** | 1.3 | 1.96 | -26.12 | -0.88 | -25.4 | 0.06 |
| **34+0** | 1.24 | 0.9 | -23.35 | 0.73 | -24.35 | 0.46 |
| **34+2** | 1.1 | -1.59 | -24.3 | 0.18 | -28.11 | -0.98 |
| **34+2** | 1.2 | 0.19 | -26.55 | -1.13 | -25.99 | -0.17 |
| **34+3** | 1.13 | -1.06 | -25.39 | -0.45 | -22.14 | 1.31 |
| **34+3** | 1.14 | -0.89 | -23.69 | 0.53 | -19.34 | 2.39 |
| **34+6** | 1.26 | 1.25 | -25.14 | -0.31 | -25.56 | 0 |
| **34+6** | 1.19 | 0 | -26.2 | -0.93 | -28.22 | -1.03 |
| **35+0** | 1.24 | 0.89 | -23.31 | 0.76 | -25.2 | 0.13 |
| **35+2** | 1.16 | -0.53 | -26.56 | -1.13 | -26.12 | -0.22 |
| **35+3** | 1.15 | -0.7 | -23.31 | 0.76 | -24.57 | 0.38 |
| **35+4** | 1.16 | -0.53 | -22.61 | 1.16 | -24.54 | 0.39 |
| **35+6** | 1.1 | -1.59 | -28.36 | -2.18 | -29.28 | -1.43 |
| **36+0** | 1.23 | 0.71 | -26.7 | -1.22 | -30.42 | -1.87 |
| **36+1** | 1.26 | 1.25 | -24.01 | 0.35 | -25.67 | -0.05 |
| **36+2** | 1.22 | 0.54 | -24.42 | 0.11 | -21.33 | 1.62 |
| **36+2** | 1.29 | 1.79 | -22.59 | 1.17 | -23.01 | 0.98 |
| **36+2** | 1.15 | -0.7 | -26.8 | -1.27 | -22.54 | 1.16 |
| | | | | | | |
| **Mean** | 1.18 | | -24.61 | | -25.54 | |
| **SD** | 0.06 | | 1.71 | | 2.60 | |
| **5%** | 1.09 | | -27.42 | | -29.82 | |
| **95%** | 1.28 | | -21.80 | | -21.26 | |
| **Range** | 1.1-1.3 | | -21.37 to -28.36 | | -19.34 to -30.42 | |

Control group GSI, LV GLS and RV GLS with corresponding Z-scores for foetuses between $32^{+1}$ and $36^{+2}$ weeks gestation. Z-scores were calculated based on normative data to assess deviation from the mean. The control group demonstrated consistent values within the expected physiological range, with mean GSI of 1.18 (SD 0.06), LV GLS of -24.61% (SD 1.71) and RV GLS of -25.54% (SD 2.60).

### Tachyarrhythmia data

The raw data and z scores for the tachyarrhythmia group is presented in Table 6.3. 15 studies were analysed from 7 patient's ranging from 26 weeks to $36^{+4}$ weeks GA. GSI, LV GLS and RV GLS were recorded. LV GLS ranged from 0.91 to 1.43, with a mean of 1.16 (± 0.14). LV GLS was between -17.46% to -28.47% mean of -22.67% (±3.35%) and RV GLS was between -16.10% to -28.44%, with a mean of -23.63% (± 3.45%).

### GLS and GSI in tachyarrhythmia patients

Z-scores

Of the 15 scans performed 80% (n-12) were within the gestational age of $32^{+1}$ – 37 weeks with 20% (n-3) with a gestational age from 26 weeks to 32 weeks.

Z-scores were calculated for these 12 studies within the $32^{+1}$ – $36^{+2}$ weeks GA and are presented in Table 6.2. Z-scores for GSI of this group were within the normal range, with the exceptions of 3 studies. These Z-scores were from two patients. The first showing Z-scores of -4.95 and -4.60, these Z-scores were from the same subject (patient 5) over two different studies at $35^{+2}$ weeks and $36^{+2}$ weeks respectively. These values were from one of the two subjects that had atrial flutter. The second atrial flutter patient (patient 4) also showed a Z-score outside of the normal range, at +2.13.

Z-scores for LV GLS revealed that three participants resulting in five of the twelve measurements obtained (42%) showed Z-scores outside of the normal range (2.50 to 4.16).

RV GLS showed that all participants with the exception of one fell within the normal range of Z-scores for RV GLS. This one patient with Z-score outside of the normal

range (2.67) was also one of the two patients that had been diagnosed as having atrial flutter.

The data and Z-scores of the remaining three cases outside of the gestational age group $32^{+1}$ – $36^{+2}$ weeks can also be seen in table 6.3. Two of the three studies were from the same foetus (case 2) with GA of $26^{+0}$ weeks and $32^{+0}$ weeks. Measurements obtained for this study showed GSI Z-score at $26^{+0}$ weeks of 0.57. At $32^{+0}$ weeks the GSI Z-score was outside of the normal range at 2.31. The LV GLS Z-scores in both cases were within the normal range at -2.0 and -1.38 respectively. The RV GLS at $26^{+0}$ weeks was outside of the normal range with a Z-score of 2.49, at 32 weeks the Z-score was within the normal range at 0.39. The final case was from case 4 which were being treated for atrial flutter; in this case all Z-scores were outside of the normal range for GSI and GLS of the LV and RV.

**Table 6.2 –** GSI and GLS raw data for all tachyarrhythmia patients from GA 26 weeks to $36^{+4}$ weeks, including Z-scores

| Patient | Gestational age (weeks) | GSI | GSI Z-score | LV GLS (%) | LV GLS Z-score | RV GLS (%) | RV GLS Z-score |
|---|---|---|---|---|---|---|---|
| **1** | 34+2 | 1.10 | -1.59 | -17.46 | 4.16 | -23.25 | 0.88 |
| | 34+5 | 1.13 | -1.06 | -19.89 | 2.75 | -23.15 | 0.92 |
| **2** | 26+0 | 1.27 | 0.57 | -28.18 | -2.0 | -19.24 | 2.49 |
| | 32+0 | 1.40 | 2.31 | -28.47 | -1.38 | -25.14 | 0.39 |
| **3** | 35+6 | 1.16 | -0.53 | -22.71 | 1.10 | -28.42 | -1.10 |
| | 36+4 | 1.15 | -0.70 | -21.56 | 1.77 | -23.67 | 0.72 |
| **4 – Flutter** | 29+5 | 1.43 | 2.63 | -18.99 | 3.11 | -16.10 | 2.68 |
| | 34+2 | 1.31 | 2.13 | -20.11 | 2.62 | -18.59 | 2.67 |
| **5 – Flutter** | 34+2 | 1.13 | -1.06 | -25.37 | -0.44 | -28.44 | -1.11 |
| | 35+2 | 0.91 | -4.96 | -24.38 | 0.13 | -22.53 | 1.16 |
| | 36+2 | 0.93 | -4.60 | -25.32 | -0.41 | -25.26 | 0.11 |
| **6** | 33+4 | 1.13 | -1.06 | -20.31 | 2.50 | -26.49 | -0.36 |
| | 35+1 | 1.14 | -0.88 | -19.53 | 2.95 | -24.84 | 0.27 |
| **7** | 34+1 | 1.13 | -1.06 | -23.04 | 0.91 | -24.16 | 0.53 |
| | 35+3 | 1.13 | -1.06 | -24.68 | -0.04 | -25.23 | 0.12 |
| | | | | | | | |
| **Mean** | | 1.16 | | -22.67 | | -23.63 | |
| **SD** | | 0.14 | | 3.35 | | 3.45 | |

GSI, LV and RV GLS, and corresponding Z-scores for foetuses with tachyarrhythmia, grouped by patient and gestational age ($26^{+0}$ to $36^{+4}$ weeks). Two foetuses diagnosed with atrial flutter are highlighted separately due to the differing rhythm characteristics. Z-scores were calculated relative to normative data derived from the control cohort (table 6.1). Mean and SD values are provided for each parameter across the tachyarrhythmia group.

Comparative analysis between tachyarrhythmia and control group

The mean values and SD were calculated for the 12 tachyarrhythmia studies conducted within the gestational age range $32^{+1}$ – $36^{+2}$ weeks. The results indicate that the mean values for GSI, LV GLS and RV GLS were lower in the tachyarrhythmia group compared to the control group. A statistically significant difference was observed in GSI between the tachyarrhythmia and the control group, with a P-value <0.01 and an effect size of $r$ = 0.45, indicating a small to medium effect. Similarly, LV GLS showed a statistically significant difference between the two groups, with a P-value of <0.01 and an effect size of $r$ = 0.43, also suggesting a small to medium effect. However, no statistically significant difference was found between the groups for RV GLS (P value > 0.05). Detailed results are presented in figures 6.6 and 6.7 and Table 6.3.

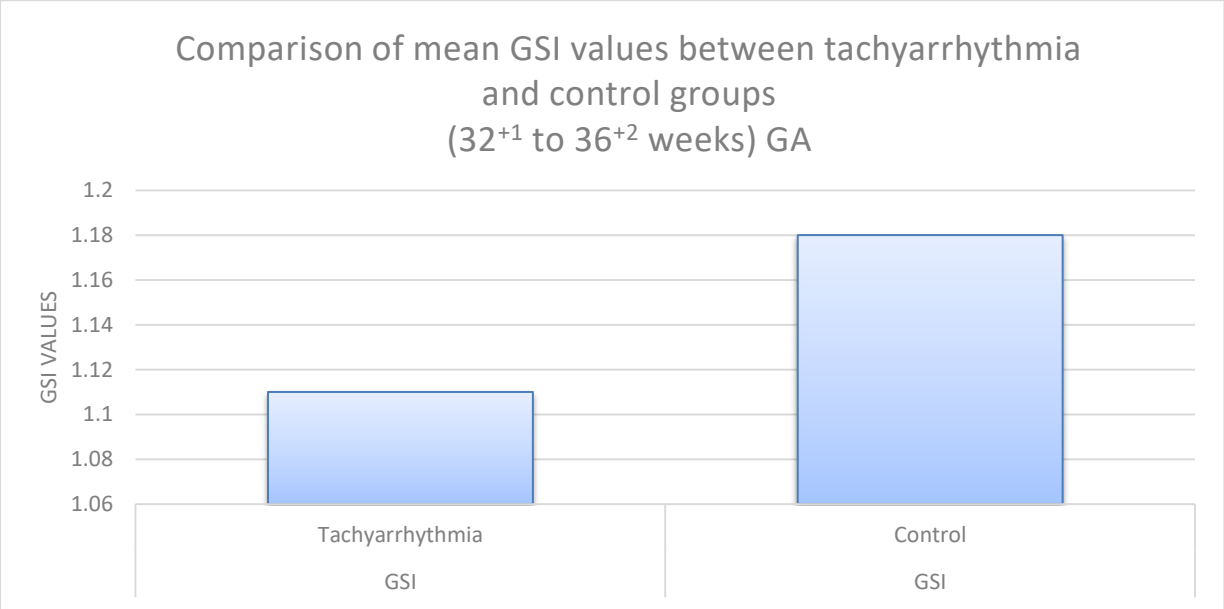


**Figure 6.6** – bar chart comparing mean GSI values between the tachyarrhythmia and control groups within the $32^{+1}$ to $36^{+2}$ weeks GA group. A reduction in mean GSI was observed in the tachyarrhythmia group compared to the control.

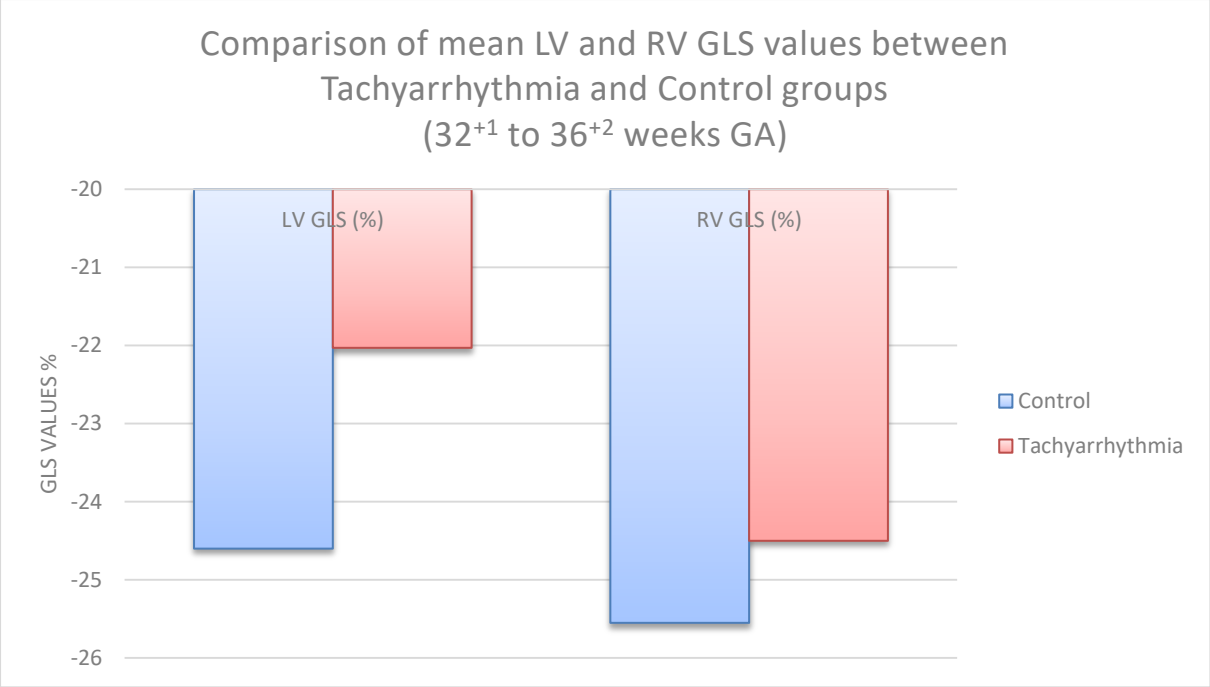


**Figure 6.7** – Grouped bar chart comparing the mean LV and RV GLS in the tachyarrhythmia and control groups. Mean LV GLS was reduced in the tachyarrhythmia group compared to the control. RV did not show a significant difference in mean RV GLS.

**Table 6.3** –Statistical analysis for tachyarrhythmia group compared to the control at $32^{+1}$ – $36^{+2}$ weeks GA.

| | P-value | Effect size (*r*) |
|---|---|---|
| **GSI** | <0.01 | 0.45 |
| **LV GLS (%)** | <0.01 | 0.43 |
| **RV GLS (%)** | 0.26 | 0.17 |

Table shows the mean and SD calculated for the tachyarrhythmia and the control group of the 12 studies analysed within the $32^{+1}$ to 37 weeks GA group. P values and effect sizes were calculated to compare the two groups

## 6.5 – Discussion

This case series aimed to evaluate the use of STE to assess foetal cardiac shape and function following the resolution of foetal tachyarrhythmia. While traditional echocardiographic techniques such as M-mode and Doppler can assess heart rate and rhythm, they lack the ability to detect subtle myocardial dysfunction. STE by contrast, offers the ability to measure myocardial strain and evaluate both global and regional ventricular function, even in the absence of overt structural abnormality (Simpson et al., 2018; Johnson et al., 2019). This is particularly relevant in tachyarrhythmia cases, where foetal cardiac function may be compromised during or after tachyarrhythmia, even if sinus rhythm is restored.

The rationale for using STE in this context lies in its ability to detect sensitive subclinical changes. Tachyarrhythmia particularly those sustained over time, can lead to alterations in loading conditions, myocardial energetics and cardiac remodelling (Hutha, 2004; Crispi and Gratacos, 2012). Conventional imaging methods may not reliably quantify these changes, especially when ventricular dimensions appear within normal range. In this study both GSI and LV GLS were significantly reduced in the tachyarrhythmia group compared to the controls, indicating there was altered myocardial geometry and function, despite the restoration to normal sinus rhythm.

The study included seven cases of tachyarrhythmia, resulting in 15 assessments. In all cases, sinus rhythm was restored during pregnancy, though at varying gestational stages. STE assessments were conducted at the points when the foetal heart had reverted to sinus rhythm.

Currently, there is a lack of research specifically investigating the use of STE in this patient cohort. However, it is well established that uncontrolled or persistent foetal

cardiac tachyarrhythmia increases the risk of foetal mortality and morbidity (Avari and Rhee, 2006; Resnik et al., 2008; Purkayastha et al., 2022). Tachyarrhythmia in foetuses who are hydronic may be more difficult to medically manage and may not respond as well to treatments initiated (Simpson et al., 1997), as absorption of drugs through the placenta at this stage may become unreliable (Purkayastha et al., 2022).

Within the seven cases being investigated, echocardiographic examination revealed five cases of SVT and two cases of atrial flutter were observed. Notably, atrial flutter cases were more challenging to manage, as they were associated with frequent episodes of breakthrough arrhythmia, making management and rhythm stabilisation more complex.

STE analysis

None of the tachyarrhythmia cases demonstrated any signs of foetal cardiac failure or developed foetal hydrops.

The analysis of the STE data in foetal tachyarrhythmia cases within the $32^{+1}$ – 37 weeks gestation revealed statistically significant differences in GSI and LV GLS compared to the controls, with a small to medium effect size noted in both cases.

Notably, GSI values were significantly lower in tachyarrhythmia cases, indicating altered myocardial contractility and potential cardiac remodelling. In cases of atrial flutter, GSI values were markedly reduced below 1.1, suggesting a shift in cardiac geometry from an elliptical shape to a more spheroidal shape. This may indicate persistent geometric cardiac remodelling due to prolonged exposure to high atrial rates and progression toward cardiac failure (Li et al., 2024; Crispi et al., 2015; Sehgal et al., 2016). Whether these foetuses exhibited 1:1 conduction or variable

block is clinically relevant, as the latter is likely to have led to lower effective cardiac output and greater haemodynamic compromise (Bravo-Valenzuela et al., 2018). Unfortunately, precise conduction ratios were not consistently documented in all cases, which limits the ability to directly correlate conduction pattern with the severity of the parameter changes.

A key observation was that LV GLS values were notably reduced in 40% (n=6) of tachyarrhythmia cases, including cases of atrial flutter, with Z-scores falling outside of the normal range. These reduced LV GLS values suggest a decline in LV myocardial function. Due to the association of reduced GSI and reduced LV GLS in the cases of atrial flutter, this could suggest a more severe impact on cardiac function with this type of arrhythmia.

Interestingly abnormal LV GLS measurements obtained from studies that had initially illustrated reduced LV GLS demonstrated improved LV GLS the longer they remained in sinus rhythm, with values and Z-scores returning to the normal range. This Suggests that cardiac dysfunction improves once the arrhythmia has been controlled, aligning with previous literature indicating that persistent arrhythmias have the potential to develop cardiac failure and potential foetal hydrops (Purkayastha et al., 2022). Early intervention of these cases may facilitate myocardial recovery. However, in this cohort, while treatment timing was recorded, the exact duration of the arrhythmia and the time between conversion and FE were not consistently available. This produces a potential cofounder, as STE may underestimate the full extent of dysfunction if recovery has begun by the time of imaging. Further protocols should consider standardising post-conversion imaging intervals to improve comparability.

While a reduction in LV GLS was evident in multiple cases. RV GLS did not show statistically significant differences between the tachyarrhythmia groups and the control groups. However, one case of atrial flutter demonstrated an abnormally reduced RV GLS Z-score suggesting potential RV dysfunction. This finding could indicate that tachyarrhythmia may have a more pronounced impact on the left ventricle, possibly due to difference in embryological development or myocardial fibre orientation.

It is also important to consider whether treatment modality may have influenced the findings. Different antiarrhythmic agents have varying pharmacological effects on myocardial function (King et al., 2024). For example, digoxin primarily slows conduction without direct negative inotropy, whereas flecainide and sotalol may have a more pronounced myocardial effects (Cuneo et al., 2017). In this case series treatment type varied across cases, and it is possible that observed strain differences were influenced in part by medication exposure or timing of administration. Larger studies would be required to assess the impact of these pharmacological effects.

The results of STE analysis for the foetal hearts being treated for atrial flutter illustrated abnormal changes in both cases. With both cases showing a reduction in GSI, and one case additionally indicating a reduction in LV and RV GLS. Importantly STE analysis identified functional myocardial changes before onset of overt clinical signs of foetal cardiac failure or hydrops, reinforcing the role of STE as a valuable tool for early detection of foetal cardiac compromise. While promising these findings should be interpreted with caution due to sample size limitations and potential variation in medication management and duration of tachyarrhythmia. Nonetheless, this case series highlights the potential role of STE as a sensitive too for assessing

functional recovery after tachyarrhythmia and may guide therapeutic decision-making and optimise outcomes. The association between atrial flutter and more pronounced reductions in GSI and LV GLS suggest that flutter may impose a greater burden on the foetal heart than SVT. Further studies are needed to explore medical management based on arrhythmia subtype.

## 6.6 – Limitations

This case series involved a small cohort of only seven arrhythmia patients. Although statistically significant differences were observed in GSI and LV GLS between groups, the limited sample size reduces the statistical power of the findings and limits generalisability. The small number of cases also precluded meaningful subgroup analysis to determine whether specific arrhythmia types such as atrial flutter, differentially impact ventricular function or cardiac geometry.

Moreover, variability in the timing of the FE assessment following conversion back to sinus rhythm may have influenced the observed myocardial recovery, as it is known that cardiac function may begin to normalise rapidly after reversion to sinus rhythm (Krapp et al., 2002), without the standardisation of imaging intervals, foetal cardiac dysfunction immediately post reversion into sinus rhythm may have been underestimated or missed altogether. These factors may compromise the reliability and consistency of the observations.

Future studies should aim to address these limitations by recruiting larger cohort numbers, standardising scan timing post tachyarrhythmia and further investigation of the mechanism of the foetal tachyarrhythmia such as atrial flutter to identify an impact on the GSI or the ventricular GLS. Further studies are needed with robust statistical analysis to prove the statistical significance or not in this cohort of patients.

It would be beneficial to include postnatal STE in future research to determine whether there is a link with abnormal GSI or ventricular GLS and persistent tachyarrhythmia in the postnatal period. This would help to establish the clinical utility of foetal STE as a tool for post tachyarrhythmia cardiac surveillance.

## 6.7 – Conclusion

Foetal tachyarrhythmia significantly alters myocardial function, as evidenced by reduced GSI and LV GLS values. These findings suggest STE may serve as a critical tool for early detection of myocardial dysfunction before overt cardiac failure or hydrops develop. However, further research needs to be conducted in order to obtain a larger cohort of tachyarrhythmia patients to identify whether the mechanism of the foetal tachyarrhythmia the timing of the FE post reversion to sinus rhythm or the treatment process has a bearing on the foetal heart shape and function. Further studies are required to look at any abnormal changes in GSI and GLS to permit a robust statistical analysis.

# Chapter 7 – Final discussion and future work

This study assessed the feasibility, reliability and reproducibility of STE in the evaluation of foetal cardiac function, specifically focussing on GSI and GLS measurements. The results demonstrated high reproducibility with good consistency in GSI and LV GLS. There was some variability in RV GLS, which could be due to the morphology of the RV. Intra- and inter-observer variability for STE, GSI and GLS parameters were assessed and demonstrated high reproducibility as detailed within chapter 4. This supports the methodological robustness of these markers within the routine clinical setting.

A key finding was the relationship between GA and LV and RV GLS, aligning with previous studies suggesting lower GLS values at higher GA (Huntley et al., 2021; Ohira et al., 2020). However, there was a stronger statistically significant correlation observed between the RV GLS and GA. This supports the notation that foetal myocardial function adapts throughout gestation (Godfrey et al., 2012). There was a statistically significant difference noted between LV and RV GLS with RV GLS values higher compared to the LV. This could be due to ongoing structural and functional maturation of the foetal myocardium and may reflect the differences in chamber compliance and load conditions between the LV and RV, which gradually equalise as gestation progresses (Dominguez-Gallardo et al., 2022; Zhu et al., 2023).

The advantage of STE over other methods of foetal cardiac functional assessment is the requirement of just a four-chamber view of the foetal heart. The acquisition of an adequate four-chamber view at as higher framerate as possible is within the normal guidelines for foetal echocardiography, with image optimisation always playing a key role in foetal echocardiography (BCCA, 2021; NHS England, 2024; Carvalho et al., 2023). Therefore, there is no need for any additional views to be obtained during the

routine foetal cardiac examination in order to obtain foetal STE analysis. Advances in ultrasound technology and transducers has improved the quality of 2D foetal echocardiography and advanced training of foetal cardiac sonographers' aids in the adequate identification of the endocardial borders of the left and right ventricles increasing the accuracy of the STE analysis for GSI measurements.

STE and disproportion

The diagnostic utility of STE lies in its ability to detect early functional myocardial changes that may precede anatomical changes. In ventricular disproportion, Underlying pathophysiological processes include altered ventricular loading conditions and pressure overload, due to obstructions such as CoA (Simpson et al., 2018). This pressure overload could lead to compensatory myocardial remodelling (Soveral et al., 2020), and reduced longitudinal strain. This study explored the role of foetal heart shape and function in cases of ventricular disproportion in the detection of an obstructive lesion. STE could potentially quantify the subclinical changes in cardiac shape and myocardial function seen in anomalies such as CoA, therefore offering prognostic insight beyond the capabilities of conventional foetal functional assessment (DeVore et al., 2021; Liu et al., 2022). Integrating STE findings with clinical context could enhance both diagnostic and prognostic planning in foetal cardiology. Previous research evaluating the use of STE in cases of ventricular disproportion have shown conflicting results, some studies have reported reduced RV GLS as well as reduced LV GLS and GSI (Germanakis et al., 2012). However earlier studies were limited by small cohort numbers, often only including two or three cases of CoA cases (Germanakis et al., 2012; Willruth et al., 2012). More recent research involved much larger cohort sizes (DeVore et al., 2021; Liu et al., 2022; Miranda et al., 2017) reinforcing the diagnostic potential of STE.

Despite advances in FE, diagnosing CoA in utero remains challenging due to high false positive rates (30%-80%), which can contribute to parental anxiety (Buyens et al., 2012; Lloyd et al., 2021). In this study 53% of cases suspected of obstruction were false positives, highlighting the difficulty in diagnosing CoA based on FE alone. However, in this study those with a confirmed obstructive lesion revealed significantly reduced GSI and LV GLS values compared to controls, aligning with previous research (DeVore et al., 2021; Miranda et al., 2017).

Statistical analysis demonstrated lower myocardial deformation in foetuses with ventricular disproportion, as reflected by reduced LV GLS values, regardless of confirmed obstruction. However, no significant differences were observed in RV GLS between the disproportion groups, the confirmed lesion group, and the controls. This finding is consistent with Liu et al. (2022) and Miranda et al. (2017), but in contrast to DeVore et al. (2021), where significant differences were found in RV GLS. These discrepancies may be due to variations in imaging techniques, ultrasound machines or software.

STE and tachyarrhythmia.

This study investigated the impact of tachyarrhythmia, including atrial flutter on myocardial function with the use of STE. The results provided evidence that foetal tachyarrhythmia may lead to significant alterations in myocardial mechanics, as demonstrated by reductions in GSI and LV GLS compared to gestational age matched controls. This may be due to the fact that in tachyarrhythmia, the sustained abnormal rhythm alters diastolic filling and myocardial perfusion, contributing to impaired ventricular relaxation and contractility. The observed reduction in GSI and GLS strain values could reflect these physiological changes, supporting the use of

STE as a potential early marker of dysfunction (Avari and Rhee, 2006; Purkayastha et al., 2022). It is known that persistent tachyarrhythmia can lead to foetal cardiac failure, foetal hydrops and ultimately intrauterine foetal demise (Avari and Rhee, 2006; Hu et al., 2023; Purkayastha et al., 2022). This case studies findings reinforced the potential use for STE as an early marker of foetal cardiac remodelling and myocardial dysfunction, even before overt clinical signs such as hydrops develop. The case series also suggested that foetuses who maintained sinus rhythm for longer durations after a tachyarrhythmia demonstrated improved LV GLS values. Incorporating STE into routine foetal echocardiographic assessments for foetal tachyarrhythmia could allow earlier risk stratification and targeted management.

While several findings reached statistical significance, particularly in LV GLS and GSI between both the subgroups compared to the controls, it is important to consider whether these differences are clinically meaningful, for example although RV GLS did not differ significantly between groups, this may not preclude clinical relevance in individual cases, especially when the complex morphology of the right ventricle is taken into consideration.

Study Aim

This study successfully achieved its primary aim of evaluating the feasibility, reproducibility and potential clinical utility of STE in routine foetal cardiac assessment. The exploration of STE's utility in cases of disproportion and foetal tachyarrhythmia provided insight into how STE can detect subclinical myocardial dysfunction in these cases before any overt clinical sign. However there were limitations particularly with relation to small subgroup sizes, particularly in the

tachyarrhythmia cohort, and lack of postnatal correlation data. These limitations may impact the generalisability and reliability of conclusions.

Future work

These results suggest that incorporating STE into routine foetal cardiac assessment is feasible, reproducible and reliable and may aid in the detection of an obstructive lesion in cases of disproportion by adding an additional functional marker to the foetal echocardiogram. Additionally STE may aid be a useful tool in the management of foetal tachyarrhythmia by assessing subclinical dysfunction of the foetal heart before overt clinic indicators or foetal hydrops are observed.

While statistically significant differences were identified in key outcomes (LV GLS and GSI), it is important to differentiate statistical from clinical significance. A statically significant result indicates that there is a low probability that the findings observed did not occur by chance, but this does not imply clinical relevance. For example the observed GSI difference between the disproportion and the arrhythmia groups compared to the mean reached statistical significance ($p < 0.01$), but whether this difference represents a meaningful alteration in cardiac geometry with clinical implications still remains uncertain.

A formal power calculation was conducted prior to data analysis (detailed in chapter 3). This was derived from a previous study assessing GLS in postnatal cases of CoA. While the target was met for the normal cohort (chapter 4), the arrhythmia and disproportion subgroups did not achieve the required sample size. These subgroup findings should therefore be interpreted with caution. Nevertheless, due to the small sample sizes effect size was reported in these cases to support interpretation of the

magnitude of observed changes and to contextualise the findings beyond p-values alone.

Future work should include multicentre studies with larger prospective cohort numbers, with postnatal follow-up for arrhythmia cases using comparable STE protocols. These larger studies will improve reference ranges and normal values and will be essential to validate these initial findings and refine clinical application of STE in foetal cardiology. Further studies are needed with robust statistical analysis to prove the statistical significance or not in the tachyarrhythmia cohort of patients. Incorporating the training of foetal HQ into foetal cardiology could aid in its use and further refine diagnostic thresholds.

The findings of this study will be disseminated through clinical education, foetal cardiology MDT meets, and future peer-reviewed publications. The ultimate goal is to improve prenatal diagnosis and management of congenital heart disease, enhance parental counselling and to in due course contribute to improved neo-natal outcomes. Over time the broader implementation of STE could potentially help to reduce unnecessary interventions in cases such as ventricular disproportion, in turn this could minimise healthcare costs and improve long-term cardiac outcomes (DeVore et al., 2021; Liu et al., 2022)

## References


1. Abuhamad, A and Chaoui R. (2022) *A Practical Guide to Fetal Echocardiography Normal and Abnormal Hearts, Fourth Edition.* Philadelphia; Lippincott Williams and Wilkins.
2. Adamo, L., Perry, A., Novak, E., Makan, M., Lindman, B. R., & Mann, D. L. (2017) 'Abnormal Global Longitudinal Strain Predicts Future Deterioration of Left Ventricular Function in Heart Failure Patients With a Recovered Left Ventricular Ejection Fraction', *Circulation. Heart failure*, *10*(6), e003788.
3. Agarwal A, Roen-Padilla S, Khemani J, Osmolovsky M, Amirtharaj C, Bhutada A, Rafii D, Ramaswamy P. (2016) 'Fetal echocardiography – A recent four year experience from a single urban centre', *Progress in Pediatric Cardiology*, 43, pp. 95-97.
4. Allan, L., Cook, A. and Huggon, I. (2009) *Fetal Echocardiography A practical Guide.* Cambridge; Cambridge University Press.
5. Anderson, R., Webb, S., Brown, N., Lamers, W. and Moorman, A. (2003) 'Development of the heart: (1) formation of the cardiac chambers and arterial trunks. *Heart*, 89(7), pp. 806-814.
6. Anuwutnavin, S., Russameecharoen, k., Ruanguvutilert, P., Viboonchard, s., Sklansky, M. and DeVore, G. (2022) 'Assessment of the Size and Shape of the 4-Chamber view and the Right and Left Ventricles Using fetal Speckle Tracking in Normal Fetuses at 17-24 Gestational Weeks', *Fetal Diagnosis and Therapy,* 49(1-2), pp. 41-51.
7. Archer. N and Manning. N. (2018) *Fetal Cardiology, second edition.* New York; Oxford University Press.

8. Arduini, D., Giannini, A., Botta, G., Bonacchi, I. and Todros, T. (2017) ‘Longitudinal strain imagining for the assessment of fetal myocardial function: A systemic review.’ *Prenatal Diagnosis*, 37(3), pp. 210-218
9. Avari, J. and Rhee, E. (2006) ‘Diagnosis and treatment of fetal tachyarrhythmias’, *US Cardiology*, *3*(2), pp.1.
10. Bansal, M. and Kasliwal R. (2013) ‘How do I do It? Speckle-tracking echocardiography’, *Indian Heart Journal,* 65, pp. 117-123.
11. Barker, P., Houle, H., Li, J., Miller, M., herlong, J. and Camitta, M. (2009) ‘Global longitudinal cardiac strain and strain rate for assessment of cardiac function: novel experience with velocity vector imaging’, *Echocardiography,* 6(1), pp. 28-36.
12. Beattie, M., Peyvandi, S., Ganisan, S. and Mood-Grady, A. (2017) ‘Toward improving the fetal diagnosis of coarctation of the aorta’, *Paediatric cardiology*, 38(2), pp. 344-352.
13. Bijnens, B., Cikes, M., Claus, P and Sutherland, G. (2009) ‘Velocity and deformation imaging for the assessment of myocardial dysfunction’, *European Journal of echocardiography,* 10(2), pp. 216-226.
14. Bravo-Valenzuela, N., Rocha, L., Machado Nardozza, L., and Araujo Júnior, E. (2018) ‘Fetal cardiac arrhythmias: Current evidence’, *Annals of pediatric cardiology,* 11(2), pp. 148–163.
15. British Congenital Cardiac Association (2021), *Fetal cardiology standards*. [Online] Available at: https//www.bcca-uk.org/fetal-cardiology [Accessed: 04 June 2024].
16. Brown, M., Burkhart, H., Connolly, H., Dearani, J., Cetta, J., Li, Z., Warnes, C. and Schaff, H. (2013) ‘Coarctation of the aorta: lifelong surveillance is

mandatory following surgical repair', *Journal of the American College of Cardiology,* 62(11), pp. 1020-1025.

17. Buckberg, G., Nanda, N., Nguyen. And Kocica, M. (2018) 'What Is the Heart? Anatomy, Function, Pathophysiology, and Misconceptions', *Journal of Cardiovascular Development and Disease*, 5(2), pp. 1-29.
18. Buyens, A., Gyselaers, W., Coumans, A., Naisiry, S., Willekes, C., Boshoff, D., Frijns, J-P, and Witters, I. (2012) 'Difficult prenatal diagnosis: fetal coarctation', *Facts, Views and Visions in obstetrics and gynecology,* 4(4), pp.230-236.
19. Cameli M. (2022) 'Echocardiography strain: why is it used more and more?', *European heart journal supplements: journal of the European Society of Cardiology*, *24*(I), pp. I38–I42.
20. Carreiro, J. (2009). An Osteopathic approach to children. The perfect companion to pediatric manual medicine by Carreiro. Second edition. Churchill Livingstone, China.
21. Carvalho, J.S., Axt-Fliedner, R., Chaoui, R., Copel, J.A., Cuneo, B.F., Goff, D., Gordin Kopylov, L., Hecher, K., Lee, W., Moon-Grady, A.J. and Mousa, H.A., (2023). ISUOG Practice Guidelines (updated): fetal cardiac screening. *Ultrasound Obstet Gynecol*, *61*(6): pp.788-803.
22. Carvalho, J., O'Sullivan, C., ShineBourne, E. and Henein, M. (2001) 'Right and left ventricular long-axis function in the fetus using angular M-mode', *Ultrasound, Obstetrics and Gynecology,* 18(6), pp. 619-622.
23. Chaudhry R, Miao JH, Rehman A. Physiology, Cardiovascular. [Updated 2022 Oct 16]. In: StatPearls [Internet]. Treasure Island (FL): StatPearls Publishing; 2023 Jan-. Available from: https://www.ncbi.nlm.nih.gov/books/NBK493197/

24. Crispi, F. and Gratacós, E. (2012) 'Fetal Cardiac Function: Technical Considerations and Potential Research and Clinical Applications', *Fetal Diagnosis and Therapy*, 32(1-2), pp. 47-64.
25. Crispi, F., Valenzuela-Alcaraz, B., Cruz-Lemini, M. and Gratacos, E. (2013) 'Ultrasound assessment of fetal cardiac function.' *Australasian Journal of Ultrasound in Medicine,* 16(4), pp. 158-167.
26. Cruz-Martinez, R., Figueras, F., Bennasar, M., Garcia-Posadas, R., Crispi, F., Hernandez-Andrade, E. and Gratacos, E. (2012) 'Normal Reference Ranges from 11 to 41 weeks' Gestation of Fetal Left modified Myocardial Performance Index by Convential Doppler with the Use of Stringent Criteria for Delimitation of the Time Periods', *Fetal Diagnosis and Therapy,* 32(1-2), pp. 79-86.
27. Cuno, B., Strasburger, J., Wakai, R. and Ovadia, M. (2017) 'Antenatal diagnosis and management of fetal arrhythmias.' Pediatric Clinics of North America, 64(6), pp. 1127-1140
28. Day T, G, Charakida, M. and Simpson J, M. (2019) 'Opinion, Using speckle-tracking echocardiography to assess fetal myocardial deformation; are we there yet?', *Ultrasound obstetrics and gynaecology*, 54, pp. 575-581.
29. Dempsey, E., Homfray, T., Simpson, J. M., Jeffery, S., Mansour, S., & Ostergaard, P. (2020) 'Fetal hydrops – a review and a clinical approach to identifying the cause', *Expert Opinion on Orphan Drugs*, *8*(2–3), pp. 51–66. Available at https://doi.org/10.1080/21678707.2020.1719827
30. Devi, G., Balakrishnan, B., Batra, M., Patil, S., Madhusoodanan, l., Hooda, R. ans Gopinathan, K. (2023) 'Role of global sphericity index in evaluation of fetal cardiac remodelling in late onset fetal growth restriction and small for gestational age fetsuses', *Journal of Clinical Ultrasound*, 51(5), pp. 796-802.

31. DeVore, G. (2005) ‘Assessing fetal cardiac function’, Seminars in Fetal and Neonatal Medicine, 10(6), pp. 515-541.
32. DeVore, G. R., Haxel, C., Satou, G., Sklansky, M., Pelka, M. J., Jone, P. N., & Cuneo, B. F. (2021) ‘Improved detection of coarctation of the aorta using speckle-tracking analysis of fetal heart on last examination prior to delivery’, *Ultrasound in obstetrics & gynecology : the official journal of the International Society of Ultrasound in Obstetrics and Gynecology*, *57*(2), 282–291. Available at: https://doi.org/10.1002/uog.21989
33. DeVore, G., Polanco, B., Satou, G and Skalansky, M. (2016) ‘The global sphericity index (GSI) of the fetal heart: its association with abnormal cardiovascular and non-cardiovascular fetal finding’, *Ultrasound in Obstetrics and Gynecology,* 48(51), pp. 69-69.
34. DeVore, G., Satou, G and Sklansky M. (2017) ‘Abnormal fetal findings associated with global sphericity Index of the four chamber view below the 5$^{th}$ centile’, *Journal of ultrasound in medicine*, 36(11), pp. 2309-2318.
35. DeVore G.R., Klas B., Satou G. and Sklansky M. (2019) ‘Quantitative evaluation of fetal right and left ventricular fractional area change using speckle-tracking technology’, *Ultrasound obstetrics and gynaecology,* 53, pp. 219-228.
36. Di Salvo, G., Russo, M., Paladini, D., Felicetti, M., Castaldi, B., Tartaglione, A., Di Pietto, L., Ricci, C., Morelli, C., Pacileo, G, and Calabro, R. (2008) ‘Two-dimensional strain to assess regional left and right ventricular longitudinal function in 100 normal foetuses’, *European Journal of echocardiography,* 9(6), pp. 754-756.

37. de Waal, K. and Phad, N. (2018) ‘A Comparison between Philips and Tomtec for Left Ventricular Deformation and Volume Measurements in Neonatal Intensive Care Patients’, *Echocardiography*, *35*, pp. 375–379.
38. Donofrio, M., Moon-Grady, A., Hornberger, L. (2014) ‘Diagnosis and treatment of fetal cardiac disease; a scientific statement from the American Heart Association.’ *Circulation*, 129(21), pp. 2183-2242.
39. Familiari, A., Morlando, M., Khalil, A., Sonesson, S.E., Scala, C., Rizzo, G., Del Sordo, G., Vassallo, C., Elena Flacco, M., Manzoli, L. and Lanzone, A., (2017) ‘Risk factors for coarctation of the aorta on prenatal ultrasound: a systematic review and meta-analysis’, *Circulation*, *135*(8), pp.772-785.
40. GE HealthCare (2020) FetalHQ Quick guide. Voluson. [Place of publication not stated]: GE HealthCare.
41. GE HealthCare (2020) ‘Voluson fetal HQ Consensus Guidelines’. Available at: https://www.volusonclub.net/download/news/file/2809 (Accessed: 2nd December 2022).
42. Gardiner, H. (2009) ‘Prenatal diagnosis of coarctation of the aorta.’ *Heart*, 95(3), pp. 246-248.
43. Germanakis, I. and Gardiner, H. (2012) ‘Assessment of fetal myocardial deformation using speckle tracking techniques’, *Fetal Diagnosis and Therapy*, 32, pp. 39-46.
44. Germanakis, I., Pepes, S., Sifakis, S. and Gardiner H. (2012) ‘Fetal Longitudinal Myocardial Function Assessment by Anatomic M-Mode*’, Fetal Diagnosis and Therapy*, 32(1-2), pp. 65-71.
45. Geyer, H., Caracciolo, G., Abe, H., Wilansky, S., Carerj, S., Gentile, F., Nesser, H. J., Khandheria, B., Narula, J., and Sengupta, P. (2010)

‘Assessment of myocardial mechanics using speckle tracking echocardiography: fundamentals and clinical applications’, *Journal of the American Society of Echocardiography: official publication of the American Society of Echocardiography*, *23*(4), pp. 351–455.

46. Godfrey, M., Messing, b., Cohen, S., Valsky, D. and Yagel, S. (2012) ‘Functional assessment of the fetal heart: a review’, *Ultrasound Obstetrics and Gynecology*, 39(2), pp. 131-144.
47. Goor, D. and Lillehei, C.W., (1975) *Congenital malformations of the heart*. NewYork; Grune & Stratton.
48. Gozar, L., Mărginean, C., Cerghit Paler, A., Gabor-Miklosi, D., Toma, D., Iancu, M., Togănel, R. and Făgărășan, A., (2021) ‘Speckle-tracking global longitudinal and regional strain analysis in neonates with coarctation of aorta: a case-control study’, *Journal of Clinical Medicine*, *10*(19), p.4579.
49. Head, C., Jowett, C., Sharland, G. and Simpson, J. (2005) ‘Timing of presentation and postnatal outcome of infants suspected of having coarctation of the aorta during fetal life’, *Heart,* 91(8), pp. 1070-1074.
50. Hede, S., DeVore, G., Satou, G. and Sklansky, M. (2020) ‘Neonatal management of prenatally suspected coarctation of the aorta’, *Prenatal Diagnosis*, 40, pp. 942-948.
51. Hernandez-Andrade, E., Benavides-Serralde, J., Cruz-Martinez, R., Welsh, A. and Mancilla-Ramirez, J. (2012) ‘Evaluation of Conventional Doppler Fetal Cardiac Function Parameters: E:A Ratios, outflow Tracts, and Myocardial Performance Index’, *Fetal Diagnosis and Therapy*, 32(1-2), pp. 22-29.
52. Ho, S. and Nihoyannopoulos, P. (2006) ‘Anatomy, echocardiography, and normal right ventricular dimensions’, Heart, 92(1), pp. i2-i13.

53. Hoit, B. (2011) ‘Strain and Strain rate Echocardiography and Coronary Artery Disease’, *Circulation Cardiovascular Imaging,* 4, pp. 179-190.
54. Hornberger, L., Sahn, D., Kleinman, C., Copel and Silverman, N. (1994) ‘Antenatal diagnosis of coarctation of the aorta: a multicenter experience’, *Journal of the American College of Cardiology,* 23(2), pp. 417-423
55. Hu, Q., Liao, H., Xu, T., Liu, H., Wang, X., and Yu, H. (2023). ‘Perinatal outcomes of intrauterine fetal arrhythmias: A 10-year retrospective cohort study’. *Medicine*, 102(10), pp. 1-8.
56. Huhta, J. (2004) ‘Guidelines for the evaluation of heart failure in the fetus with or without hydrops’, *Pediatric Cardiology*, 25(3), pp. 274-286.
57. Hunter, L. and Seale, A. (2018) ‘Prenatal diagnosis of congenital heart disease’, *Echo research and practice*, 5(3), pp. 81-100.
58. Huntley, S., Hernandez-Andrade, E., Soto, E., DeVore, G. and Sibai, B. (2021) ‘Novel Speckle Tracking Analysis Showed Excellent Reproducibility for Size and Shape of the Fetal Heart and Good Reproducibility for Strain and Fractional Shortening’ *Fetal Diagnosis and Therapy*, 48(7), pp. 541-550.
59. Johnson, C., Kuyt, K., Oxborough, D. and Stout, M. (2019) ‘Practical Tip and Tricks in Measuring Strain, Strain-Rate, Twist and Area-Deformation for the Left and Right Ventricles’, *Echo research and Practice,* 6(3), pp. R87-R98.
60. Kapusta, L., Mainzer, G., Weiner, Z., Deusch, L., Khoury, A., Haddad, S. and Lorber, A. (2013) ‘Changes in fetal left and right ventricular strain mechanics during normal pregnancy’, *Journal of the American Society of Echocardiography*, 26(10), pp. 1193-1200.
61. Koestenberger, M., Ravekes, W., Stueger, H., Heinzl, B., Gamillscheg, A., Cvirn, G., Boysen, A., Fandl, A. and Nagel, B. (2009) ‘Right ventricular

function in infants, children and adolescents; reference values of the tricuspid annular plane systolic excursion (TAPSE) in 640 healthy patients and calculation of z score values', *Journal of the American Society of echocardiography*, 22(6), pp. 715-719.

62. Krause, K., Möllers, M., Hammer, K., Falkenberg, M., Möllmann, U., Görlich, D., Klockenbusch, W. and Schmitz, R. (2017) 'Quantification of mechanical dyssynchrony in growth restricted fetuses and normal controls using speckle tracking echocardiography (STE)', *Journal of Prenatal Medicine*, 45(7), pp. 821-827.
63. Leitman,M., Lysyansky, P., Sidenko, S., Shir, S., Peleg, F., Binebaum, m., Kaluski, M., Kaluski, E., Krakover, R. and Vered, Z. (2004) 'Two-dimensional strain – a noval software for real-time quantitative echocardiographic assessment of myocardial function', *Journal of the American Society of Echocardiography,* 17, pp. 1021-1029.
64. Lee-Tannock, A., hay, K., Gooi, A. and Kumar, S. (2020) 'Global longitudinal reference ranges for fetal myocardial deformation in the second half of pregnancy', *Journal of Clinical Ultrasound*, 48(7), pp. 396-404.
65. Li S, Wang L, Yang H, Fan L. (2024) 'Changes in the shape and function of the fetal heart of pre- and gestational diabetes mothers', *BMC Pregnancy Childbirth,* 24(57), pp. 1-11.
66. Li, X., Ge, Q., Wu, Q., Hu, Y. and Liu, J. (2019) 'Developmental Changes in fetal right and left ventricular deformation: A speckle-tracking echocardiography study.' *Echocardiography*, 36(4), pp. 739-746
67. Liu, J., Cao, H., Zhang, L., Hong, L., Cui, L., Song, X., Ma, J., Shi, J., Zhang, Y., Li, Y. and Wang, J., (2022) 'Incremental value of myocardial deformation

in predicting postnatal coarctation of the aorta: establishment of a novel diagnostic model', *Journal of the American Society of Echocardiography*, *35*(12), pp.1298-1310.

68. Lloyd, D., Poppel, M., Pushparajah, K., Vigneswaran, T., Zidere V., Steinweg, J., Van Amerom, J., Roberts, T., Schulz, A., Charakida, M., Miller, O., Sharland, G., Rutherford, M., Hajnal, J., Simpson, J. and Razavi, R. (2021) 'Analysis of 3-Dimensional Arch Anatomy, Vascular Flow, and Postnatal Outcome in Cases of Suspected Coarctation of the Aorta Using Fetal Cardiac Magnetic Resonance Imaging', *Circulation – Cardiovascular Imaging,* 14(7), pp. 583-593
69. Lou, Y., Zhao, B., Pan, M., Huang, L., Lu, X., Zhang, X and Peng, X. (2024) 'Quantitative Analysis of Morphology and Function in the Fetal Heart with Severe Tricuspid Regurgitation by Speckle Tracking Imaging', *Pediatric Cardiology,* 45, pp. 740-748.
70. Luo, L., Liu, H., Zhou, S., Zhao, F., Zhu, Q., Guo, N. and Chen, J. (2021) 'Quantitative evaluation of fetal ventricular function by speckle tracking echocardiography', *Echocardiography*, *38*(11), pp.1924-1931.
71. Maskatia, S., Pignatelli, R., Ayres, N., Altman, C., Sangi-Haghpeykar, H., and Lee, W. (2016) 'Fetal and Neonatal Diastolic Myocardial Strain Rate: Normal Reference Ranges and Reproducibility in a Prospective, Longitudinal Cohort of Pregnancies', *Journal of the American Society of Echocardiography, 29*(7), pp. 663–669. Available at: https://doi.org/10.1016/j.echo.2016.02.017
72. Matsui, H., Mellander, M., Roughton, M., Jicinska, H. and Gardiner, H. M. (2008) 'Morphological and physiological predictors of fetal aortic coarctation', *Circulation*, 118(18), pp. 1793-1801.

73. Maulik D., Nanda N., Maulik D. and Vilchez G. (2017) ‘A brief history of fetal echocardiography and its impact on the management of congenital heart disease’, *Echocardiography,* 34(12), pp. 1760-1767.
74. Miranda, J., Hunter, L., Tibby, S., Sharland, G., Miller, O. and Simpson, J. (2017) ‘Myocardial deformation in fetuses with coarctation of the aorta: a case-control study’, *Ultrasound in obstetrics & gynecology : the official journal of the International Society of Ultrasound in Obstetrics and Gynecology*, 49(5), pp. 623–629.
75. Moon-Grady, A., Tacy, T., Lee, W. and Donofrio, M. (2021) ‘Strain imagining in the fetus: evolving clinical utility for myocardial deformation assessment.’ *Journal of the American Society of Echocardiography*, 34(8), pp. 820-831
76. Myocardial Mechanics: Structure and Function of Myocardial Fibers – Cardiovascular Education (ecgwaves.com) (accessed 07/03/2024)
77. Negishi, T and Negishi K. (2022) ‘How to standardize the measurement of global longitudinal strain’, *Journal of Medical Ultrasonics*, 49, pp. 45-52.
78. NHS England (2024) *Fetal anomaly screening programme handbook*. [Online] Available at: http://www.gov.uk/government/publicaions/fetal-anomaly-screening-programme-handbook [Accessed on 15 August 2024].
79. Ohira, A., Hayata, K., Mishima, S., Tani, K., Maki, J., Mitsui, T., Eto, E. and Masuyama, H. (2020) ‘The assessment of the fetal heart function using two-dimensional speckle tracking with a high frame rate’, *Early Human Development,* 151, pp. 105160.
80. OpenStax College (2013), *Development of the heart* [image]. Available at: https://en.wikipedia.org/wiki/Heart_development#/media/File:2037_Embryonic_Development_of_Heart.jpg [Accessed: 23 June 2025].

81. Opie, L., Commerford, P., gersh., B and Pfeffer, M. (2006) ‘Controversies in ventricular remodelling’, *The Lancet*, 367(9506), pp. 262-272.
82. Pasquini, L., Mellander, M., Seale, A., Matsui, H., Roughton, M., Ho, S.Y. and Gardiner, H.M., (2007) ‘Z-scores of the fetal aortic isthmus and duct: an aid to assessing arch hypoplasia’, *Ultrasound in Obstetrics and Gynecology: The Official Journal of the International Society of Ultrasound in Obstetrics and Gynecology*, *29*(6), pp.628-633.
83. Patti, L., Horenstein, M.S. and Ashurst, J.V., 2025 Supraventricular Tachycardia. *StatPearls [Internet]*. Treasure Island (FL): StatPearls Publishing. [Updated 18 February 2025]. Available from: https://www.ncbi.nlm.nih.gov/books/NBK441972/ [Accessed 29th July 2025].
84. Peixoto, A., Bravo-valenzuela, N., Martins, W., Tonni, G., Mattar, R., Moron, A., Pares, D. and Junior, E. (2020) ‘Reference ranges for the fetal mitral, tricuspid, and interventricular septum annular plane systolic excursions (mitral annular plane systolic excursion, tricuspid annular plane systolic excursion, and septum annular plane systolic excursion) between 20 and 36+6 weeks of gestation’, *Journal of Perinatal Medicine,* 48(6), pp. 601-608.
85. Pérez-Cruz, M., Cruz-Lemini, M., Fernández, M.T., Parra, J.A., Bartrons, J., Gómez-Roig, M.D., Crispi, F. and Gratacós, E., (2015) ‘Fetal cardiac function in late-onset intrauterine growth restriction vs small-for-gestational age, as defined by estimated fetal weight, cerebroplacental ratio and uterine artery Doppler’, *Ultrasound in Obstetrics & Gynecology*, *46*(4), pp.465-471.
86. Purkayastha, S., Weinreich, M., Fontes, J. D., Lau, J. F., Wolfe, D. S., & Bortnick, A. E. (2022) ‘Fetal Supraventricular Tachycardia: What the Adult

Cardiologist Needs to Know', *Cardiology in review*, *30*(1), pp. 31–37. Available at: https://doi.org/10.1097/CRD.0000000000000370

87. Rajiah P, Mak C, Dubinksy M. (2011) 'Ultrasound of Fetal Cardiac Anomalies', *The American Journal of roentgenology.* 197(4), pp. 747-760.
88. Remien K, Majmundar SH. Physiology, Fetal Circulation. [Updated 2023 Apr 26]. In: StatPearls [Internet]. Treasure Island (FL): StatPearls Publishing; 2025 Jan-. Available from: https://www.ncbi.nlm.nih.gov/books/NBK539710/
89. Resnik, R., Creasy, R.K., Iams, J.D., Lockwood, C.J., Moore, T. and Greene, M.F., 2008. *Creasy and Resnik's maternal-Fetal medicine: Principles and practice E-book*. Elsevier Health Sciences.
90. Riffel, J., Keller, M., Aurich, M., Sander, Y., Andre, F., Giusca, S., Siepan, F., Seitz, S., Galuschky, C., Korosoglou, G., Merele, d., Katus, H. and Buss, s. (2015) *'*Assessment of global longitudinal strain using standardized myocardial deformation imaging: a modality independent software approach', *Clinical Research in Cardiology,* 104, pp. 591-602.
91. Robinson, S., Ring, L., Oxborough, D., Harkness, A., Bennett, S., Rana, B., Sutaria, N., Lo Giudice, F., Shun-Shin, M., Paton, M., Duncan, R., Willis, J., Colebourn, C., Bassindale, G., Gatenby, K., Belham, M., Cole, G., Augustine, D., and Smiseth, O. A. (2024) 'The assessment of left ventricular diastolic function: guidance and recommendations from the British Society of Echocardiography', *Echo research and practice*, *11*(1), pp. 16.
92. Rocha, L., Rolo, C. and Junior, E. (2019) 'How to perform a functional assessment of the fetal heart: a pictorial review*', Ultrasonography* 38(4), pp. 365-373.

93. Rosenthal, E. (2005) ‘Coarctation of the aorta from fetus to adult: curable condition or lifelong disease process’, *Heart,* 100(6), pp. 2286-2290.

94. Sadler, T.W. (2018). *Langmans Medical Embryology*. 14th edition. Philadelphia: Wolters Kluwer

95. Semmler J., Day, T., Georgiopoulos g., Garcia-Gonzalez, C., Aguilera, J., Vigneswaran, T., Zidere, V., Miller, O., Sharland, G., Charakida, M, and Simpson J. (2020) ‘Fetal Speckle-Tracking: Impact of Angle of Insonation and Frame Rate on Global Longitudinal Strain’, *Journal of the American Society of Echocardiography*, 33(9), pp. 1141-1146.

96. Sharland, G. (2013). *Fetal Cardiology Simplified: A Practical Manual.* United Kingdom; Tfm Publishing.

97. Shen, Y., Tan, F., Yang, J., Fan, S., Zhang, L. and Ji, X. (2022) ‘A preliminary study on fetal cardiac morphology and systolic function of normal and anaemic pregnant women by fetal heart quantification technology’, *Translational Pediatrics,* 11(8), pp. 1336-1345.

98. Simpson, J. (2018) *Fetal Cardiac function* in Simpson, J., Zidere, V. and Miller, O. *Fetal Cardiology. A practical Approach to Diagnosis and Management.* London; Springer International Publishing.

99. Simpson, J. (2011) ‘Speckle tracking for the assessment of fetal cardiac function’, *Ultrasound Obstetrics and Gynecology,* 37(2), pp.133-134.

100. Simpson, J. (2004) ‘Echocardiographic evaluation of cardiac function in the fetus’, *Prenatal Diagnosis*, 24(13), pp. 1081-1091.

101. Singh, S., Hakim, F.A., Sharma, A., Roy, R.R., Panse, P.M., Chandrasekaran, K., Alegria, J.R. and Mookadam, F. (2015) ‘Hypoplasia,

pseudocoarctation and coarctation of the aorta–a systematic review', *Heart, Lung and Circulation*, 24(2), pp.110-118.

102. Soveral, I., Crispi, F., Walter, C., Guirado, L., García-Cañadilla, P., Cook, A., Bonnin, A., Dejea, H., Rovira-Zurriaga, C., Sánchez de Toledo, J., Gratacós, E., Martínez, J.M., Bijnens, B. and Gómez, O. (2020), 'Early cardiac remodeling in aortic coarctation: insights from fetal and neonatal functional and structural assessment'. *Ultrasound Obstetrics and Gynecology*, 56(1), pp. 837-849.

103. Van Mieghem, T., Gucciardo, L., Lewi, P., Lewi, L., Van Schoubroeck, D., Devlieger, R., De Catte, L., Verhaeghe, J. and Deprest, J. (2009) 'Validation of the fetal myocardial performance index in the second and third trimesters of gestation', *Ultrasound, Obstetrics and Gynecology*, 33(1), pp. 58-63.

104. Van der Linde D, Konings E.E.M, Slager M.A, Witsenburg M, Helbing W.A, Takkenberg J.J.M, Roos-Hesselink J.W. (2011) 'Birth Prevalence of Congenital Heart Disease Worldwide. A systematic Review and Meta-Analysis', *Journal of the American College of Cardiology*, 58(21), pp. 2241-2247.

105. Van Nisselrooij, A., Rozendaal, L., Clur, S., Hruda, J., Pajkrt, E., Van Velzen, C., Blom, N. and Haak, M. (2018) 'Postnatal outcome of fetal isolated ventricular size disproportioin in the absence of aortic coarctation', *Ultrasound in Obstetrics and Gynecology.* 52(5), pp. 593-598.

106. Van Oostrum, N., De Vet, C., Van De Woude.,Kemps, H., Guid Oei, S, and Van Laar, J. (2020) 'fetal strain and strain rate during pregnancy measured with speckle tracking echocardiography: A systemic review'

*European journal of obstetrics and Gynecology and Reproductive Biology*, 250, pp. 178-187.

107. Van Oostrum, N., De Vet, C., Clur, S., Van De Woude., Van Den Heuvel., Oei, S. and Van Laar, J. (2022) 'Fetal Myocardial deformation measured with two-dimensional speckle-tracking echocardiography: longitudinal prospective cohort study of 124 healthy foetuses', *Ultrasound in Obstetrics and Gynecology.* 59(5), pp 651-659.

108. Vigneswaran, T., Zidere, V., Chivers, S., Chorkida, M., Akolekar, R. and Simpson J. (2020) 'Impact of prospective measurement of outflow tracts in prediction of coarctation of the aorta', *Ultrasound obstetrics and gynaecology,* 56(6), pp. 850-856.

109. Wang, D., Liu, C., Liu, X., Zhang, Y., & Wang, Y. (2021) 'Evaluation of prenatal changes in fetal cardiac morphology and function in maternal diabetes mellitus using a novel fetal speckle-tracking analysis: a prospective cohort study', *Cardiovascular ultrasound*, *19*(1), pp. 25. Available at: https://doi.org/10.1186/s12947-021-00256-z

110. Willruth, A., Geipel, A., Merz, W, and Gembruch, U. (2012) 'Speckle tracking – a new ultrasound tool for the assessment of fetal myocardial function', *Z Geburtshilfe Neonatol*, 216(3), pp. 114-121.

111. Yang, J., Tan, F., Shen, Y., Zhao, Y., Xia, Y., Fan, S. and Ji, X., (2023) 'Assessing Coarctation of the Aorta with Fetal Heart Quantification Technology', *Maternal-Fetal Medicine*, 3(6), pp.147-155.

112. Yingchoncharoen, T., Agarwal, s., Popovic, Z and Marwick, T. (2013) 'Normal ranges of left ventricular strain: a meta-analysis', *Journal of the American Society of Echocardiography,* 26, pp. 185-191.

113. Yuan, S. (2019) ‘Fetal arrhythmias: Surveillance and management.’ *Hellenic Journal of Cardiology,* 60(2), pp. 72-81.

114. Weber, R., Stambach, D., and Jaeggi, E. (2011) ‘Diagnosis and management of common fetal arrhythmias’, *Journal of the Saudi Heart Association*, 23(2), pp 61–66. Available at: https://doi.org/10.1016/j.jsha.2011.01.008

# Appendices

## Appendix 1 - Voluson, fetal HQ Quick Guide

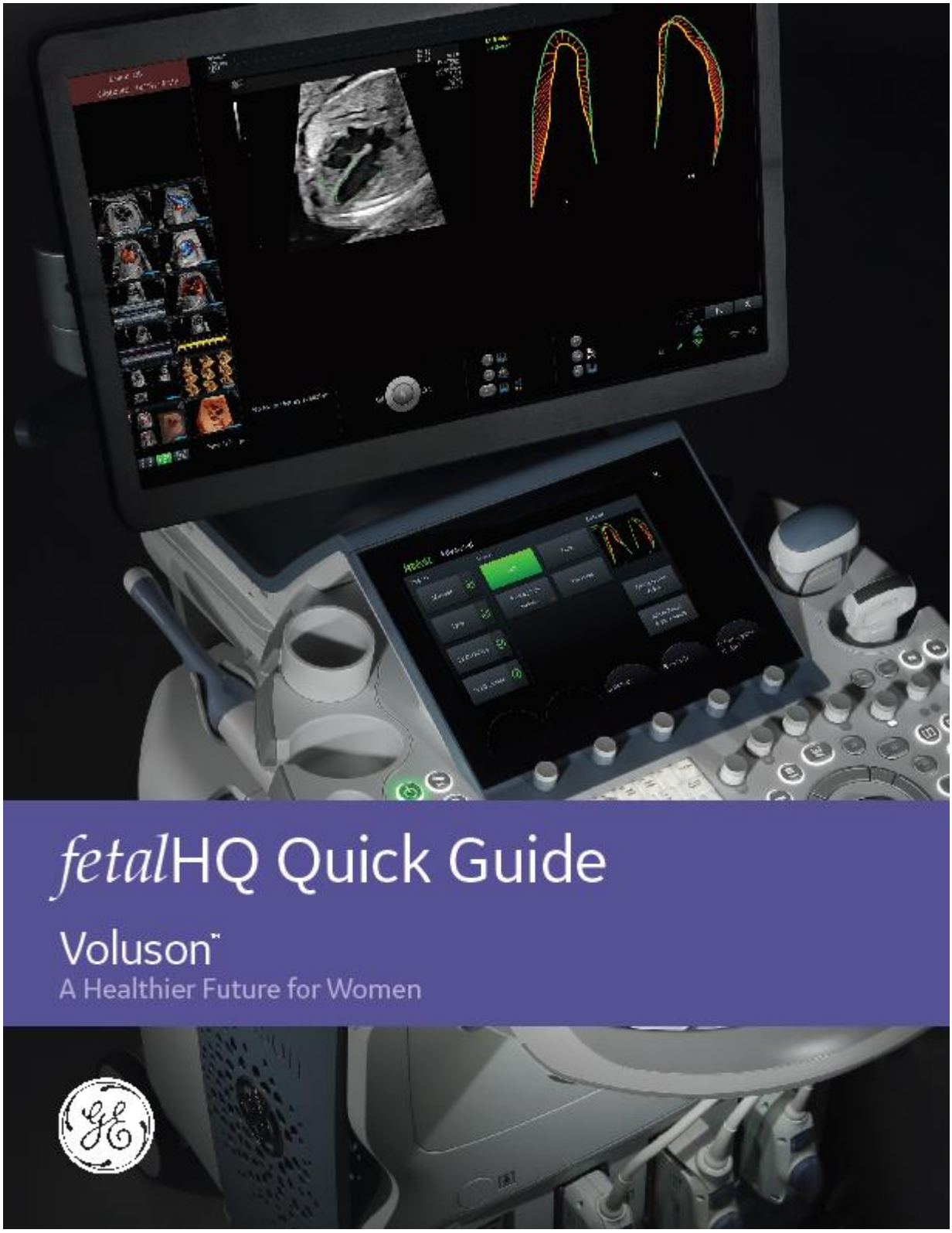

## Appendix 2 - GE Healthcare Voluson fetal HQ Consensus Guidelines

# Voluson™ *fetal*HQ Consensus Guidelines

Conduct an easy and comprehensive evaluation of the size, shape and contractility of the fetal heart from the 4-chamber view using measurements based on 2D imaging and speckle tracking. *fetal*HQ contains an in-depth report page including z-scores and percentiles for each of the cardiac measurements. These consensus guidelines can provide steps to optimize your *fetal*HQ exams.

### ACQUISITION OF AN IDEAL 4-CHAMBER VIEW FOR *fetal*HQ

**Septal Orientation**

- Choose Fetal Cardiac Preset – Harmonic mid or low, narrow angle, low depth
- Frame rate: min. 80 Hz*
- Heart located centrally within the image
- Orientation:
  - Septum horizontal, 3 or 9 o'clock position, up to ±45° from horizontal – orientations marked in green are preferred
  - Scan between the ribs, no rib shadow visible

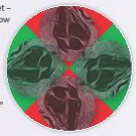

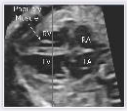


Optimal 4-chamber view from a 25 week fetus.


B-Plane at the desired level (blue line should be between the two papillary muscles of the left ventricle, and just off center to the papillary muscle of the right ventricle at the maximum width of the heart.

**Left ventricle: papillary muscles should not be visible.**
**Right ventricle: papillary muscle can be visible during systole, moderator band can be visible.**

- Obtain recording in absence of fetal corporal and respiratory movements
- Consider asking mother to hold her breath
- Avoid arrhythmia during the acquisition, repeat if necessary
- Save 2-3 seconds clip (approximately 3-5 cardiac cycles)

* Goal of *fetal*HQ is to have a good contour detection to outline the endocardium in ES and ED. Frameretes < 100 Hz are considered acceptable because ES and ED tracings are adjusted manually if needed. For Strain Analysis of the entire cardiac cycle, frameretes > 100 Hz are recommended.

### OBTAIN GLOBAL SPHERICITY INDEX – SIZE AND SHAPE


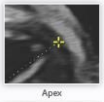




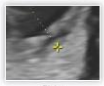


Go to end diastolic image (1st image where AV valves are closed)

- Set 4CV-Length: Epicardium (apex), parallel to the ventricular septum to epicardium (between right and left atrium, outside the atrial septum)
- Set 4CV-Width: Epicardium to epicardium on the widest diameter, perpendicular to the septum

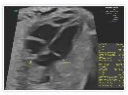

Image of normal size and shape results

- Size: 4CV-Length, 4CV-Width, Area
- Shape: GSI (Global Sphericity Index)

Image highlights abnormal size and shape due to aortic stenosis.

### VENTRICULAR ANALYSIS FOR CONTRACTILITY

**STEP 1 | DEFINE ORIENTATION**


Orientation acceptable

Orientation not acceptable – flip

- Left ventricle should be on the left, if apex is up – Left ventricle should be clockwise before the right ventricle
- If not, flip function on touch panel

**STEP 2 | SELECT ONE CARDIAC CYCLE**

Draw M-Mode line from apex through the lateral base of the right ventricle (tricuspid valve lateral anulus).

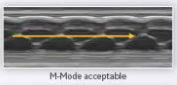

M-Mode acceptable

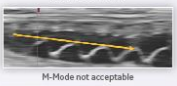

M-Mode not acceptable

On M-Mode tracing, ensure there is no drifting (due to fetal movement or maternal breathing).

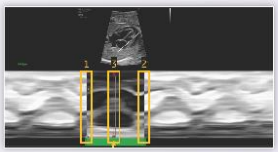


1. Select end diastole (mid portion of the lowest anulus position on M-Mode trace); if visible, 1st image after AV-valves closed
2. Select end diastole to mark end of selected cycle
3. Select end systole between the 2nd diastole markers (highest anulus position on M-Mode trace); if visible, 1st image before AV-valves open

**STEP 3 | DEFINE LEFT VENTRICULAR END-SYSTOLIC ENDOCARDIAL TRACING**

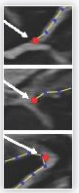

Adjust tracing if needed:
1. Adjust **red** anchor points first
2. Fine tune on **blue** dots

Tracing should be placed on the endocardial border.
1. Septal mitral valve insertion
2. Lateral mitral valve insertion
3. Apex

**STEP 4 | DEFINE LEFT VENTRICULAR END-DIASTOLIC TRACING**

Adjust **red** dots if needed (contour should follow endocardial border).

**STEP 5 | DEFINE RIGHT VENTRICULAR END-SYSTOLIC ENDOCARDIAL TRACING**

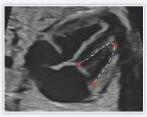

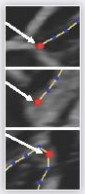

Adjust tracing if needed:
1. Adjust **red** anchor points first
2. Fine tune on **blue** dots

Tracing should be placed on the endocardial border.
1. Septal tricuspid valve insertion
2. Lateral tricuspid valve insertion
3. Apex

Papillary Muscle should be inside the contour.
Moderator Band (if visible) should be inside contour.

**STEP 6 | DEFINE RIGHT VENTRICULAR END-DIASTOLIC TRACING**

Adjust **red** dots if needed (contour should follow endocardial border).

### *fetal*HQ REPORT AND RESULTS

**Advanced Report**

**Global Analysis**

- Size: 4CV-Length, 4CV-Width, Area
- Shape: GSI (4CV-Length/4CV-Width)


Based on 24 segment analysis for right and left ventricle.

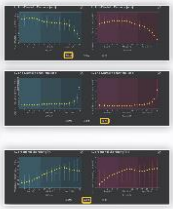

- Size – End Diastolic Diameter (ED)
- Shape – Sphericity Index (SI): ventricular length/ end diastolic diameters
- Contractility – Fractional Shortening (FS): (end-diastolic diameter-end-systolic diameter)/ end-diastolic diameter x 100

* Goal of *fetal*HQ is to have a good contour detection to outline the endocardium in ES and ED. Frameretes < 100 Hz are considered acceptable because ES & ED tracings are adjusted manually if needed. For Strain Analysis of the entire cardiac cycle, frameretes > 100 Hz are recommended.

GE would like to thank the following expert contributors for their scientific guidance: Prashant Acharya, Hagai Avnet, Greggory DeVore, Christian Ehlendorfer, Edgar Hernandez Andrade, Kwang Jun Kim, Wesley Lee, Jose Ochoa, Katsuzoku Ozawa, Olga Patey, Luigi Raio, Mette Tind Tindholdt, Renato Ximenes, Simcha Yagel and Satoshi Yasukochi.

## Appendix 3 - Quick Guide for the use of fetal HQ.

# Fetal HQ Image acquisition and data collection quick guide

## Obtain and store a 4- chamber heart clip

- Choose fetal cardiac pre-set
- Include mitral/tricuspid valve insertions, clear view of apex, **NOT** in apical view for optimal view of endocardium.
- Frame rate ≥80Hz For strain analysis of the entire cardiac cycle frame rate >100Hz are recommended
- Heart located centrally within the image
- Septum horizontal, 3 or 9 o'clock position.
- Obtain in-between ribs to avoid shadows.
- 2-3 second clip
- Minimal fetal movement.
- Heart should be orientated with left ventricle and right ventricle in a clockwise position. Flip image if necessary.

Figure 1

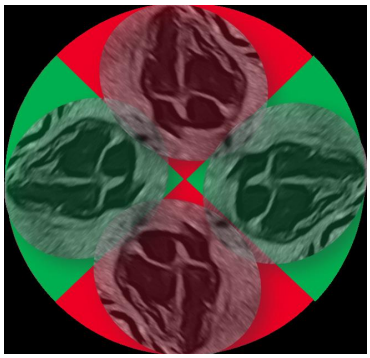

**Septum horizontal, 3 or 9 o'clock position, up to ±45° from horizontal orientations marked in green are preferred**

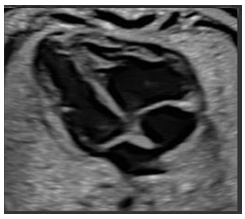

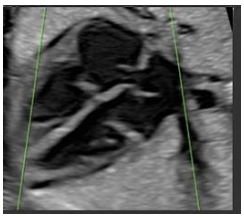

Accepted Orientation

Flipping does not affect any measurement data.

**Left ventricle**: papillary muscles should not be visible

Orientation not acceptable – image can be flipped

**Right ventricle**: Papillary muscle can be visible during systole, moderate band can be visible.

- Recording should be obtained in the absence of fetal corporal and respiratory movements.
- Avoid arrhythmia during the acquisition.

Consider asking mother to hold her breath if necessary.

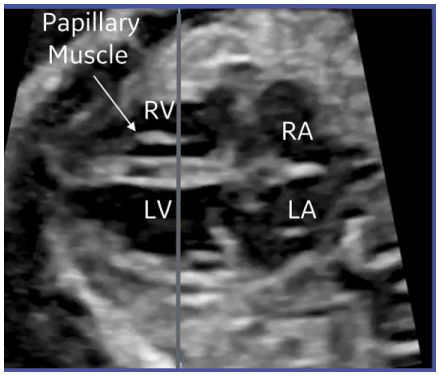


Optimal 4-chamber view from 25 week fetus

## Global Sphericity Index Measurement (GSI)

## Provides information as to the size and shape of the *entire* fetal heart

- Recall the clip and scroll to the end diastole frame.
- Select Calc key, then FetalHQ from the touch panel
- Select Global Size and Shape Study and measure the length and width of the heart, **epicardrdium to epicardium in end diastole.**
- Set 4CV-length: epicardium(apex), parallel to the ventricular septum to epicardium (between right and left atrium, outside of atrial septum)
- Set 4CV-width: Epicardium to epicardium on the widest diameter, perpendicular to the septum.

Image shows fetal heart in end diastole where the AV valves are closed. 4CV is measured from epicardium to epicardium in length and width.

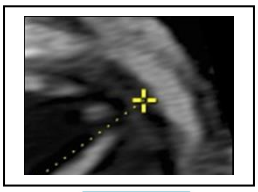

Apex

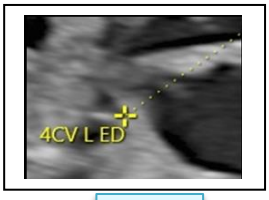


BASE

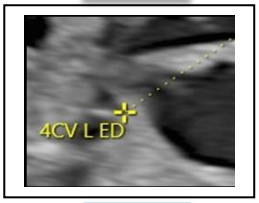


Left

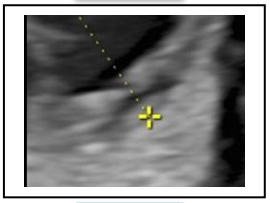

Right

## Ventricular analysis for contractility

**Step 1. – Define orientation**

Left ventricle should be on the left if apex is up – left ventricle should be clockwise before the right ventricle. If not, then the image needs to be flipped using the function on the touch panel.

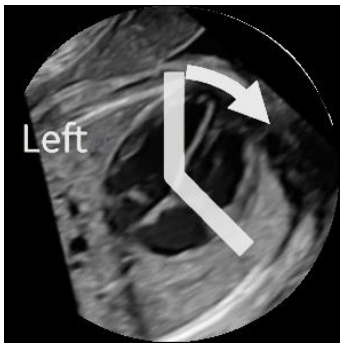


Image shows four chamber view with left ventricle in clockwise position before the right ventricle.

Acceptable orientation can be seen in acquisition section at the beginning of this paper.

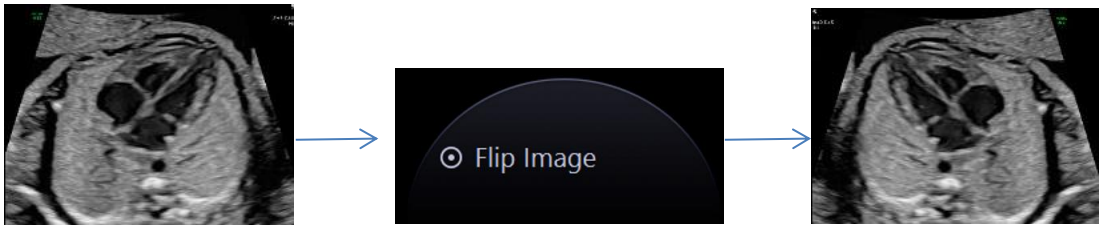


**Step 2. – Select one cardiac cycle**

Draw M-mode line from apex through the lateral base of the right ventricle (TV annulus)

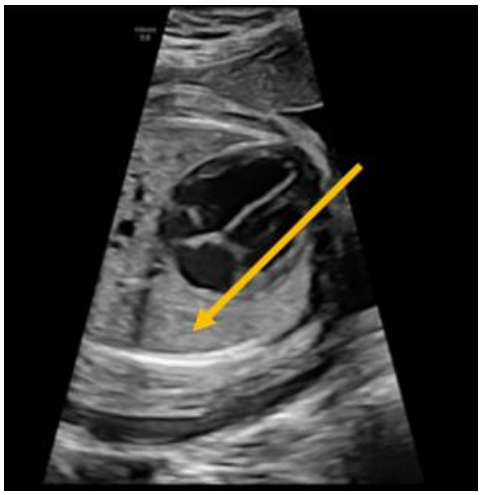

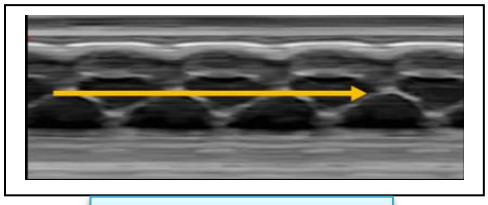

M-mode acceptable

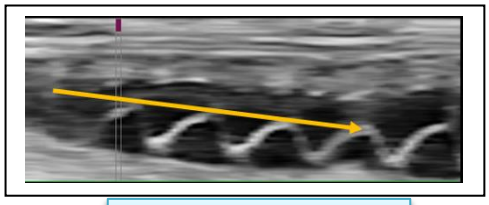

M-mode not acceptable

On M-mode tracing, ensure there is no drifting (due to fetal movement or maternal breathing)

1. Select end diastole (mid-portion of the lower annulus position on M-mode trace); If visible, 1st image after AV-valves closed.
2. Select end diastole to mark end of selected cycle
3. Select end systole between the 2nd diastole markers (highest annulus position on M-mode trace)

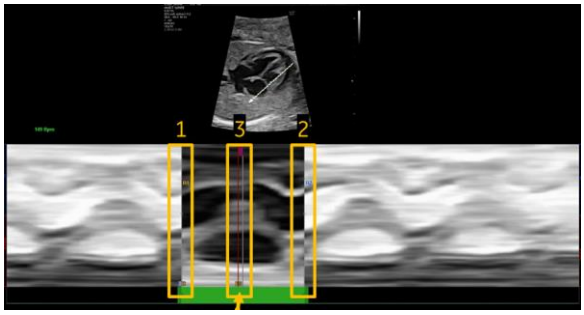


**Choose Left or Right Ventricle to begin analysis.**

**Step 3, Define Left Ventricular end –systolic endocardial tracing**

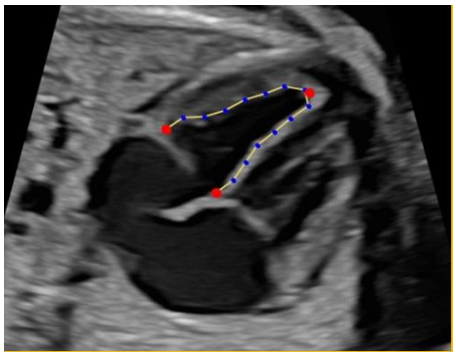

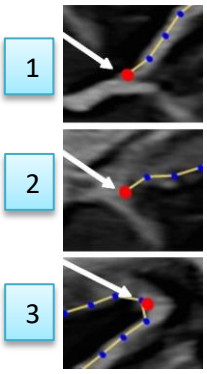


Adjust tracing if needed:
1. Adjust **red** anchor points first
2. Fine tune on **blue** dots

Tracing should be placed on the endocardial border.
1. Septal mitral valve insertion
2. Lateral mitral valve insertion
3. Apex

Once all 3 are selected, trace line will appear along the endocardium.

**Step 4 - Define Left Ventricular end –systolic endocardial tracing**

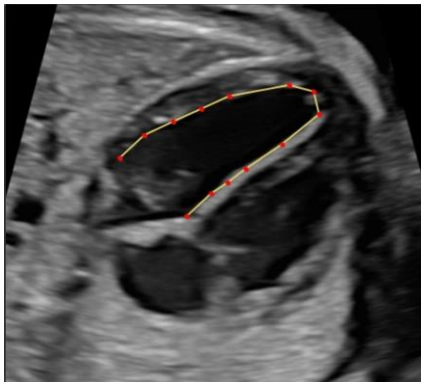

A proposed trace of the endocardium in ED will appear.

Confirm tracing or adjust dots as needed to meet endocardium.

Once tracing is confirmed, select Accept on touch panel to complete.

**Step 5 – Define the right ventricle –** using the same principles as above

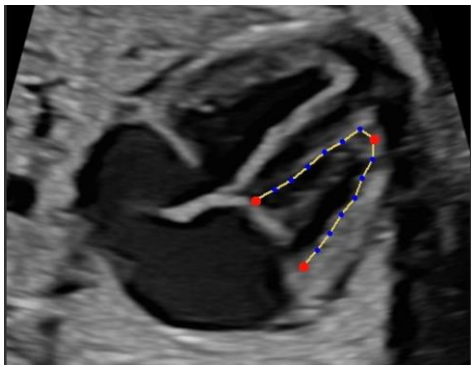

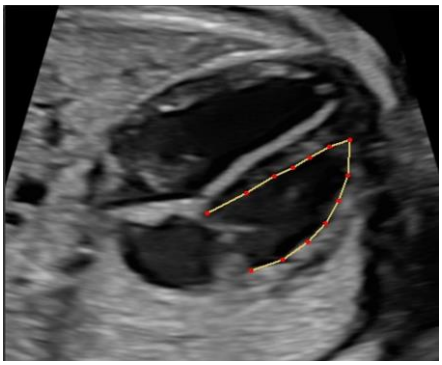

Papillary Muscle should be inside the contour.

Moderator Band (if visible) should be inside contour.

TRACE TIPS

Play or scroll the cine for each phase as needed to help recognize location of endocardium, valve insertions, etc.

For the right ventricle, ensure moderator band is inside the trace line (included in trace).

Ensure modifications are done on yellow trace lines – blue trace lines indicate the cine frame is out of phase of the ED frame and will alter the results.

Goal of *fetal*HQ is to have a good contour detection to outline the endocardium in ES and ED. Framerates < 100 Hz are considered acceptable because ES & ED tracings are adjusted manually if needed. For Strain Analysis of the entire cardiac cycle, framerates > 100 Hz are recommended.

## References


1. GE HealthCare (2020) FetalHQ Quick guide. Voluson. [Place of publication not stated]: GE HealthCare.
2. GE HealthCare (2020) 'Voluson fetal HQ Consensus Guidelines'. Available at: https://www.volusonclub.net/download/news/file/2809